End of Degree Project
Degree in Industrial Technologies Engineering

Analysis of sensitivity of parameters in an active orthosis assisting the human walking

Author: Guillermo Muñoz Pérez
Tutor: Daniel García Vallejo

Mechanical Engineering and Manufacturing Department
Higher Technical School of Engineering
Seville, 2018

End of Degree Course
Degree in Industrial Technologies Engineering

Analysis of sensitivity of parameters in an active orthosis assisting the human walking

Author:

Guillermo Muñoz Pérez

Tutor:

Daniel García Vallejo

Mechanical Engineering and Manufacturing Department

Higher Technical School of Engineering

University of Seville

Seville, 2018

End of Degree Project: Analysis of sensitivity of parameters in an active orthosis assisting the human walking

Author: Guillermo Muñoz Pérez

Tutor: Daniel García Vallejo

El tribunal nombrado para juzgar el Proyecto arriba indicado, compuesto por los siguientes miembros:

Presidente:

Vocales:

Secretario:

Acuerdan otorgarle la calificación de:

El Secretario del Tribunal   Sevilla, 2013

A mi familia
A mis maestros

Agradecimientos

Me gustaría comenzar recordando a todos mis Maestros y Profesores del Colegio y del Instituto, que me aportaron los conocimientos básicos no sólo de Física o Matemáticas, sino también las herramientas necesarias para poder expresar mediante la escritura todo ese aprendizaje. También quiero agradecer a todos aquellos Profesores de Inglés que me han ayudado a alcanzar el nivel suficiente para redactar este Trabajo en esa lengua.

Por supuesto, agradecer a todos los Profesores que, durante estos años en el Grado, han aportado su grano de arena con sus enseñanzas, así como a los amigos y compañeros que me han ido acompañando. Todos ellos son responsables de que alguien como yo haya podido completar, con mucho trabajo y esfuerzo mediante, este Grado en Ingeniería en Tecnologías Industriales.

Yendo más a lo particular, es obligado agradecer a Daniel su tutelaje y su ayuda para realizar este Trabajo. Sin duda, su accesibilidad y disponibilidad en todo momento, así como su amabilidad para explicar cualquier concepto han resultado de mucha ayuda y me han permitido obtener un intenso aprendizaje sobre las órtesis activas. Tanto es así, que espero en el futuro seguir estudiando más a fondo el campo de los exoesqueletos, en general.

Por último, pero no menos importante, mi familia. No puedo ser más afortunado de tenerlos a ellos, que me transmiten un ambiente familiar inmejorable para poder desarrollarme. Os quiero.

x

Resumen

Este trabajo servirá para estudiar la influencia de algunos parámetros de una órtesis en un ciclo de marcha humana, realizado por una persona con un cierto grado de lesión que lleva una órtesis activa. Partiendo de una solución de referencia correspondiente a una persona sana, se estudiará cómo los cambios introducidos en el exoesqueleto afectan al ciclo de marcha humana en términos de energía, desviación de la referencia y otros parámetros definidos como variables de diseño. El problema consiste en un algoritmo de optimización en el que la función de coste tiene en cuenta el coste metabólico y la desviación con respecto al patrón, mientras que las variables de diseño deben cumplir una serie de restricciones en los puntos de control. Estas variables de diseño se evalúan en los nodos, para buscar la solución más óptima.

La órtesis portada por la persona lesionada consiste en un exoesqueleto active SCKAFO, que contiene un actuador rotacional que aporta un par en cada una de las rodillas, así como un tobillo flexible Klenzak, que ayuda a flexionar el tobillo. Un encóder permite controlar el ángulo de flexión y corregir la posición si es necesario. Los resultados incluyen la evolución temporal a lo largo del ciclo de marcha de las coordenadas generalizadas, las fuerzas de reacción, los pares generados en las articulaciones y en los dispositivos de la órtesis (el motor y el tobillo Klenzak), la activación muscular y la excitación neuronal. Las conclusiones obtenidas servirán como guía para el diseño de futuras órtesis.

Abstract

This work will serve to study the influence of some parameters from an orthosis in a human walking cycle, performed by an injured person while wearing an active orthosis. Parting from a reference solution corresponding to an injured individual, it will be studied how the changes introduced in the exoskeleton affect to the walking cycle in terms of energy, deviation from the reference and other parameters defined as design variables. The problem consists on an optimization problem where the cost function bears the metabolical cost and the deviation from reference, while the design variables must fulfill a set of constraints in control points. These design variables are evaluated in node points, so as to look for the more optimal solution.

The orthosis worn by the injured individual consists on an SCKAFO active orthosis, which includes a rotational actuator in each knee that supplies a torque, and a flexible Klenzak ankle, that also helps to bend the ankle. An encoder serves to control the bending angle and correct the position if necessary. The results will include the temporary evolution through the walking cycle of generalized coordinates, reaction forces, torques generated both at the human body and the orthosis devices (motor and Klenzak ankle, muscle activation and neural excitation. The obtained conclusions will serve as a guide for future orthosis designing.

Index

LIST OF TABLES

LIST OF FIGURES

1 INTRODUCTION

This research deals with the influence of certain parameters from an active orthosis, when the person wearing the exoskeleton performs a walking cycle. The main objective consists on, after implementing some changes into the exoskeleton, studying how these changes affect to some important features relating a walking cycle performed by an injured individual wearing the orthosis, such like the metabolical cost or the torques generated during the cycle. The results which may be obtained will serve to reach some conclusions about how future active orthosis can be designed and manufactured, focusing on those parameters which really could cause an impact in the cycle, and ignoring those which do not really affect the most important parameters in the walking cycle.

In order to measure the influence of the orthosis parameters, a non-linear optimization problem, coded in a MATLAB algorithm by García Vallejo [23] is used, taking a linear combination of the metabolical cost and the deviation from the reference motion as the cost function. First of all, data corresponding to healthy individuals, appearing in Ackerman and Gross [9], may be used to build a reference solution parting from them. This reference solution does correspond to a person suffering a certain grade of injury, and it will serve as the basis for the rest of optimizations. All of them will be compared to this reference solution.

In addition to the aim of this project, just explained in the previous paragraphs, this introduction contains a descriptive summarize about every contents appearing in this research, including the most important bibliographical sources, which were useful to obtain every needed information.

In Section 2, an introduction to the spinal cord and its typical injuries, based in the information submitted by Mayo Clinic [4], Johns Hopkins [5] and The Shepherd Center [6]. Following with the theoretical presentation, the active orthosis subject to this study is presented in Section 3, describing its parts and mechanical devices, as well as its main functionalities, as appears in Font-Llagunes, García Vallejo and Schliehen [1]. The SCI classification according to the damage level is also presented, as it is necessary to understand the aim of the exoskeleton.

Henceforth, every mathematical models used are described. Section 4 serves to present the musculoskeletal model, its generalized coordinates, the equations of motion and where do their terms come from. Every mathematical models appearing in this research, especially the musculoskeletal model and restrictions can be found and further explained in the works made by Font-Llagunes, García Vallejo and Schliehen [1-2-3]. On the other hand, the Section 5 contains a complete development of the mathematics describing the muscle modelling (especially Hill's model) and the activation dynamics, essential to understand how the human being performs a movement using the limbs. Most of the information about muscle dynamics has been obtained from the works by García Vallejo [3], Martínez Reina [16] and Nagano and Gerritsen [20].

The optimization problem is introduced and developed in Section 6. The vector of design variables is deconstructed so as to understand what each term means. The interpolation method, the cost function, the constraints and, by last, the options required by MATLAB to describe completely the problem. Also, some useful algorithms are detailed, explaining their sequential relations, their relation to the main algorithm and their role in the optimization problem. The description of the problem finishes at Section 7, where the six types of parameters subject to changes during the optimization are presented.

After presenting the problem, it is the moment to introduce the results. The Section 8 contains a complete display of every results obtained during the optimization, described both quantitative and qualitatively.

Graphics and tables shows the evolution of generalized coordinates, ground forces, joint moments, artificial torques, muscle activation, neural excitation, metabolical expenditure and deviation from pattern, when an orthosis parameter is changed.

By last, Section 9 contains a small summary of every results just described, including conclusions which may be obtained from them.

2 SPINAL CORD INJURIES. EXOSKELETONS

In this section, the Spinal Cord and its injuries, denoted as Spinal Cord Injuries, will be presented, as they are one of the main causes of damage in the musculoskeletal human system. More detailed information can be found in the bibliography [4-5-6-15]. Then, a theoretical introduction about exoskeletons is made, focusing on their purpose on serving as a mechanical device to improve injured people's quality of life.

2.1   An introduction to the spinal cord

The Shepherd Center defines the spinal cord as a on a major bundle of nerves, which serves as a road for nerve impulses from the brain to the muscles and vice versa [6]. Along with the brain they constitute the central nervous system, responsible for receiving and processing all information arriving to the body, and coordinating the movements the musculoskeletal system can carry out.

The spinal cord extends from the base of the brain to the conus medullaris, located in the waist, along 44 cm, approximately. It is connected to the brain through the upper motor neurons (UMNs), which transport the information from and to the brain through the spinal tract. The spinal cord is connected to the rest of parts of the body through the lower motor neurons (LMNs). There are LMNs at each vertebral level, so as every members in the body to be communicated with the spinal cord.

The LMNs are divided into two parts: the sensory part and the motor part. The first one is responsible for informing the brain about the sensations felt by the skin and body parts. The second one makes the inverse road: it broadcasts the movement orders from the brain to the body parts.
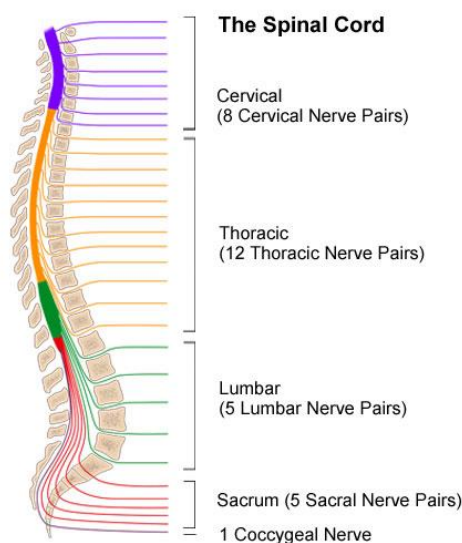
Figure 2-1: Subdivisions in the spinal cord. The Hopkins Medicine University [5]

The Figure 4-1 shows the parts the spinal cord divides into, the nerves getting out from the spinal to the body parts, and how the spinal cord is protected by the vertebral column. As it is shown, the vertebral column comprises 8 cervical vertebrae (right below the neck), 12 thoracic vertebrae (in the upper back), five lumbar vertebrae (considered to be in the low back), five sacrum vertebrae (placed in the pelvis) and four coccygeal vertebrae (also located within the pelvis).

2.2 Spinal Cord Injuries

According to the Mayo Clinic [4], a Spinal Cord Injury (henceforth, SCI) can be defined as the damage produced in any part of the spinal cord, or the nerves at the end of the spinal canal, which affects severely some important body functions below the place of injury, as well as strength and sensory in some of these parts.

A SCI implies an important loss of self-control to perform movements, in a total or a partial way. The importance of the injury depends on two factors: the place of the injury, and its severity. The highest site a SCI is placed in the spinal cord, the most serious the injury can result to be, as the damage produced in a determined location in the spinal cord normally affects to the rest of the cord, situated right below the injury. The first criterion used to classify the SCI is their completeness, according to Mayo Clinic [4]:

a) Complete injury: when the sensory and self-control of the movements right below the affected zone in the spinal cord are completely lost.

b) Incomplete injury: when some sensory and movement skills remain unaffected. As there are some grades of severity in uncomplete spinal cord injuries, complete injuries can be considered as a particular case of uncomplete injuries.

Depending on the amount of affected members, SCI can also be referred as:

a) Quadriplegia: when the SCI affects practically every members in the body, including upper and lower extremities, the trunk and the pelvis.

b) Paraplegia: when upper extremities are not affected.

Hopkins Medicine adds a third type of SCI [5]:

c) Triplegia: when the loss of movement affects to both legs and only one arm.
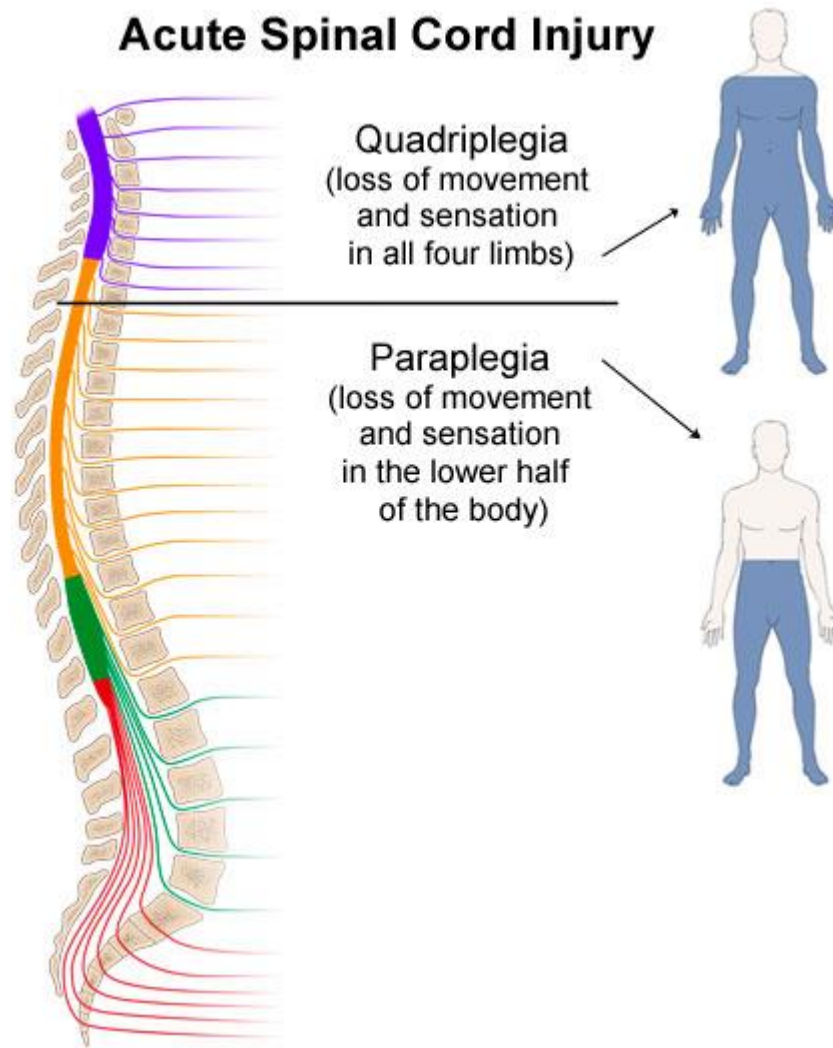
Figure 2-2: Spinal Cord Injuries according to the affected movement area. The Hopkins University [5].

There is a huge set of causes which can be responsible for provoking SCIs. Most of them are classified as traumatic because they consist on sudden events which cause the injury, such like car accidents, gunshots or stabbings. Not even the professional sport is away from spinal injuries. Well known it is the case of Slobodan Janković [6]. This Yugoslavian basketball player ended prematurely his sports career at 29 years old, in 1993, while playing for Panionios a Greek League playoff game in Athens, against Panathinaikos. The referee called Janković's fifth foul, which meant his foul out. Janković angered and kicked his head against the basket supporting post, damaging severely his vertebral column and thus, his spinal cord. He could not walk again, and died due to a heart attack in 2006 at 42 years old. To summarize, an injury in the vertebral column can be decisive to suffer a SCI.

Other causes for SCI's are not considered as traumatic and they involve diseases like cancer, arthritis, inflammation or neurodegenerative diseases. These last ones can result in a progressive loss of motor skills, starting with fingers and hands, and following with extremities.

Figure 2-3: Slobodan Janković right after getting severely injured. Libertad Digital [8].

Exoskeletons field has developed itself considerably for the last decades, to face several purposes they have been designed to. Undoubtedly, these devices have contributed to improve life quality in our society. But starting from the beginning, what is an exoskeleton like?

2.3   Exoskeletons

An exoskeleton is a wearable, mechanical device that provides an additional energy to the person wearing it, allowing him not to exert the whole required strength to perform a movement [12]. According to the energy source, exoskeletons can be divided into two types [13]:

a) Passive exoskeletons: the additional energy is supplied by a set of mechanical elements such like springs, dampers or spring-like cilinders, which store energy during the beginning of the movement, and release it subsequently [10-11]. They do not have any electrical energy source, and their production is economically more affordable. Especially designed for manufacturing industry, they allow workers not to overload their muscles, and so on to reduce the risk to suffer musculoskeletal diseases like low-back pain. Passive exoskeletons can assist workers in tasks involving almost any type of limbs in thir body. Figure 1-1 shows an operator wearing the PLAD, a typical passive exoskeleton, while performing a typical task in automotive industry. These devices are not necessarily worn by injured people.

Figure 2-4: Industrial worker wearing PLAD exoskeleton. Graham et al. [10].

b) Active exoskeletons: powered by an electrical actuator, they usually generate more strength than their passive counterparts [12]. Usually more expensive than passive exoskeletons, they are focused on assist patients suffering spinal cord injuries (SCI), providing them the needed torque to manage basic and daily activities like walking. They usually incorporate sensors and encoders so as to measure the position of the body, and correct it if necessary. Also, a flexible Klenzak ankle, placed at the ankle joint, controls its bending, locking it during the swing phase in a gait, as García Vallejo, Font-Llagunes and Schliechen explain [1]. Figures 1-2 and 1-3 show a typical active exoskeleton and its actuator, placed in the knee.

Figure 2-5: Active orthosis for lower limbs. Yale University [14].

Figure 2-6: Example of an exoskeleton actuator placed in the knee. Yale University [14].

3 DESCRIPTION OF THE ACTIVE ORTHOSIS

In this section, the active orthosis used in every experiments appearing in this research will be presented. As explained in the previous section, the main object at designing active orthosis is to provide an additional power to people suffering a spinal cord injury (SCI), to ease them at walking. According to the University of Wisconsin [15], the American Spinal Injury Association (ASIA) classifies the SCI injuries according to the Table 2-1:

Table 3–1. SCI classification according to ASIA

Range	Description
A	No motor skills or sensory function below the affected area
B	Little sensitivity under the injured area
C	Half of muscles under affected area can defy gravity
D	Most of muscles (not all) can move against gravity
E	Complete motor and sensory function returned

The orthosis in question in this research is a SCKAFO orthosis (Stance Control Knee Ankle Foot Orthosis), which assists incomplete SCI subjects, around C-D range. The exoskeleton allows these people to perform low-speed gaits. The SCKAFO includes some important features [1]:

a) A knee-locking system that forbids the knee movement so as to prevent an overload in the quadriceps, which can not support big loads. It is activated upon heel strike detection, using a set of sensors.

b) An actuator providing force to help the walker to flex and extend the knee joint during the swing phase.

c) A Klenzak passive ankle joint, including a spring which produces a torque, and an optical incremental encoder, responsible for controlling the ankle angle.

During the gait cycle, the orthosis works the following way: when the heel strike makes its appearance, the knee-locking system goes into action, forbidding any torque produced by the actuator. The sensors and the encoder obtain information about the gait. When the walker lifts the foot from the ground, and so the contact has finished, the locking system stops working and the motor produces a torque to perform the swing phase. When the foot touches the ground again, a new cycle starts.
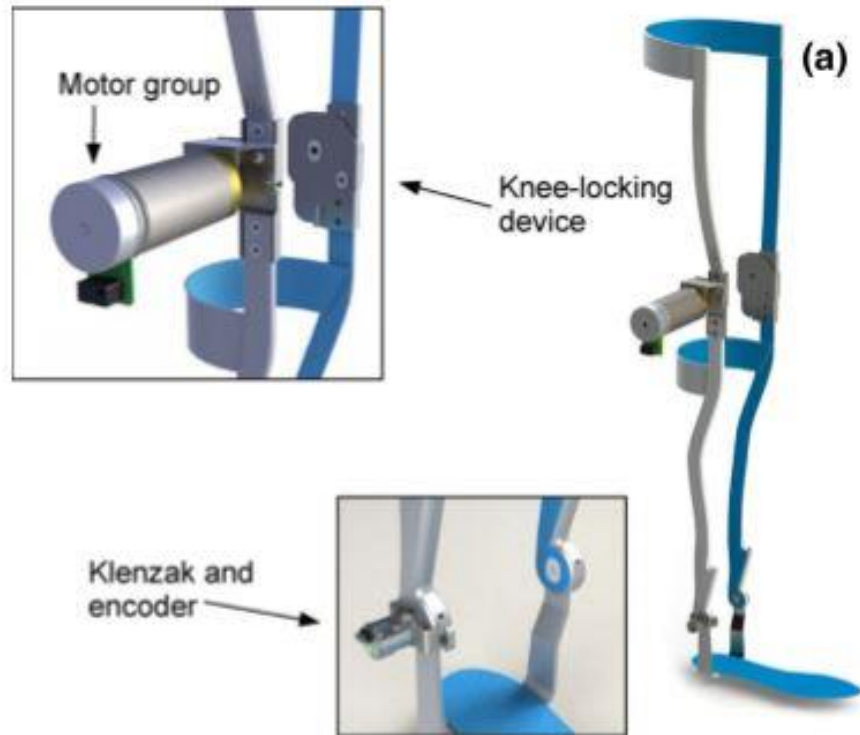
Figure 3-1: SCKAFO exoskeleton, used in this report. It contains an electrical actuator placed in the knee, a Klenzak flexible ankle and an encoder, these two sited in the ankle. Font-Llagunes, García Vallejo and Schliehen [1].

The Figure 3-1 shows the devices just presented: the actuator, the knee-locking system and the Klenzak flexible ankle.

4 MODEL DESCRIPTION

In this section, the human body model used in the research by Font-Llagunes. García Vallejo and Schliehen [1] will be presented, as well as the system of equations which describe the motion, the conditions of contact modelling the foot-ground contact, and the eight phases describing a walking cycle.

This model parts of an original tridimensional model used in other researches (meter cita). Nonetheless, as this work deals completely with a bidimensional model, and so every results and graphics obtained, the bidimensional model of the human body will be the only one presented here.

4.1 Bidimensional musculoskeletal model

This bidimensional human body model can be found in Ackermann [9] and García Vallejo [2]. As it is shown in the Figure 3-1, it is fully contained in the sagital plane, and it will be very useful to work with this model due to its simplicity. In fact, it reduces significantly the number of parameters in the optimization and, therefore, the number of design variables. The effect of the orthosis and the Klenzak ankle on the generalized coordinates will also be included, as every experiments and results obtained will bear the presence of both mechanical elements. As it will be explained later, the symmetry of the model will also allow to obtain results quicker.

7 bodies and 9 generalized coordinates are defined in this model. The seven bodies consist on two shanks, two thighs, two feet and a body named HAT, which includes the pelvis, the trunk, the arms and the head. It shall be noted that the motion of the lower part of the human body is given much more importance than the upper part, as this one is being comprised in a single body. The 9 generalized coordinates can be defined as:

a) x_{11}: longitudinal displacement of the HAT (measured in absolute coordinates)
b) z_{11}: vertical displacement of the HAT (measured in absolute coordinates)
c) β_{11}: pitch rotation of the pelvis
d) β_{13}: right hip flexion angle
e) β_{34}: right knee flexion angle
f) β_{45}: right ankle flexion angle
g) β_{16}: left hip flexion angle
h) β_{67}: left knee flexion angle
i) β_{78}: left ankle flexion angle

If the walking cycle is divided into two equivalent halves, the symmetry of the model allows to make the next simplifications:

- The motion of the pelvis is the same in the first and the second half of the cycle.

13

- In the second half, the left leg moves the same as the right leg in the first half of the motion cycle.
- Equivalently, the left leg is submitted to the same muscle forces during the second half of the cycle, as the right leg in the first one.

To sum up, only 6 generalized coordinates can be considered as design variables for the trajectory, in the optimization of parameters.
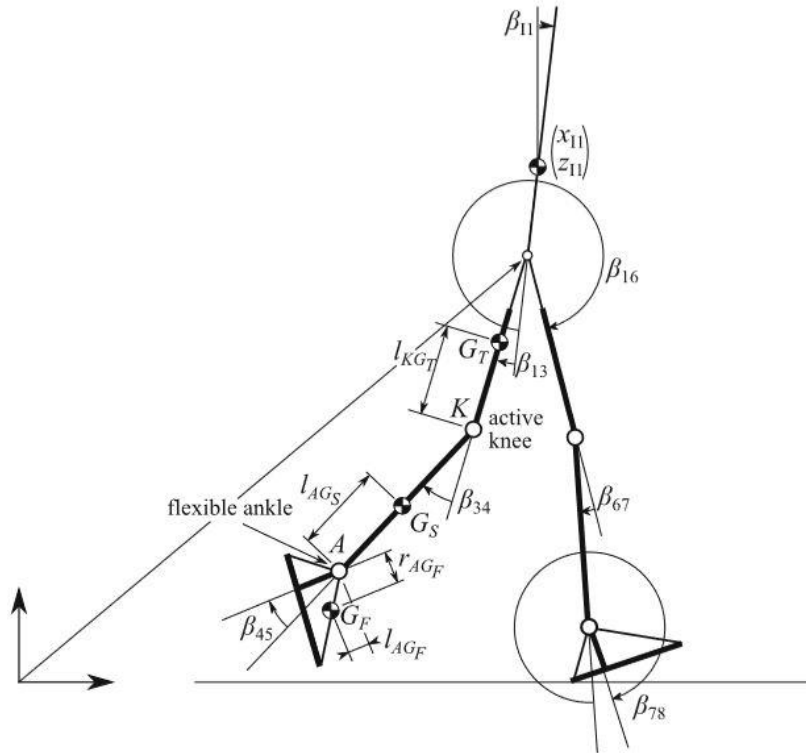
Figure 4-1: Musculoskeletal system used in this report, representing generalized coordinates. Font-Llagunes, García Vallejo and Schliehen [1].

4.2 Equations of motion

Defining n_c as the number of generalized coordinates, N_m as the number of actuating muscles, and n_b the number of actuated joints, and considering in a first place the model as an open kinematic chain, built with a set of bodies connected by a set of holonomic joints, and described by n_c generalized coordinates, the classical equations of Newton-Euler allow to express the system as a set of equations of motion where the unknowns parameters are the generalized coordinates (according to d'Alembert's Principle) as follows [2]:

$$M(q)\ddot{q} + k(q, \dot{q}) = q_r(q, \dot{q}) + BAf^m + q_{act} + q_{ank}(y) \qquad \text{(4-1)}$$

14

Where $M(q)$ is the (n_c x n_c) square mass matrix of the system, $k(q, \dot{q})$ is a (n_c x1) vector containing the generalized Coriolis forces, $q_r(q, \dot{q})$ is a (n_c x 1) vector including generalized gravitational forces, generalized moments in the joints due to the interaction between them and the tissues as it appears in Riener and Edrich [21], and generalized viscous damping torques in the knees according to the model presented in Stein [22], and BAf^m, a (n_c x1) vector, represents the effect in terms of generalized forces of the muscle actuating in the system.

This term is formed by B, a (n_c x n_b) matrix which includes the generalized torques in the actuated joints; A, a (n_b x N_m) matrix containing every moment arms needed to calculate the torques produced by muscles during their actuation; and f^m is the (N_m x1) vector containing every muscle forces.

The terms q_{act} and $q_{ank}(y)$ are (n_c x 1) vectors that make reference to the actuation of the orthosis and the Klenzak ankle, respectively. Both of them expressed in function of the generalized coordinates, they can be written as follows:

$$q_{act} = [0 \ \ 0 \ \ 0 \ \ 0 \ \ T_{kr} \ 0 \ \ 0 \ \ T_{kl} \ 0]^T$$

$$q_{ank} = [0 \ \ 0 \ \ 0 \ \ 0 \ \ 0 \ \ T_{ar}(q) \ 0 \ \ 0 \ \ T_{al}(q)]^T$$

Of course, $q, \dot{q}$ and $\ddot{q}$ are the generalized coordinates, velocities and accelerations, respectively.

4.2.1 Foot-Ground contact modelling

What is concerning to the modelling of the contact between the feet and the ground, it can be expressed by a set of conditions of contact which vary according to the phase of the cycle. First of all, some variables must be defined, starting with the geometrical parameters of feet. Denoting H as the height of an individual, the next relations described by Ackermann and Gross [9], also collected by García Vallejo in [3], appearing in the Figure 3-2, can be used:
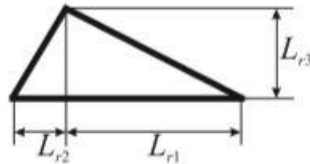
$$L_{r1} = L_{l1} = 0.10 \, H$$
$$L_{r2} = L_{l2} = 0.04 \, H$$
$$L_{r3} = L_{l3} = 0.06 \, H$$

Figure 4-2: Geometrical parameters needed to define feet. García Vallejo [3].

Where L_{r1}, L_{r2} and L_{r3} are geometrical constants that define the feet, and are the same for both feet. The following constants may also be used during the parameterization:

1) L_R: it is the length of the right step, considering it the distance between the left and the right toe (this one is in front of the left one).
2) L_L: it is the length of the left step, considering it the distance between the right and the left toe (now this one is in front of the right one).
3) T_R and T_L: denote the right and left toe, respectively.
4) H_R and H_L: denote the right and left heel respectively.

Now the conditions of contact between the ground and the feet can be presented. As explained before, each walking cycle is divided into eight phases, and each phase has its own conditions of contact. They can be described as follows:

1) Phase 1: the left toe and the right heel have their displacements constrained.
2) Phase 2: the same as in phase 1, adding a vertical constraint in the right toe.
3) Phase 3: the left foot is fully released, the right one remains the same way as in phase 3.
4) Phase 4: the right heel is released, whereas the right toe has its displacements constrained. The left foot remains with no constraints.
5) Phase 5: constraints are imposed on the left heel and the right toe.
6) Phase 6: the same as right before, adding a vertical constraint in the left toe.
7) Phase 7: the right foot is unconstrained, while the left one remains with no changes.
8) Phase 8: the left heel is liberated, and displacements constraints are added in the left toe. The right foot remains released.

It shall be noted that phases 5 to 8 are the same as 1 to 4, but with the right and the left foot interchanging their roles. The conditions of contact for each phase can be observed in the Figure 3-3:
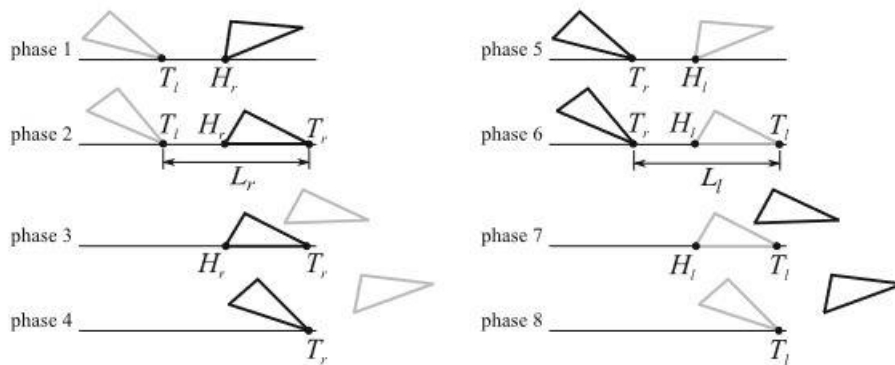
Figure 4-3: Eight phases of the walking cycle. García Vallejo [3].

Where L_R and L_L represent the respective lengths of a right and a left step.

As the conditions of contact have been defined, the system is now a closed kinematic chain, and the effect of those conditions must be reflected in the equations of motion, in terms of contact forces expressed in function of the generalized coordinates. The new system of equations is defined:

$$M(q)\ddot{q} + k(q, \dot{q}) = q_r(q, \dot{q}) + BAf^m + q_{act} + q_{ank}(y) + C_{ph}^T\lambda_{ph} \tag{4-2}$$

Where C_{ph}^T denotes the jacobian matrix of the kinematic constraints at the phase ph of the motion, and λ_{ph} is the vector of Lagrange multipliers, also at the phase ph.

5 MUSCLE MODELLING

In this section, muscles intervening in the walking cycle right described will be presented, as well as the biological model followed to describe the dynamics of muscles activation and contraction, better known as Hill model.

5.1 Muscles intervening in the cycle. Hill's model

The muscles taking part in the walking cycle are the following [1-3]:

a) Soleus (represented in this research as SOL)
b) Tibialis anterior (TA)
c) Gastrocnemius (GAS)
d) Vastii (VAS)
e) Rectus femoris (RF)
f) Harmstrings (HAMS)
g) Gluteus (GLU)
h) Iliopsoas (ILPSO)
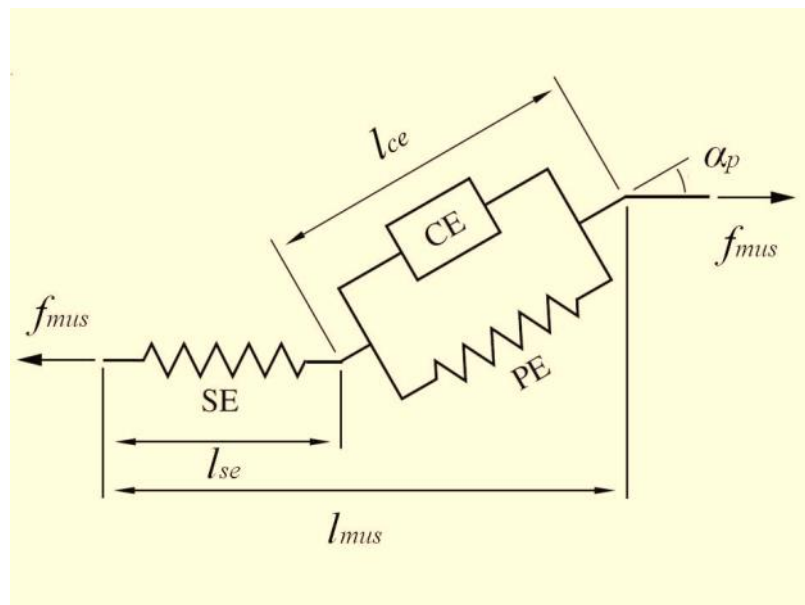
Figure 5-1: Muscle model developed by Hill. Martínez Reina [16].

The Figure 5-1 shows the typical Hill muscle-tendon model. The SE is the elastic element, and it represents the tendon as a spring with a determined stiffness, joined to the muscle. This one is represented by the union of CE and PE. CE is the contractile element, which generates the force, while PE is the non-linear elastic element, parallel to the contractile element. This one represents the stiffness of the structures

parallel to the muscle fibers. The angle α_p is known as the pennation angle, and it represents the angle formed by the tendon and the muscle. The Figure 5-2 shows a more reliable representation of this angle:
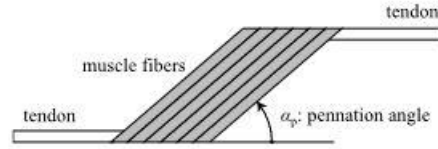
Figure 5-2: Representation of the pennation angle. Font-Llagunes, García Vallejo and Schliehen [1].

Denoting f_m as the muscle force, l_m as its length, l_{SE} as the length of the tendon, f_{PE} as the force generated by PE, and l_{CE} as the length of the contractile element, and projecting the length and the force actuated by CE and PE in an axis parallel to the tendon, the next relations can be stablished:

$$l_m = l_{CE}\cos(\alpha_p) + l_{SE} \tag{5-1}$$

$$f_m = (f_{CE} + f_{PE})cos(\alpha_p) \tag{5-2}$$

As the force powered by PE, $f_{PE,}$ is considered to be negligible in this research, the relation between the muscle force and the contractile element force is now expressed as:

$$f_{CE} = \frac{f_m}{\cos(\alpha_p)} \tag{5-3}$$

Derivating respect to the time the equation…, the velocity of lengthening of the muscle can be obtained:

$$v_m = v_{CE}\cos(\alpha_p) + v_{SE} \tag{5-4}$$

which can also be written this way:

$$v_{CE} = (v_m - v_{SE})\cos(\alpha_p) \tag{5-5}$$

A last parameter can also be defined. It is W, the muscle thickness, and it can be mathematically described as the projection of the aggregate CE-PE in an axis perpendicular to the tendon line of action. It is easier to understand its definition by looking the figure below:
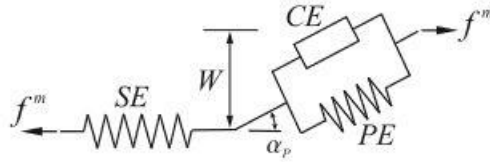
Figure 5-3: Muscle Hill's model.

This mathematical definition leads to an interesting trigonometrical relation between W, α_p and l_{CE}, which can be written as follows[16]:

$$\cos(\alpha_p) = \sqrt{1 - \left(\frac{W}{l_{CE}}\right)^2}$$

(5-6)

Another way to express this relation is the next one:

$$l_{CE} = \sqrt{(l_m - l_{SE})^2 + W^2}$$

(5-7)

5.2 Muscle dynamics

After determining all these geometrical relations, muscle dynamics can be faced. It is governed by two differential equations [1-2-3-21]:

$$\dot{f}_m = f(a, f_m, l_m, v_m)$$

(5-8)

$$\dot{a} = (u - a) * (t_1 * u - t_2)$$

(5-9)

The first equation represents the first derivative of the muscle force as a function of f_m, l_m, v_m (already

20

described) and a. This last one is the muscle activation, and will be bounded in the interval [0, 1], with $a = 1$ being the full activation, and $a = 0$ a total lack of activation.

The second equation relates the muscle activation and its first derivative, with u, t_1 and t_2. The parameter u is defined as the neural excitation, while the other two are two time constants, expressed the next way:

$$t_2 = \frac{1}{t_d} \tag{5-10}$$

$$t_1 = \frac{1}{t_a - t_2} \tag{5-11}$$

Where t_a and t_d are the activation and deactivation time constants, respectively. The significance of these constants can be better understood in the Figure 5-4:
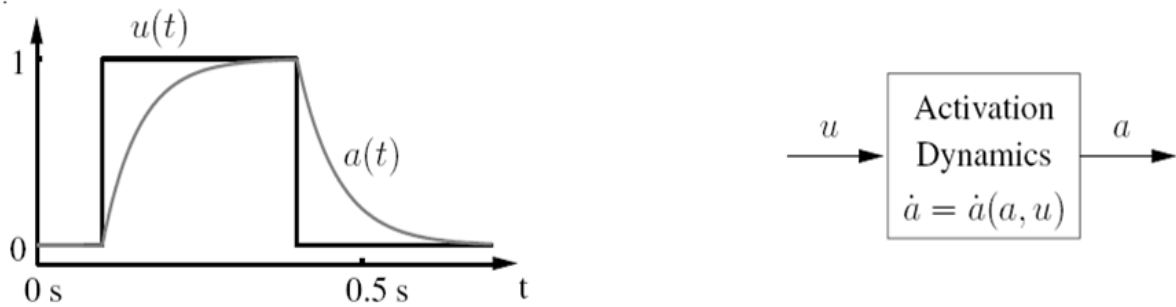
Figure 5-4: Activation and deactivation time. Martínez Reina [16].

The activation time reflects the moment when the muscle starts to receive the influence of the neural excitation, while the deactivation time signs the time that influence ends.

The objective now is to get the parameter a and its first derivative. First, the muscle force and its first and second derivative $(f_m, \dot{f}_m$ and $\ddot{f}_m)$ must be determined using a spline interpolation subroutine. Next, the length of the muscle and its first and second derivative $(l_m, v_m$ and $\dot{v}_m)$ are obtained from the generalized coordinates, as they are a function of them:

$$l_m = l_m(\boldsymbol{y}(t)) \tag{5-12}$$

$$v_m = v_m(\boldsymbol{y}(t), \dot{\boldsymbol{y}}(t)) \tag{5-13}$$

$$v_m = v_m(y(t), \dot{y}(t), \ddot{y}(t)) \tag{5-14}$$

By last, the following muscle properties table (Figure 5-5) will be used to get some important values such like the pennation angle (α_p), the optimus length of the contractile element (l_{opt}^{ce}), the muscle length in the slack state (l_{slack}) and the maximum force the contractile element can power (f_{max}^{ce}).

Muscle group	f_{max}^m (N)	l_{opt}^{ce} (m)	l_{slack} (m)	α_p (°)	$r_{H\beta}$ (cm)	$r_{K\beta}$ (cm)	$r_{A\beta}$ (cm)	l_0^{lm} (cm)	ft (%)	Width
ILPSO	821	0.102	0.142	7.5	−5.00	0	0	24.8	50	1.298
RF	663	0.081	0.398	5.0	−3.40	−5.00	0	47.4	65	1.443
GLU	1705	0.200	0.157	3.0	6.20	0	0	27.1	45	0.625
HAMS	1770	0.104	0.334	7.5	7.20	3.40	0	38.3	35	1.197
VAS	7403	0.093	0.223	4.4	0	−4.30	0	27.1	50	0.627
GAS	1639	0.055	0.420	14.3	0	2.00	5.30	48.7	50	0.888
TA	1528	0.082	0.317	6.0	0	0	−3.70	40.6	25	0.442
SOL	3883	0.055	0.245	23.6	0	0	5.30	28.4	20	1.039

Figure 5-5: Muscle properties table used in this research. Font-Llagunes, García Vallejo and Schliehen [1].

Here on, the muscle thickness (W) and the stiffness of the contractile element (K_T) are defined:

$$W = l_{opt}^{ce} \sqrt{1 - cos^2(\alpha_p)} \tag{5-15}$$

$$K_T = \frac{f_{max}^{ce}}{(0.04 l_{slack})^2} \tag{5-16}$$

Now, the next magnitudes to determine will be the length of the tendon and its derivatives, first and second, using the next equations:

$$l_{SE} = l_{slack} + \sqrt{\frac{f_m}{K_T}} \tag{5-17}$$

$$v_{SE} = \frac{\dot{f}_m}{2K_T(l_{SE} - l_{slack})} \tag{5-18}$$

$$a_{SE} = \frac{\ddot{f}_m - 2K_T v_{SE}^2}{2K_T(l_{SE} - l_{slack})} \tag{5-19}$$

The next step consists on determine the second derivative of the contractile element length $(\dot{v}_{CE})$ and the first derivative of its force $(\dot{F}_{CE})$. Before, the next trigonometrical relation of the pennation angle may be defined:

$$tan^2(\alpha_p) = \frac{1}{cos^2(\alpha_p)} - 1 \tag{5-20}$$

Now, it is easier to write the derivatives right presented:

$$\dot{f}_{CE} = \frac{\dot{f}_m}{cos(\alpha_p)} - \frac{f_{CE}v_{CE}tan^2(\alpha_p)}{l_{CE}} \tag{5-21}$$

$$\dot{v}_{CE} = (a_{SE} - \dot{v}_m)cos(\alpha_p) + \frac{v_{CE}^2 tan^2(\alpha_p)}{l_{CE}} \tag{5-22}$$

The objective now is to get the muscle activation and its first derivative so as to solve the differential equation **(5-9).** The relations appearing in Nagano and Gerritsen [21] are used to obtain the next parameters: the contractile element force at the maximum activation $(\widehat{f_{CE}})$, and the partial derivatives of this parameter with respect to the contractile element length and its derivative $\frac{\partial \widehat{f_{CE}}}{\partial l_{CE}}$ and $\frac{\partial \widehat{f_{CE}}}{\partial v_{CE}}$. For further details read the reference.

As it can be deducted from the definition of $\widehat{f_{CE}}$, the muscle force given a determined value for activation is proportional to the activation so that:

$$f_{CE} = a\widehat{f_{CE}} \tag{5-23}$$

Now there is nothing more but clear the muscle activation:

$$a = \frac{f_{CE}}{\widehat{f_{CE}}} \tag{5-24}$$

To determinate the derivative of the activation, a relation present in Nagano and Gerritsen [21] is also used:

$$\dot{a} = \frac{1}{\widehat{f_{CE}}} (\dot{f_{CE}} - a \frac{\partial \widehat{f_{CE}}}{\partial l_{CE}} \dot{l}_{CE} - a \frac{\partial \widehat{f_{CE}}}{\partial v_{CE}} \dot{v}_{CE})$$

<div align="right">(5-25)</div>

The neural excitation, u, can already be cleared, as every factors in the equation **(5-25)** are known. As it is now a second grade equation, and taking the solution which makes physical sense, the next expression for u results:

$$u = \frac{1}{2}\left(a - \frac{t_2}{t_1}\right) + \frac{1}{2}(a + \frac{t_2}{t_1})\sqrt{1 + \frac{4a\dot{t_1}}{(at_1 + t_2)^2}}$$

<div align="right">(5-26)</div>

6 OPTIMIZATION PROBLEM

In this section, the optimization problem is approached. Every elements required to understand the process will be presented, including design variables, the cost function, the constraint expressions and the initial estimation. The procediment to obtain the values at the control points will also be explained. Further explanations about the interpolation method based in splines can be found in Section 7.

6.1 Design variables

The aim of this research is to measure the influence of the orthosis parameters in a typical human walking cycle, taking into consideration the metabolical cost during the cycle. In other words, the human walking simulation is modeled as an optimization parameters problem [1], where the cost function includes the metabolical cost and the deviation from the regular walking pattern. A set of parameters, called design variables, are used to reconstruct the generalized coordinates histories and the muscle force histories of the walking cycle [1-2-3].

The generalized coordinates and the muscle forces must fulfill a set of constraints so as to ensure the fulfillment of the equations of motion of the multibody system, the kinematic constraints and other physical and physiological relations.

The complete set of design variables form the vector X, whose length depends on the number of nodes used in the parameterization, NN. Considering NC the number of generalized coordinates, and NM the number of muscles in the multibody system, the vector X can be deconstructed into four smaller groups of vectors as it appears in García Vallejo's reports [1-2-3]:

a) The first group consists on a set of NC vectors, each one including all nodal values for each generalized coordinate. As the trajectory of each coordinate in the walking cycle can be described with a vector of NN nodal values, the dimension of the vector corresponding to the trajectory of the multibody system is NN x NC. The vector used for a single coordinate can be denoted as y_i, i=1,2… NN.

b) The second group consists on a set of NM vectors, that includes all nodal values of the muscle forces during the walking cycle. Each vector can be denoted as f_{mi}, i=1,2… NM. As each muscle has NN nodal values for its force during a single cycle, the length of this whole second group of vectors is NN x NM.

c) The third group refers to the parameterization of the motor torque, including all nodal values of the torque during the walking cycle. As the multibody system is considered to be symmetrical, there is only a vector of NN components representing the design variables for the parameterization of the motor torque.

d) The fourth group deals with the parameterization of duration of each of the eight phases forming a walking cycle. Therefore, this vector, T_{ph}, has eight components. As it will be explained later, this vector can be split into two equal vectors, so as the first phase of the motion has the same duration as the fifth one, the second takes the same time as the sixth, and so on.

e) The fifth vector includes a set of geometrical parameters which describe the kinematical constraints in the ground, PG. These parameters can be listed as Lr (the length of a right step) and Ll (the length of a left step).

f) The sixth and last group of vectors, PO, contains a set of design parameters of the orthosis. They are the torque and the stiffness. As the problem is symmetrical, this vector only includes these two components.

6.2 Nodes and control points. Parameterization

In order to ease the study and analysis of the movement during the walking cycle, it must be parameterized by using spline functions. This situation makes indispensable to know the value of design variables in determined points of the cycle, named as nodes [3]. The walking cycle will be divided into a determined number of nodes, NN. The most nodes are used in optimization, the most reliable and accurate results will be obtained, but at the same time the largest will be the vector containing design variables, something harmful in terms of computational time. Most of the optimizations performed in this research have been done using 25 nodes, a number found to be reliable to get accurate results in a reasonable time. Also, a 29-node optimization was performed so as to check and compare it with the 25-nodes solution.

So, taking NN = 25 nodes, each walking cycle is composed of 25 nodes. The objective is to build time stories of parameterized variables from their values at nodes, by using fifth-order spline functions with periodical boundary conditions [3]. These periodical conditions are used to take into account the periodical nature of the walking cycle. However, the measured walking cycle is not perfectly periodical, due to small deviations from the reference pattern. Moreover, other imperfections appear as a consequence of numerical reasons in the procediment. What is more, a problem appears when imposing periodical boundaries to non-periodical points: a non-desirable swing-like trajectory that makes more difficult to find a convergent solution (see Figure 6-1). The way to solve this problem consists on imposing periodicity to the values in nodes. Concretely, two conditions are imposed in node values:

a) The first node value must be the same as the last one in the cycle, to ensure the cycle fulfillment

b) The two first and the two last node values are calculated from previous node values (for further information about the calculation method, consult García Vallejo's report [3]).

This last condition makes that only NN-4 node values are considered as design variables during optimization, so in the 25-nodes solution, only 21 correspond to the design variables vector.
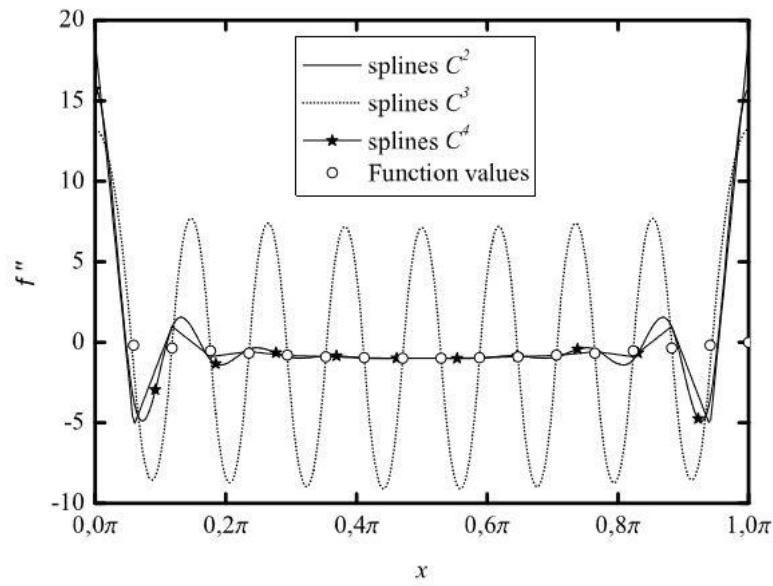
Figure 6-1: Diverse examples of spline functions. García Vallejo [1]

Node values are not enough to ensure a reliable and fully parameterization of the walking cycle. Also, a set of control points must be defined to ensure the fulfillment of constraints expressions at those points (see Ackerman and Gross [9]). These control points do not coincide necessarily with node points, in fact, there are much more control points than nodes, which allows a more accurate fulfillment of constraints. Each phase has a determined number of control points according to its duration, as it appears in the Table 6-1:

Table 6-1. Control points in each phase

Phase	Number of control points
1	3
2	4
3	18
4	15
5	3
6	4
7	18
8	15

As it can be observed in the table, the cycle can be divided into two equal halves, so that the phase 1 has the same number of control points as the phase 5, the phase 2 has the same number as the same 6, and so on for the rest. This means that the last control point in a gait phase is the same as the first one in the next gait phase. The total number of control points comes from the next equation [3]:

$$N_{cp} = 1 + \sum_{ph=1}^{8} (N_{cp}^{ph} - 1)$$

<div align="right">(6-1)</div>

So, there is a total of 73 control points in the whole walking cycle. The Figure 6-2 shows the distribution of nodes and control points in a typical walking cycle.
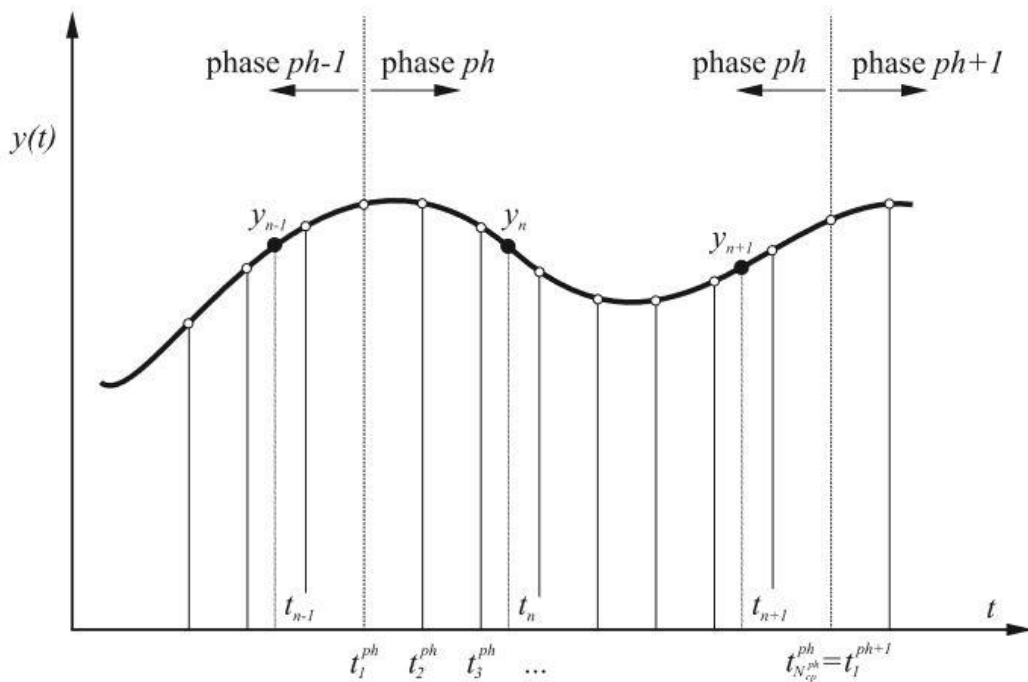
Figure 6-2: Distribution of nodes and control points in the walking cycle [3].

6.2.1 Design variables vector breakdown

The explanation of the distribution of node points in a walking cycle is necessary to understand the length of the components in the design variables vector. Looking the algorithm coded by García Vallejo [23], it is easy to understand the length of its part in the vector.

```
X(3*(NNM-4)+(NCS-3)*(NN-4)+NMS*(NN-4)+(NAS)*(NN-4)+8+2+2)
```

The first term refers to the three coordinates describing the pelvis movement. Each one of them describes a symmetrical movement, and following the interpolation rule right described, the length of each vector is (NNM-4), being NNM the number of the node placed in the middle. The second term makes reference to

the rest of the coordinates. As they do not describe a symmetrical motion, each one has a (NN-4)-components length. The third and fourth parts of the X vector describe themselves analogously to the second one, but referring to the muscles and the actuators, respectively. This way, the third part has a (NMS*(NN-4))-components length, while the fourth one is (NAS*(NN-4)) components long.

By last, the number 8 makes reference to the eight phases of the optimization, while the last two numbers indicate the two foot geometrical parameters and the two orthosis parameters.

6.3 Cost function

The objective of the optimization problem consists on finding the best trajectories minimizing the metabolical expenditure. This is a logical criterion according to biological and physical reasons, as the human being tries to spend the less energy power possible when executing its movements. Therefore, the design variables presented right before will be obtained by minimizing the objective function which will be explained in the next paragraphs.

In this report, the energy expenditure model developed by Umberger [19] will be used, as it represents in a reliable way the metabolical cost during the human act of walking. This model considers the thermal and mechanical energy liberation rates during simulated muscle contractions at normal body temperature. The energy rate for a single muscle can be described as:

$$\dot{E} = \dot{E}(l^{ce}, v^{ce}, f^{ce}, a, u, p_m) \qquad \text{(6-2)}$$

Where l^{ce} is the CE length, v^{ce} is the CE velocity, f^{ce} is the CE force, a refers to the muscle activation, u is the neural excitation, and p_m is a vector that includes every muscle constants parameters needed to measure accurately the energy rate. This expression can be integrated in a determinate period of time, to represent the whole quantity of energy used in a walking cycle, as follows:

$$E = \int_{t_0}^{t_f} \dot{E}(l^{ce}, v^{ce}, f^{ce}, a, u, p_m) dt \qquad \text{(6-3)}$$

Where t_0 and t_f are the inicial and final times of the walking cycle, respectively.

In this research, as long distances are considered to measure the energy gate during the walking cycle, it is more comfortable to use the average energy per distance walked. It is said, the total energy consumpted divided by the total length walked during the process. This quantity, defined as the metabolical cost of transportation, can be written as follows:

$$E^t = \frac{E}{L_r + L_l}$$

(6-4)

In order to avoid non-logical solutions trying the find the most optimum trajectories and muscle forces, a regular motion pattern will be followed. This is important for aesthetical reasons, as one of the purposes in the designing of orthosis is to make the person wearing it to walk the most similar possible way to a regular person. Moreover, the resulting contact forces in the simulated model will be very similar to the ones in the non-damaging feet model.

The deviation from the walking standard motion is expressed below:

$$J_{dev} = \int_{t_0}^{t_f} \sum_{i=1}^{n_x} \frac{(x_i(t) - x_i^m(t))^2}{\sigma_i^2} dt$$

(6-5)

In that equation, $x_i(t)$ refers to the variable measured for the regular motion pattern, $x_i^m(t)$ is the same variable, but experimentally obtained, and σ_i^2 measures the variability of the variable $x_i(t)$. Each variable is represented with a vector containing as many variables as the number of nodes used in the interpolation. The variability before presented can be defined as follows:

$$\sigma_i^2 = \frac{1}{T} \int_{t_0}^{t_f} (x_i(t) - X_i)^2$$

(6-6)

Where T makes reference to the duration of the period, and X_i is the mean value of the considered variable, calculated in the following way:

$$X_i = \frac{1}{T} \int_{t_0}^{t_f} x_i(t) dt$$

(6-7)

Now, the first cost function used in this research, f_A, can be defined as the next way:

$$f_A = w_E * \frac{E^t}{E_0^t} + w_J * J_{dev} \qquad\qquad \textbf{(6-8)}$$

Where E_0^t consists on a reference value to scale the energy rating, and make it to have the same magnitude order as the deviation from the motion pattern, J_{dev}. It shall be noted that two weight coefficients were added. The first one, w_E, measures the influence of the metabolical cost of transportation, while the second one, w_J, makes the same with the deviation from the standard motion of walking. These two coefficients will be modified during the experiments so as to examine their influence in the optimization parameters problem.

The expression defined right before will be the cost function used in the optimization, although it is not the most accurate, as it ignores the efficiency of the orthosis. In order to bear it, two more objective functions can be described [1], although they will not be used finally.

The first new parameter used will be the root mean square of the power consumption, P_{RMS}. This one measures the efficiency of the actuator in terms of power, and can be calculated as follows:

$$P_{RMS} = \sqrt{\frac{1}{T}\int_{t_0}^{t_f}(T_k * \beta_{34})^2\, dt}$$

$$\textbf{(6-9)}$$

Where T is the duration of the gait cycle, T_k is the power of the actuator in the right leg (only this one was included due to the symmetry of the model) and β_{34} is the angle of the right knee. Now, this term can be added to the first cost function, resulting the following one:

$$f_B = w_E * (\frac{E^t}{E_0^t} + \frac{P_{RMS}}{P_{RMS0}}) + w_J * J_{dev} \qquad\qquad \textbf{(6-10)}$$

Equivalently to the procediment followed before, the root mean square of the power consumption has been divided by a reference value, P_{RMS0}, so as to have the same magnitude order in the two terms of the equation (it shall be remembered that J_{dev}, the deviation from the motion pattern, was obtained by dividing the difference between the standard and the experimental variable, by the variability, σ_i^2).

The third and last cost function which can be described bears the torque of the motor, represented by its root mean square, in an equivalent way as the power consumption:

$$T_{RMS} = \sqrt{\frac{1}{T} \int_{t_0}^{t_f} (T_k)^2 \, dt}$$

Being T the duration of the gait cycle, and T_k the torque of the actuator. Its influence in the cost function is beared the same way as the power consumption:

$$f_C = w_E * (\frac{E^t}{E_0^t} + \frac{T_{RMS}}{T_{RMS0}}) + w_J * J_{dev}$$

The coefficients w_E and w_J have the same function in the three cost functions.

6.4 Constraint expressions

The optimization algorithm must fulfill as much as possible a set of constraints that will be presented in the next paragraphs. Constraints can be either linear or non-linear, and can also be classified according to if they are equations or inequations. As explained before, the fmincon function of Matlab allows to introduce linear and non-linear, equalities and inequalities as constraints.

6.4.1 Bounds

Each design variable has associated an upper and a lower bound, according to biological and physiological reasons. Concerning to generalized coordinates bounding:

6.4.1.1 Generalized coordinates

a) The three first generalized coordinates, which express the HAT motion (x_{11}, z_{11}, and β_{11}) are bounded by taking the mean of the reference motion (for x_{11}, the deviation from the mean motion is also beared), and allowing a bit upper and lower tolerance, proportional to the amplitude of the reference motion.

b) The rest of the generalized coordinates are the belonging to the joints in the hip, the knees and the ankles. Assuming the symmetry of the model, ($\beta_{13} = \beta_{16}$, $\beta_{34} = \beta_{67}$ and $\beta_{45} = \beta_{78}$), there are only three coordinates remaining to bound. Now, the procediment is the same as the described for the three first coordinates, with two exceptions:

b.1) The lower bound for the knees is imposed to be zero, so as to avoid an unnatural knee rotation. Therefore,

$$\beta_{34} > 0 \tag{6-13}$$

b.2) The Klenzak ankle imposes the rotation of the ankle. This mechanical device forbids a positive rotation of this joint, and as it has a limited maximum rotation, it imposes the following bounds:

$$\beta_{45} = \beta_{78} < 0 \tag{6-14}$$

$$\beta_{45} = \beta_{78} > -\frac{\pi}{9} rad \tag{6-15}$$

6.4.1.2 Muscle forces

The forces actuated by muscles are bounded by the following way: their lower bound is zero, as it does not make physical sense to consider a negative force, while their upper bound is calculated according to the next equation:

$$f_{up_i}^m = f_{max_i} * \cos(\alpha_{p_i}) \tag{6-16}$$

Where f_{max_i} and α_{p_i} are the maximum force and the pennation angle of the muscle i. The equation consists on nothing but the projection of the maximum muscle force in the direction of the tendon, according to Hill's model, as it is shown in the Figure 6-3.
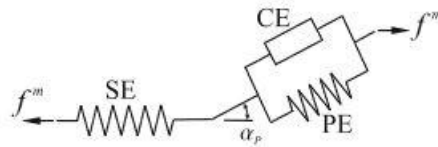
Figure 6-3: Muscle model developed by Hill. Font-Llagunes, García Vallejo and Schliehen [1].

The information for the eight muscles can be found in the Table 6-2, where the first column represents f_{max_i} and the second one, α_{p_i}.

Table 6-2: Maximum forcé and pennation angle for each muscle group taking part in the cycle.

Muscle group	Maximum force, f_{max}(N)	Pennation angle, α_p (°)
ILPSO	821	7.5
RF	663	5
GLU	1705	3
HAMS	1770	7.5
VAS	7403	4.4
GAS	1639	14.3
TA	1528	6.0
SOL	3883	23.6

6.4.1.3 Motor torque

The torque powered by the motor placed in the knee has a maximum value which will be modificated as part of the research, to examine its influence in the parameters optimization. Anyway, as the nodal values for the motor torque are normalized, the only bounds applied to them will consist on the following:

$$T_i < 1 \tag{6-17}$$

$$T_i > -1 \tag{6-18}$$

Being T_i a random nodal value for the motor torque.

6.4.1.4 Phases duration

The lower bounds imposed to these design variables make them to be at least 0.01, while the upper bounds force them not to occupy more than a half of the cycle. Therefore,

$$t_{ph_i} > 0.01 \tag{6-19}$$

$$t_{ph_i} < T/2 \tag{6-20}$$

Being T the whole duration of a cycle. Later, some linear equality constraints referring phases duration will be added.

6.4.1.5 Step lengths

Both step lengths, right and left, are forced to be in the interval [0.1, 1.5]. So,

$$L_R < 0.1 \tag{6-21}$$

$$L_L < 0.1 \tag{6-22}$$

$$L_R > 1.5 \qquad\qquad\qquad \text{(6-23)}$$

$$L_L > 1.5 \qquad\qquad\qquad \text{(6-24)}$$

Equivalently to before, linear equality constraints affecting the step lengths will be added.

6.4.1.6   Klenzak ankle

The last bounds are imposed in two parameters of the flexible Klenzak ankle: its torque and its stiffness. Their minimum value is zero, while their maximum values are 20 and 200, respectively. Expressing them in form of inequalities:

$$T_k > 0 \qquad\qquad\qquad \text{(6-25)}$$

$$T_k < 20 \qquad\qquad\qquad \text{(6-26)}$$

$$K_k > 0 \qquad\qquad\qquad \text{(6-27)}$$

$$K_k < 200 \qquad\qquad\qquad \text{(6-28)}$$

6.4.2   Linear constraints

In this optimization there are not linear inequation constraints. Instead, there is a set of linear equation constraints the algorithm must fulfill. These constraints can be divided into three groups:

6.4.2.1   Velocity constraint

It is the only linear constraint referring to the motion itself. It can be written as follows:

$$\sum_{i=1}^{8} t_{ph_i} - \frac{L_R + L_L}{v} = 0 \qquad\qquad\qquad \text{(6-29)}$$

Where L_R and L_L are the lengths of a right and a left step, respectively, and v the velocity of those steps. This constraint expresses that the duration of both steps must be the same as the duration of the whole cycle. This velocity is always constant.

6.4.2.2 Phases duration

In order to make more symmetrical the motion and to ease its analysis, the eight phases of a cycle can be divided into two equal halves, in a way that the first phase of the first half takes the same time as the first phase of the second half, and so on for the rest of phases. So, these constraints would be written as in the following way:

$$t_{ph_1} - t_{ph_5} = 0 \qquad\qquad \text{(6-30)}$$

$$t_{ph_2} - t_{ph_6} = 0 \qquad\qquad \text{(6-31)}$$

$$t_{ph_3} - t_{ph_7} = 0 \qquad\qquad \text{(6-32)}$$

$$t_{ph_4} - t_{ph_8} = 0 \qquad\qquad \text{(6-33)}$$

6.4.2.3 Symmetrical steps

Another way to simplify the problem will be to consider the same value the length of the right and the left step. This can be written as in the next way:

$$L_R - L_L = 0 \qquad\qquad \text{(6-34)}$$

6.4.3 Non-linear constraints

Now, non-linear constraints will be described. There are no inequality constraints in this optimization problem, so every non-linear constraints will be equations. These can be divided in several groups:

6.4.3.1 Motion constraints

As explained before, the walking gait cycle divides itself into eight phases. Generalized coordinates have different constraints according to the phase they are experimenting. The jacobian matrix of the constraints is also required to calculate other constraints. It is calculated by derivating each constraint by each generalized coordinate.

Assuming the generalized coordinates as the ones described in 4.1., and the parameters presented in 4.2., these constraints can be written in terms of non-linear equations as follows:

1) Phase 1:

$$c_{11} = x_{11} - d_2 \sin(\beta_{11}) - l_6 \sin(\beta_{16} + \beta_{11}) - l_7 \sin(\beta_{16} + \beta_{11} + \beta_{67}) \tag{6-35}$$
$$+ L_{l1} \cos(\beta_{16} + \beta_{11} + \beta_{67} + \beta_{78}) - L_{l3} \sin(\beta_{16} + \beta_{11} + \beta_{67} + \beta_{78}) - x_0$$

$$c_{12} = z_{11} - d_2 \cos(\beta_{11}) - l_6 \cos(\beta_{16} + \beta_{11}) - l_7 \cos(\beta_{16} + \beta_{11} + \beta_{67}) \tag{6-36}$$
$$- L_{l1} \sin(\beta_{16} + \beta_{11} + \beta_{67} + \beta_{78}) - L_{l3} \cos(\beta_{16} + \beta_{11} + \beta_{67} + \beta_{78})$$

$$c_{13} = x_{11} - d_2 \sin(\beta_{11}) - l_3 \sin(\beta_{11} + \beta_{13}) - l_4 \sin(\beta_{11} + \beta_{13} + \beta_{34})$$
$$- L_{r2} \cos(\beta_{11} + \beta_{13} + \beta_{34} + \beta_{45}) \tag{6-37}$$
$$- L_{r3} \sin(\beta_{11} + \beta_{13} + \beta_{34} + \beta_{45}) - x_0 - LR + L_{r1} + L_{r2}$$

$$c_{14} = z_{11} - d_2 \cos(\beta_{11}) - l_3 \cos(\beta_{13} + \beta_{11}) - l_4 \cos(\beta_{11} + \beta_{13} + \beta_{34}) \tag{6-38}$$
$$+ L_{r2} \sin(\beta_{11} + \beta_{13} + \beta_{34} + \beta_{45}) - L_{r3} \cos(\beta_{11} + \beta_{13} + \beta_{34} + \beta_{45})$$

$$c_{15} = \beta_{34} - \beta_{34_{block}} \tag{6-39}$$

$$c_{16} = \beta_{67} - \beta_{67_{block}} \tag{6-40}$$

Being $\beta_{34_{block}}$ and $\beta_{67_{block}}$ the limit values for β_{34} and β_{67}, respectively.

2) Phase 2:

$$c_{21} = x_{11} - d_2 \sin(\beta_{11}) - l_6 \sin(\beta_{16} + \beta_{11}) - l_7 \sin(\beta_{16} + \beta_{11} + \beta_{67}) \tag{6-41}$$
$$+ L_{l1} \cos(\beta_{16} + \beta_{11} + \beta_{67} + \beta_{78}) - L_{l3} \sin(\beta_{16} + \beta_{11} + \beta_{67} + \beta_{78}) - x_0$$

$$c_{22} = z_{11} - d_2 \cos(\beta_{11}) - l_6 \cos(\beta_{16} + \beta_{11}) - l_7 \cos(\beta_{16} + \beta_{11} + \beta_{67}) \tag{6-42}$$
$$- L_{l1} \sin(\beta_{16} + \beta_{11} + \beta_{67} + \beta_{78}) - L_{l3} \cos(\beta_{16} + \beta_{11} + \beta_{67} + \beta_{78})$$

$$c_{23} = x_{11} - d_2 \sin(\beta_{11}) - l_3 \sin(\beta_{11} + \beta_{13}) - l_4 \sin(\beta_{11} + \beta_{13} + \beta_{34}) \tag{6-43}$$
$$- L_{r2} \cos(\beta_{11} + \beta_{13} + \beta_{34} + \beta_{45})$$
$$- L_{r3} \sin(\beta_{11} + \beta_{13} + \beta_{34} + \beta_{45}) - x_0 - LR + L_{r1} + L_{r2}$$

$$c_{24} = z_{11} - d_2 \cos(\beta_{11}) - l_3 \cos(\beta_{13} + \beta_{11}) - l_4 \cos(\beta_{11} + \beta_{13} + \beta_{34})$$
$$+ L_{r2} \sin(\beta_{11} + \beta_{13} + \beta_{34} + \beta_{45}) - L_{r3} \cos(\beta_{11} + \beta_{13} + \beta_{34} + \beta_{45})$$

(6-44)

$$c_{25} = z_{11} - d_2 \cos(\beta_{11}) - l_3 \cos(\beta_{13} + \beta_{11}) - l_4 \cos(\beta_{11} + \beta_{13} + \beta_{34})$$
$$- L_{r1} \sin(\beta_{11} + \beta_{13} + \beta_{34} + \beta_{45}) - L_{r3} \cos(\beta_{11} + \beta_{13} + \beta_{34} + \beta_{45})$$

(6-45)

$$c_{26} = \beta_{34} - \beta_{34_{block}}$$

(6-46)

$$c_{27} = \beta_{67} - \beta_{67_{block}}$$

(6-47)

3) Phase 3:

$$c_{31} = x_{11} - d_2 \sin(\beta_{11}) - l_3 \sin(\beta_{11} + \beta_{13}) - l_4 \sin(\beta_{11} + \beta_{13} + \beta_{34})$$
$$- L_{r2} \cos(\beta_{11} + \beta_{13} + \beta_{34} + \beta_{45})$$
$$- L_{r3} \sin(\beta_{11} + \beta_{13} + \beta_{34} + \beta_{45}) - x_0 - LR + L_{r1} + L_{r2}$$

(6-48)

$$c_{32} = z_{11} - d_2 \cos(\beta_{11}) - l_3 \cos(\beta_{13} + \beta_{11}) - l_4 \cos(\beta_{11} + \beta_{13} + \beta_{34})$$
$$+ L_{r2} \sin(\beta_{11} + \beta_{13} + \beta_{34} + \beta_{45}) - L_{r3} \cos(\beta_{11} + \beta_{13} + \beta_{34} + \beta_{45})$$

(6-49)

$$c_{33} = z_{11} - d_2 \cos(\beta_{11}) - l_3 \cos(\beta_{13} + \beta_{11}) - l_4 \cos(\beta_{11} + \beta_{13} + \beta_{34})$$
$$- L_{r1} \sin(\beta_{11} + \beta_{13} + \beta_{34} + \beta_{45}) - L_{r3} \cos(\beta_{11} + \beta_{13} + \beta_{34} + \beta_{45})$$

(6-50)

$$c_{34} = \beta_{34} - \beta_{34_{block}}$$

(6-51)

4) Phase 4:

$$c_{41} = x_{11} - d_2 \sin(\beta_{11}) - l_3 \sin(\beta_{11} + \beta_{13}) - l_4 \sin(\beta_{11} + \beta_{13} + \beta_{34})$$
$$+ L_{r1} \cos(\beta_{11} + \beta_{13} + \beta_{34} + \beta_{45})$$
$$- L_{r3} \sin(\beta_{11} + \beta_{13} + \beta_{34} + \beta_{45}) - x_0 - LR$$

(6-52)

$$c_{42} = z_{11} - d_2 \cos(\beta_{11}) - l_3 \cos(\beta_{13} + \beta_{11}) - l_4 \cos(\beta_{11} + \beta_{13} + \beta_{34})$$
$$- L_{r1} \sin(\beta_{11} + \beta_{13} + \beta_{34} + \beta_{45}) - L_{r3} \cos(\beta_{11} + \beta_{13} + \beta_{34} + \beta_{45})$$

(6-53)

$$c_{43} = \beta_{34} - \beta_{34_{block}}$$

(6-54)

5) Phase 5:

$$c_{51} = x_{11} - d_2 \sin(\beta_{11}) - l_3 \sin(\beta_{13} + \beta_{11}) - l_4 \sin(\beta_{11} + \beta_{13} + \beta_{34}) \qquad \textbf{(6-55)}$$
$$+ L_{r1} \cos(\beta_{11} + \beta_{13} + \beta_{34} + \beta_{45})$$
$$- L_{r3} \sin(\beta_{11} + \beta_{13} + \beta_{34} + \beta_{45}) - x_0 - LR$$

$$c_{52} = z_{11} - d_2 \cos(\beta_{11}) - l_3 \cos(\beta_{11} + \beta_{13}) - l_4 \cos(\beta_{11} + \beta_{13} + \beta_{34}) \qquad \textbf{(6-56)}$$
$$- L_{r1} \sin(\beta_{11} + \beta_{13} + \beta_{34} + \beta_{45}) - L_{r3} \cos(\beta_{11} + \beta_{13} + \beta_{34} + \beta_{45})$$

$$c_{53} = x_{11} - d_2 \sin(\beta_{11}) - l_6 \sin(\beta_{11} + \beta_{16}) - l_7 \sin(\beta_{11} + \beta_{16} + \beta_{67}) \qquad \textbf{(6-57)}$$
$$- L_{l2} \cos(\beta_{11} + \beta_{16} + \beta_{67} + \beta_{78})$$
$$- L_{l3} \sin(\beta_{11} + \beta_{16} + \beta_{67} + \beta_{78}) - x_0 - LR - LL + L_{l1} + L_{l2}$$

$$c_{54} = z_{11} - d_2 \cos(\beta_{11}) - l_6 \cos(\beta_{11} + \beta_{16}) - l_7 \cos(\beta_{11} + \beta_{16} + \beta_{67}) \qquad \textbf{(6-58)}$$
$$+ L_{l2} \sin(\beta_{11} + \beta_{16} + \beta_{67} + \beta_{78}) - L_{l3} \cos(\beta_{11} + \beta_{16} + \beta_{67} + \beta_{78})$$

$$c_{55} = \beta_{34} - \beta_{34_{block}} \qquad \textbf{(6-59)}$$

$$c_{56} = \beta_{67} - \beta_{67_{block}} \qquad \textbf{(6-60)}$$

6) Phase 6:

$$c_{61} = x_{11} - d_2 \sin(\beta_{11}) - l_3 \sin(\beta_{13} + \beta_{11}) - l_4 \sin(\beta_{11} + \beta_{13} + \beta_{34}) \qquad \textbf{(6-61)}$$
$$+ L_{r1} \cos(\beta_{11} + \beta_{13} + \beta_{34} + \beta_{45})$$
$$- L_{r3} \sin(\beta_{11} + \beta_{13} + \beta_{34} + \beta_{45}) - x_0 - LR$$

$$c_{62} = z_{11} - d_2 \cos(\beta_{11}) - l_3 \cos(\beta_{11} + \beta_{13}) - l_4 \cos(\beta_{11} + \beta_{13} + \beta_{34}) \qquad \textbf{(6-62)}$$
$$- L_{r1} \sin(\beta_{11} + \beta_{13} + \beta_{34} + \beta_{45}) - L_{r3} \cos(\beta_{11} + \beta_{13} + \beta_{34} + \beta_{45})$$

$$c_{63} = x_{11} - d_2 \sin(\beta_{11}) - l_6 \sin(\beta_{11} + \beta_{16}) - l_7 \sin(\beta_{11} + \beta_{16} + \beta_{67}) \qquad \textbf{(6-63)}$$
$$- L_{l2} \cos(\beta_{11} + \beta_{16} + \beta_{67} + \beta_{78})$$
$$- L_{l3} \sin(\beta_{11} + \beta_{16} + \beta_{67} + \beta_{78}) - x_0 - LR - LL + L_{l1} + L_{l2}$$

$$c_{64} = z_{11} - d_2 \cos(\beta_{11}) - l_6 \cos(\beta_{11} + \beta_{16}) - l_7 \cos(\beta_{11} + \beta_{16} + \beta_{67}) \qquad \textbf{(6-64)}$$
$$+ L_{l2} \sin(\beta_{11} + \beta_{16} + \beta_{67} + \beta_{78}) - L_{l3} \cos(\beta_{11} + \beta_{16} + \beta_{67} + \beta_{78})$$

$$c_{65} = z_{11} - d_2\cos(\beta_{11}) - l_6\cos(\beta_{11} + \beta_{16}) - l_7\cos(\beta_{11} + \beta_{16} + \beta_{67})$$
$$- L_{l1}\sin(\beta_{11} + \beta_{16} + \beta_{67} + \beta_{78}) - L_{l3}\cos(\beta_{11} + \beta_{16} + \beta_{67} + \beta_{78})$$

(6-65)

$$c_{66} = \beta_{34} - \beta_{34_{block}}$$

(6-66)

$$c_{67} = \beta_{67} - \beta_{67_{block}}$$

(6-67)

7) Phase 7:

$$c_{71} = x_{11} - d_2\sin(\beta_{11}) - l_6\sin(\beta_{11} + \beta_{16}) - l_7\sin(\beta_{11} + \beta_{16} + \beta_{67})$$
$$- L_{l2}\cos(\beta_{11} + \beta_{16} + \beta_{67} + \beta_{78})$$
$$- L_{l3}\sin(\beta_{11} + \beta_{16} + \beta_{67} + \beta_{78}) - x_0 - LR - LL + L_{l1} + L_{l2}$$

(6-68)

$$c_{72} = z_{11} - d_2\cos(\beta_{11}) - l_6\cos(\beta_{11} + \beta_{16}) - l_7\cos(\beta_{11} + \beta_{16} + \beta_{67})$$
$$+ L_{l2}\sin(\beta_{11} + \beta_{16} + \beta_{67} + \beta_{78}) - L_{l3}\cos(\beta_{11} + \beta_{16} + \beta_{67} + \beta_{78})$$

(6-69)

$$c_{73} = z_{11} - d_2\cos(\beta_{11}) - l_6\cos(\beta_{11} + \beta_{16}) - l_7\cos(\beta_{11} + \beta_{16} + \beta_{67})$$
$$- L_{l1}\sin(\beta_{11} + \beta_{16} + \beta_{67} + \beta_{78}) - L_{l3}\cos(\beta_{11} + \beta_{16} + \beta_{67} + \beta_{78})$$

(6-70)

$$c_{74} = \beta_{67} - \beta_{67_{block}}$$

(6-71)

8) Phase 8:

$$c_{81} = x_{11} - d_2\sin(\beta_{11}) - l_6\sin(\beta_{11} + \beta_{16}) - l_7\sin(\beta_{11} + \beta_{16} + \beta_{67})$$
$$+ L_{l1}\cos(\beta_{11} + \beta_{16} + \beta_{67} + \beta_{78})$$
$$- L_{l3}\sin(\beta_{11} + \beta_{16} + \beta_{67} + \beta_{78}) - x_0 - LR - LL$$

(6-72)

$$c_{82} = z_{11} - d_2\cos(\beta_{11}) - l_6\cos(\beta_{11} + \beta_{16}) - l_7\cos(\beta_{11} + \beta_{16} + \beta_{67})$$
$$- L_{l1}\sin(\beta_{11} + \beta_{16} + \beta_{67} + \beta_{78}) - L_{l3}\cos(\beta_{11} + \beta_{16} + \beta_{67} + \beta_{78})$$

(6-73)

$$c_{83} = \beta_{67} - \beta_{67_{block}}$$

(6-74)

By computational reasons, it is impossible to fulfill with a 100% accuracy the constraints right presented, so a certain tolerance, $\varepsilon_k = 0.005\,m$, must be allowed. Denoting $c_{ph,j}(X), ph = 1, 2, \dots, 8,\ j = 1, 2, \dots, N_{cp}$ as the complete set of kinematics equations, the two following constraints are defined:

$$c_{ph,j}(X) \le \varepsilon_k \tag{6-75}$$

$$-\varepsilon_k \le c_{ph,j}(X) \tag{6-76}$$

They can be better expressed as:

$$\frac{-c_{ph,j}(X)}{\varepsilon_k} - 1 \le 0 \tag{6-77}$$

$$\frac{c_{ph,j}(X)}{\varepsilon_k} - 1 \le 0 \tag{6-78}$$

There by, kinematic constraints are imposed on the eight phases of the walking cycle, for every control points.

6.4.3.2   Excitation constraints

Neural excitations will be normalized, so as they have to be in the interval [0, 1]. However, this criterion will only be acceptable for healthy muscles. Damage in muscles will be beared by imposing a limit to the neural excitation they receive. Therefore, the parameter u_{lim} can be defined, so as $u_{lim}<1$. Right below the Table 6-3 shows the value of u_{lim} for each muscle present in the walking cycle.

Table 6-3: Limit neural excitation for each muscle group

Muscle group	u_{lim}
ILPSO	1
RF	0.6
GLU	1
HAMS	0.6
VAS	0.6
GAS	0.4
TA	0.4
SOL	0.4

Now the muscle forces are ensured to be consistent with the activation and contraction dynamics presented in section 5.

6.4.3.3   Clearance constraints

These constraints are imposed so as to maintain the feet above the ground in every moment, and avoid it to penetrate it. Therefore, the vertical coordinate for the toe and the heel in both feet must be zero or positive. As it is very difficult to fulfill the constraint with a complete accuracy, a certain tolerance will be allowed, so as the coordinates right presented can penetrate the ground until a depth, which is the same as the defined tolerance. This tolerance will be:

$$Tol = -2.5E - 5 \qquad \textbf{(6-79)}$$

The only points in the musculoskeletal system where the contact with the ground is studied are the toe and the heel in both feet. Therefore, the clearance constraints will only affect them. Moreover, as the conditions of contact change for each phase, there will be different constraints for each phase. First of all, the vertical coordinate for the respective toes and heels, expressed in function of the generalized coordinates and the parameters before described, may be presented:

a) Left heel

$$z_{11} = d_2 \cos(\beta_{11}) + l_6 \cos(\beta_{11} + \beta_{16}) + l_7 \cos(\beta_{11} + \beta_{16} + \beta_{67}) \qquad \textbf{(6-80)}$$
$$- L_{l2} \sin(\beta_{11} + \beta_{16} + \beta_{67} + \beta_{78}) + L_{l3} \cos(\beta_{11} + \beta_{16} + \beta_{67} + \beta_{78})$$

b) Left toe

$$z_{11} = d_2 \cos(\beta_{11}) + l_6 \cos(\beta_{11} + \beta_{16}) + l_7 \cos(\beta_{11} + \beta_{16} + \beta_{67}) \qquad \textbf{(6-81)}$$
$$+ L_{l1} \sin(\beta_{11} + \beta_{16} + \beta_{67} + \beta_{78}) + L_{l3} \cos(\beta_{11} + \beta_{16} + \beta_{67} + \beta_{78})$$

c) Right heel

$$z_{11} = d_2 \cos(\beta_{11}) + l_3 \cos(\beta_{11} + \beta_{13}) + l_4 \cos(\beta_{11} + \beta_{13} + \beta_{34}) \qquad \textbf{(6-82)}$$
$$- L_{r2} \sin(\beta_{11} + \beta_{13} + \beta_{34} + \beta_{45}) + L_{r3} \cos(\beta_{11} + \beta_{13} + \beta_{34} + \beta_{45})$$

d) Right toe

$$z_{11} = d_2 \cos(\beta_{11}) + l_3 \cos(\beta_{11} + \beta_{13}) + l_4 \cos(\beta_{11} + \beta_{13} + \beta_{34})$$
$$+ L_{r1} \sin(\beta_{11} + \beta_{13} + \beta_{34} + \beta_{45}) + L_{r3} \cos(\beta_{11} + \beta_{13} + \beta_{34} + \beta_{45}) \tag{6-83}$$

The clearance constraints required for each phase are the ones shown in the Table 6-4 (YES if constraint required):

Table 6-4: Ground constraints activated in each phase

Phase	Left heel	Left toe	Right heel	Right toe
1	YES			YES
2	YES			
3	YES	YES		
4	YES	YES	YES	
5		YES	YES	
6			YES	
7			YES	YES
8	YES		YES	YES

6.4.3.4   Equations of motion

Analog to kinematic constraints, equations of motion cannot be fulfilled with 100% accuracy, so a small tolerance must be allowed. May the system defined in Section 2:

$$M(q)\ddot{q} + k(q, \dot{q}) = q_r(q, \dot{q}) + BAf^m + q_{act} + q_{ank}(y) + C_{ph}^T \lambda_{ph} \tag{6-84}$$

Lagrange multipliers, λ_{ph}, which represent the ground forces in the contact feet-ground, can be easily calculated the next way:

$$\lambda_{ph} = (C_{ph}^T)^+ (M(q)\ddot{q} + k(q, \dot{q}) - q_r(q, \dot{q}) - BAf^m - q_{act} - q_{ank}(y)) \tag{6-85}$$

Now, assuming the definition of torques at the joints as:

$$\tau^m = Af^m \tag{6-86}$$

And taking into account that a small error must be allowed, and so on small residual torques make their

appearance, these ones can be evaluated as follows:

$$\tau_{res}^m = (B)^{-1}(M(q)\ddot{q} + k(q, \dot{q}) - q_r(q, \dot{q}) - q_{act} - q_{ank}(y))$$

<div align="right">(6-87)</div>

The error at calculating torques at joints is calculated the next way:

$$e_{mj} = \tau^m - \tau_{res}^m$$

<div align="right">(6-88)</div>

So, defining the allowed tolerance as $\varepsilon_m = 2 \ Nm$, the two following constraints are defined:

$$e_{i,j}(X) \le \varepsilon_m$$

<div align="right">(6-89)</div>

$$-\varepsilon_m \le e_{i,j}(X)$$

<div align="right">(6-90)</div>

Analog to kinematic constraints, these ones can be easier to understand if they are written as follows:

$$\frac{-e_{i,j}(X)}{\varepsilon_m} - 1 \le 0$$

<div align="right">(6-91)</div>

$$\frac{e_{i,j}(X)}{\varepsilon_m} - 1 \le 0$$

<div align="right">(6-92)</div>

6.4.3.5 Ground forces

Foot sliding must be avoided as much as possible, so another set of constraints is introduced so as to make tangent forces consistent with Coulomb's friction model. Moreover, to avoid two-sides constraints in the foot-ground contact, normal reaction forces are made to be positive. Thereby, denoting **wgt** as the total weight of the system, and **v** as the friction coefficient, the next set of constraints is defined:

$$\frac{-F_z}{wgt} \leq 0 \qquad\qquad (6\text{-}93)$$

$$\frac{F_{tan}}{v*wgt} \leq 0 \qquad\qquad (6\text{-}94)$$

6.4.3.6 Motor torque

When the legs are fully extended ($\beta_{34} = 0$, $\beta_{67} = 0$) the motor is not actuating. That circumstance can be written the next way:

$$T_{kr} = 0 \text{ if } \beta_{34} = 0 \qquad\qquad (6\text{-}95)$$

$$T_{kl} = 0 \text{ if } \beta_{67} = 0 \qquad\qquad (6\text{-}96)$$

Being T_{kr} and T_{kl} the generated torques at the right and left legs, respectively.

6.4.3.7 Physiological constraints

By last, another set of constraints is included, to get a more optimal convergence in the optimization problem. These constraints include bounds to the maximum knee flexion measured during the oscillation phase, and the maximum hip extension during the stance phase [1]. Further information can be consulted in Ackerman and Gross [9].

6.5 MATLAB Script

The MATLAB script used to perform optimizations includes several algorithms, variables and functions that will be furtherly explained in the next paragraphs. The whole main MATLAB algorithm, which serves as the basis for the optimization and is exceuted to perform them, was fully programmed by García Vallejo [23]. First of all, some global variables may be defined, so as they can be called for any function in the script. These global variables can be classified as García Vallejo explained in the MATLAB algorithm he coded [23]:

a) Specific features describing the musculoskeletal model and the optimization algorithm: number of coordinates (both for the whole (NC) and the symmetrical model (NCS), number of muscles (both for the whole (NM) and the symmetrical model (NMS)), number of actuators (NAS), number of nodes (NN) and number of control points (NCP). All of them are scalars.

b) Variables describing the reference pattern: time instants vector (`Tex`) and its length (`NTex`), generalized coordinates (`Qex2D`) and ground reaction forces (`GRFex2D`), both of them being vectors.

c) Variables defining useful statistic values, to compare the obtained results to the reference patterns: the mean longitudinal motion vector (`xIlm`), and the deviation appearing in the coordinates and the ground forces from the pattern, expressed as the variance vector (`Sig_Q` and `Sig_GRF`, respectively).

d) Tolerances allowed for motion equations constraints (`eps_m`) and kinematic constraints (`eps_k`), both are scalars.

e) Typical characteristics of the model, such like the Poisson friction coefficient (it is an scalar, `nu`), the matrix containing muscle properties (`propM`), and the vector including the musculoskeletal body and orthosis features (`sys`). Also, the maximum torque the motor can generate (`KneeTorq`) and the two mechanical devices describing the Klenzak ankle in the orthosis (the maximum moment, `Tank0`, and the stiffness, `Kank`) may be included here.

f) Variables needed for the interpolation, `Aex` and `ANN`.

g) Upper bounds for knee rotation angles (`bet34block` and `bet67block`).

Once every needed global variables are defined, they start to be filled out. The general procediment in this research consists on taking data from the experiments made by Ackermann and Gross [9], use them as the reference pattern, and build a reference solution parting from this pattern. Every optimizations are made from this reference solution, what makes way faster the optimization process.

So, after choosing one of the multiple files containing information about subjects appearing in Ackermann [9], the selected file is loaded using the function extract_alldata, being the information reordered conveniently using `start_at_HSr2`. As the Ackermann experiments deals with 3D models, and the research consists on studying a bidimensional, only a few parameters from the system are needed. Further details about generalized bidimensional coordinates can be found in Section 2. Also, the velocities and accelerations are obtained, saved in the vectors `QEx_2D_p` and `QEx_2D_pp`, respectively. The deviation from pattern is calculated by calling the function deviation, which contains `Tex`, `QEx2D` and `GRFex2D` as arguments.

The initial conditions of the contact points are defined by a set of functions (`FOl_A_r` and `FOl_B_r` for the left foot, `FOr_A_r` and `FOr_B_r` for the right one) and then, so on with the linear constraints (see more information in Section 6). Concerning bounds, defined as the upper and lower values design variables can reach, they are set into two vectors: `ub` for upper bounds, and `lb` for the lower ones, while the initial estimation for design variables are defined in the vector `X0`.

It shall be noted this initial estimation will only be used once in this research: to build a reference solution which will serve as the starting point for the rest of the optimizations. This initial optimization takes considerably more time than the following, so parting from a reference solution will be useful to decrease the computing time.

Once every vectors needed for the optimization algorithm have been defined, they may be implemented in the function fmincon. This subroutine presents the following argument:

```
X = fmincon(@costfunSC,X0,A,b,Aeq,beq,lb,ub,@nolinconSC_1xb,options);
```

Where `@costfunSC` is the objective function, further described in Section 5, `X0` is the initial estimation, `A` and `b` form the linear inequality constraints, `Aeq` and `beq` form the linear equality constraints, `lb` and `ub` refers to the lower and upper bounds, respectively, `@nolinconSC_1xb` is a subroutine which returns the non-linear constraints, and `options` is another subroutine calling a vector containing every additional information about the algorithm (more information in Section 6). The `fmincon` routine returns the design variables vector, `X`.

After defining the cost function, the initial estimation and every needed constraints, the optimization problem is programmed in MATLAB using an Active Set method. The Active Set [17] distinguishes active from inactive constraints, considering active those constraints defined as $f_i(x) = 0$, and inactive the constraints written as $f_i(x) \geq 0$. It shall be noted that equality constraints are always active. This method calculates what constraints will influde in the final optimization.

Algorithm argument in MATLAB includes the following options, collected in the Table 6-5:

Table 6-5: Activated options during the optimization

Options	Description
Diagnostics	It gives information about the cost function. It is active.
Algorithm	It indicates the used algorithm, Active Set in this case.
Display	It displays each iteration found in the problem.
TolCon	The algorithm will stop when the constraints reach this value, 0.001.
TolFun	Analog to the function, 0.001.
TolX	Analog to the design variables vector, 0.0001
MaxFunEvals	Maximum number of function evaluations during the optimization, 1e6
DiffMaxChange	Maximum change allowed for finite difference gradients, 1e-7
MaxIter	Maximum number of iterations allowed, 800.

When the screen displays the solution, the next step consists on saving it in a file, so as it can be opened whatever the user wants to obtain the graphics representing design variables. To display these results, a MATLAB algorithm was coded, parting from the one made by García Vallejo. This file, named as `analisis_4_variables`, asks the user for the name of three files:

a) The first file may be the reference solution, which will be used as a pattern.

b) The second, third and fourth file are those which will be compared and evaluated.

It shall be noted not every optimizations will require to compare four magnitudes; only those affecting the inertia. For example, when the changed parameters are the weight coefficients of the cost function, the function used to compare results is `analisis_2_variables`, which results to be analog to the first one, but it only ask for two files, instead of four.

This file works the next way: it gets the design variable vector, saved in the selected file, X, and builds the graphics parting from it. It reconstructs the time histories referring the generalized coordinates by interpolating the respectives components from X which refer to these coordinates, using the functions `spl5rv` and `spl5rv_eval`. They consist on fifth-order-splines. Next, it makes the same with muscle forces and the actuator. In the muscle forces case, each muscle design variable is multiplied by its correspondent column from the muscle properties matrix `propM`, just before interpolation. Analogously, actuator variables are multiplied by the scalar `KneeTorq`, already defined before. On the other hand, feet geometrical parameters are not modified, while Klenzak parameters are multiplied by `Tank0` and `Kank`, respectively. This code was also made by García Vallejo, and it was written as follows:

```
% Trunk coordinates
kk=1;   qn = spl5rV(tn(1:NNM),[0,0,X((kk-1)*(NNM-4)+1:kk*(NNM-4)),0,0],tn,5);
YPV=[YPV,qn(3:NN-2)];
kk=2;   qn = spl5rV(tn(1:NNM),[0,0,X((kk-1)*(NNM-4)+1:kk*(NNM-4)),0,0],tn,5);
YPV=[YPV,qn(3:NN-2)];
kk=3;   qn = spl5rV(tn(1:NNM),[0,0,X((kk-1)*(NNM-4)+1:kk*(NNM-4)),0,0],tn,5);
YPV=[YPV,qn(3:NN-2)];

% Leg coordinates
id = 3*(NNM-4);
YS=[YPV,X(id + 1:id + (NCS-3)*(NN-4))];

% Muscle forces
id = 3*(NNM-4)+(NCS-3)*(NN-4);
F = X(id+1 : id+NMS*(NN-4));
for KMSC=1:NMS
    kmsc=KMSC;
    F((KMSC-1)*(NN-4)+1:KMSC*(NN-4))=F((KMSC-1)*(NN-4)+1:KMSC*(NN-
4))*propM(kmsc,1);
    qn=spl5rV_eval(tn,[0,0,F((KMSC-1)*(NN-4)+1:KMSC*(NN-4)),0,0],tdf,5);
    F=[F,qn(3:NN-2)];
end

% Actuator
id = 3*(NNM-4)+(NCS-3)*(NN-4) + NMS*(NN-4);
Tmotr = X(id+1 : id+NAS*(NN-4))*KneeTorq;
wa = spl5rV_eval(tn,[0,0,Tmotr,0,0],tdf,5);
```

```
Tmotl = wa(3:NN-2);


% Step sizes
id = 3*(NNM-4)+(NCS-3)*(NN-4) + NMS*(NN-4) + NAS*(NN-4) + 8;
LR = X(id+1);
LL = X(id+2);


% Ankle parameters
id = 3*(NNM-4)+(NCS-3)*(NN-4) + NMS*(NN-4) + NAS*(NN-4) + 8 + 2;
TorqAnk0 = X(id+1)*Tank0
RigiAnk0 = X(id+2)*Kank


% Fix the value of the parameters from the optimization
sys.userVar.data.LR = LR;
sys.userVar.data.LL = LL;


% Make symmetrical motion
Y = YS;
kk=4;   qn = spl5rV_eval(tn,[0,0,YS((kk-1)*(NN-4)+1:kk*(NN-4)),0,0],tdf,5);
Y=[Y,qn(3:NN-2)];
kk=5;   qn = spl5rV_eval(tn,[0,0,YS((kk-1)*(NN-4)+1:kk*(NN-4)),0,0],tdf,5);
Y=[Y,qn(3:NN-2)];
kk=6;   qn = spl5rV_eval(tn,[0,0,YS((kk-1)*(NN-4)+1:kk*(NN-4)),0,0],tdf,5);
Y=[Y,qn(3:NN-2)];
```

Next, values of generalized coordinates are calculated at control points, so as to represent them on the plots. Newly, the spline function spl5rv_eval is used.

```
% Values of the generalized coordinates (measured and simulated) at control
points
QGex = zeros(ncp,NC);


QG = zeros(ncp,NC);
QGp = zeros(ncp,NC);
QGpp = zeros(ncp,NC);


for KGC=1:NC
    if KGC==1
        qcp = spl5rV_eval(Tex,Qex2D(:,KGC)-xI1m(1)*Tex'-xI1m(2),tcp,6);
        QGex(:,KGC) = qcp'+xI1m(1)*tcp'+xI1m(2);
    else
        qcp = spl5rV_eval(Tex,Qex2D(:,KGC),tcp,6);
        QGex(:,KGC) = qcp';
    end
    q = Y((KGC-1)*(NN-4)+1:KGC*(NN-4));
    q = [0,0,q,0,0];
    [qcp,qcp_p,qcp_pp] = spl5rV_eval(tn,q,tcp,5);
    QG(:,KGC)=qcp';
    QGp(:,KGC)=qcp_p';
    QGpp(:,KGC)=qcp_pp';
end
```

Next, the function Qankle obtains the torque generated in the ankles, evaluated at the control points. Otherwise, the generalized coordinates and their first derivative are corrected by adding the mean motion, so what to make the first generalized coordinate non-periodical.

```
% Cálculo de los pares que hace la rodilla y los tobillos
Tak = zeros(ncp,2);
```

```
for KCP = 1:ncp
    Qank = Qankle(QG(KCP,:),TorqAnk0,RigiAnk0);
    Tak(KCP,1) = Qank(6);
    Tak(KCP,2) = Qank(9);
end


% Mean motion must be added
QG(:,1) = QG(:,1)+(xI1m(1)*tcp+xI1m(2))';
QGp(:,1) = QGp(:,1)+xI1m(1);
```

Then, García Vallejo calculates the metabolical expenditure based on the procediment described by Umberguer et al. [19]. This procedure is further detailed in Section 5, including their theoretical suppositions and equations. In this part of the algorithm, muscle forces are calculated at the control points using the same spline function as before, `spl5rv_eval`. The subroutine `tau_m` obtains the moment values at control points, while the function `mkinen` makes the same with muscle lengths, velocities and accelerations.

```
% Calculation of the Energy expendidure according to Umberguer et al. [115]

E = zeros(1,ncp);
Em = zeros(1,ncp);
TAU = zeros(ncp,NC);
U = zeros(ncp*NM,1);
A = zeros(ncp*NM,1);
for KMSC=1:NM

    mforce = F((KMSC-1)*(NN-4)+1:KMSC*(NN-4));
    mforce = [0,0,mforce,0,0];                % Forces at time nodes
    [fm,fmp,fmpp]=spl5rV_eval(tn,mforce,tcp,5);  % Now we have the muscle
force at control points

    TAU = TAU+tau_m(KMSC,ncp,fm);

    [Lm,Vm,Vmp] = mkinen(QG,QGp,QGpp,KMSC);       % Calculates the lengths,
velocities and accelerations of the muscle at control points
```

Then, the energy rate is calculated with the function `energy`, while the subroutine `neural2` is used to obtain the muscle activation and the neural excitation.

```
    Ep = energy(fm,fmp,fmpp,Lm,Vm,Vmp,KMSC);      % Energy rate can be
calculated for each muscle from the muscle forces, lengths... there is no
need for having visible am and um here

        [U(ncp*(KMSC-1)+1:ncp*KMSC,1),A(ncp*(KMSC-
1)+1:ncp*KMSC,1)]=neural2(fm,fmp,fmpp,Lm,Vm,Vmp,KMSC); % Neural excitations
are needed here to stablish bounds on them
```

By last, as `Ep` makes reference to a rate, it must be multiplied by a time increment so as to obtain the real energetic value, following this equation:

51

```
    Em(1)=0;
    for kk=2:ncp
        Em(kk)=Em(kk-1)+(Ep(kk-1)+Ep(kk))*(tcp(kk)-tcp(kk-1))/2;
    end
    E=E+Em;
end
```

The motor torque and ground reaction forces are calculated at control points, using a specific subroutine, `GRforces`, in the second case:

```
% Motor torque at control points
Tmcpr = spl5rV_eval(tn,[0,0,Tmotr,0,0],tcp,5);
Tmcpl = spl5rV_eval(tn,[0,0,Tmotr,0,0],tn(NNM)+tcp,5);

% Calculating reaction forces
GRF = GRforces(QG,QGp,QGpp,tcp,TAU,jPH,Tmcpr,Tmcpl,TorqAnk0,RigiAnk0);
```

The deviation from pattern is calculated following the equations in Font-Llagunes, García Vallejo and Schliehen [1], further explained in Section 6. Finally, the cost function `f` is also obtained at its optimal value.

```
Jp=zeros(1,ncp);
for KGC=1:NC
    Jp=Jp+((QG(:,KGC)'-QGex(:,KGC)')/Sig_Q(KGC)).^2;   % Ahora se está
utilizando la desviación media con respecto a la media
end

Fex=zeros(ncp,1);
for KL=1:2
    for KGR=1:2
        Fex=spl5rV_eval(Tex,GRFex2D(:,2*(KL-1)+KGR),tcp,5);
        Jp=Jp+((GRF(:,2*(KL-1)+KGR)'-Fex)/Sig_GRF(2*(KL-1)+KGR)).^2;     %
Ahora se usa la desviación media con respecto a la media
    end
end

J=zeros(1,ncp);
for kk=2:ncp
    J(kk)=J(kk-1)+(Jp(kk-1)+Jp(kk))*(tcp(kk)-tcp(kk-1))/2;
end

% Total cost function using weights

w1=1;
w2=1;

f=(w1/100)*(E(ncp)/(LR+LL))+w2*J(ncp);
```

The code explained above has been repeated three times, to represent the reference motion and the other two which must be compared to the reference. Now, it is the moment to represent them in graphics. For that, the reference motion is represented with blue lines, while the first increment above the reference appears represented with red lines, and the second one with green lines. The original code by García Vallejo only included two magnitudes to compare with the healthy individuals; this one has been modified to represent the variables right described.

```
plot(tcpref/tcpref(ncpref),GRFref(:,1),'b',tcp/tcp(ncp),GRF(:,1),'r',tcpref1/
tcpref1(ncpref1),GRFref1(:,1),'g');
title('Right leg tangent reaction
force','FontSize',fontsize,'FontName',fontname);
xlabel('Normalized time','FontSize',fontsize,'FontName',fontname);
ylabel('Force (N)','FontSize',fontsize,'FontName',fontname)
grid on;hold on;
```

This small example serves to illustrate the procediment to plot results.

By last, after each optimization, a Table collects every numerical results so as to make a quantitative analysis of the studied parameter. For that, an algorithm named cuantitativo has been made. It must be called right after complete the optimization, and it calculates the maximum amplitude for every design variables, for the first and the last increment imposed in the optimization. Then, it calculates the relative variation of the amplitude between the two set of variables. It has been coded as follows:

```
col_2=zeros(27,1);
col_3=zeros(27,1);
col_4=zeros(27,1);

for i=1:9
    col_2(i)=max(QG(:,i))-min(QG(:,i));
    col_3(i)=max(QGref1(:,i))-min(QGref1(:,i));
    col_4(i)=100*abs(col_3(i)-col_2(i))/col_2(i);
end

for i=1:4
    col_2(i+9)=max(GRF(:,i))-min(GRF(:,i));
    col_3(i+9)=max(GRFref1(:,i))-min(GRFref1(:,i));
    col_4(i+9)=100*abs(col_3(i+9)-col_2(i+9))/col_2(i+9);
end

    col_2(14)=max(Tmcpr)-min(Tmcpr);
    col_3(14)=max(Tmcprref1)-min(Tmcprref1);
    col_4(14)=100*abs(col_3(14)-col_2(14))/col_2(14);

    col_2(15)=max(Tmcpl)-min(Tmcpl);
    col_3(15)=max(Tmcplref1)-min(Tmcplref1);
    col_4(15)=100*abs(col_3(15)-col_2(15))/col_2(15);

for i=1:2
    col_2(i+15)=max(Tak(:,i))-min(Tak(:,i));
    col_3(i+15)=max(Takref1(:,i))-min(Takref1(:,i));
    col_4(i+15)=100*abs(col_3(i+15)-col_2(i+15))/col_2(i+15);
end

for i=1:6
    col_2(i+17)=max(TAU(:,i+3))-min(TAU(:,i+3));
    col_3(i+17)=max(TAUref1(:,i+3))-min(TAUref1(:,i+3));
```

```
        col_4(i+17)=100*abs(col_3(i+17)-col_2(i+17))/col_2(i+17);
end

    col_2(24)=max(TAU(:,5)+Tmcpr')-min(TAU(:,5)+Tmcpr');
    col_3(24)=max(TAUref1(:,5)+Tmcprref1')-min(TAUref1(:,5)+Tmcprref1');
    col_4(24)=100*abs(col_3(24)-col_2(24))/col_2(24);

    col_2(25)=max(TAU(:,8)+Tmcpl')-min(TAU(:,8)+Tmcpl');
    col_3(25)=max(TAUref1(:,8)+Tmcplref1')-min(TAUref1(:,8)+Tmcplref1');
    col_4(25)=100*abs(col_3(25)-col_2(25))/col_2(25);

    col_2(26)=max(TAU(:,6)+Tak(:,1))-min(TAU(:,6)+Tak(:,1));
    col_3(26)=max(TAUref1(:,6)+Tak(:,1))-min(TAUref1(:,6)+Tak(:,1));
    col_4(26)=100*abs(col_3(26)-col_2(26))/col_2(26);

    col_2(27)=max(TAU(:,9)+Tak(:,2))-min(TAU(:,9)+Tak(:,2));
    col_3(27)=max(TAUref1(:,9)+Tak(:,2))-min(TAUref1(:,9)+Tak(:,2));
    col_4(27)=100*abs(col_3(27)-col_2(27))/col_2(27);
```

7 OPTIMIZATION PARAMETERS

As explained before, multiple parameters have been modified so as to examine their influence in the cost function. These parameters include:

a) Mass parameters of the orthesis (and their influence in the moments of inertia)
b) Geometrical parameters (and its influence in the moments of inertia)
c) Mass and geometrical parameters combined (and their influence in the moments of inertia)
d) Weight coefficients of the cost function
e) Maximum torque of the orthesis
f) Ankle parameters: torque and stiffness

Each of the points presented above correspond to a phase in the optimization. Modification of the parameters has been made by taking the reference values and increasing them progressively, in order to obtain reliable results which display the correct evolution of the cost function, the design variables and the rest of ítems studied in this research.

7.1   Geometrical parameters of the orthesis

In a first aproximation, some geometrical values were modified, including the lengths of the shank, the thigh and the feet, and the distance between the joints and the center of gravity of each element. The changes in values were imposed to be symetrical, so as the left parameters to be the same as the right ones. Given that the studied model is two-dimensional, no width parameters were altered.

The alteration of pelvis-trunk parameters was not finally included in this research, due to the lack of convergence in the cost function when that modification was implemented.

Small changes were firstly imposed to these parameters, starting with a variation of 1% in every values with respect to the reference ones. The same procidiment was taken by increasing this change to 2, 5 and 10% finally, considering the last one an enough increasement to obtain a reliable result.

As it is known, the inertia of an element with respect to an axis is proportional to the square of the length of that axis, so the inertia has been modified by multiplying the reference value by the square of the variation imposed to the length.

7.2   Mass

The second influencer factor modificated was the mass. The total mass includes the mass of the pelvis trunk, the thighs, the shanks and the feet. The procidiment was equivalent to the one followed for the geometrical modifications, so that the mass might be the same one for the right and the left side of the model. Also, 1% variations were firstly imposed, following with 2, 5 and 10%, to obtain a notable result.

Newly, the pelvis-trunk system was not affected by the changes, as a minimum variation in its parameters implies a lack of convergence in the cost function.

In order to consider the gravitatory effect of mass, and equivalently done before with lengths, the inertia values were also increased the same quantity as the mass values, as mass is proportional to the inertia.

7.3 Mass and geometrical parameters combined

After modifying the mass and the lengths, both types of parameters were considered in the third phase. Every changes introduced before were included together in this section.

As the inertia is proportional to the mass and the square of the length, it was multiplied by the cube of the variation introduced (volver a explicar lo de la inercia). Increasements of 1, 2, 5 and 10% were imposed over the reference value.

Evaluating the effect of the variation of the combined mass and geometrical parameters is more senseful and adjusted to reality, than measuring their effects separately, as it does not imply a change in the density of the material of the orthosis. Thereby, results obtained by this procediment will be considered very important for final conclusions.

7.4 Weight coefficients of the cost function

As described before, the cost function contains two coefficients, w_E and w_J, which measure the influence of the metabolical expenditure and the deviation from normal walking patterns, respectively. These coefficients can be altered so as to give more importance to the expenditure or the deviation.

To increase the first coefficient, w_E, means that the optimization algorithm will focus on reduce the energy expenditure while looking for the most optimal solution, rather than the aestethical appearance of the movement, while incrementing the second coefficient, w_J, will have the opposite effect. Later, when results are obtained, it will be analyzed if it is worth taking into account only one coefficient or both of them.

The reference values to both coefficients are $w_E = 1$ and $w_J = 1$. Increasements will consists on impose values of 1.5 and 3 to the coefficients by separately, and see how they affect to the design parameters and, especially, the metabolical expenditure and the deviation from the pattern.

7.5 Maximum orthosis torque

The fifth phase in the optimization will consist on incrementing the maximum torque the motor sited in the orthosis can generate. Therefore, the torque range of the orthosis is extended to see if this change is costworthy in terms of efficiency. The change will consist on implementing 25 and 100% increments over the reference maximum torque, stipulated in 20 Nm.

7.6 Ankle parameters: torque and stiffness

By last, the sixth and last phase in the optimization will face the study of the Klenzak artificial ankle, by modifying its two main mechanical characteristics: the generated torque and the stiffness. The procedure

is similar as other used in previous phases in the optimization: the values are multiplied by 1.05 and 1.1, by separately. The respective reference values for the torque and stiffness are 17.156 Nm and 293.885 N/m.

The next page shows a framework (Figure 7-1) summarizing the optimizations performed in this research, ordered sequentially. There are 23 optimizations in total.
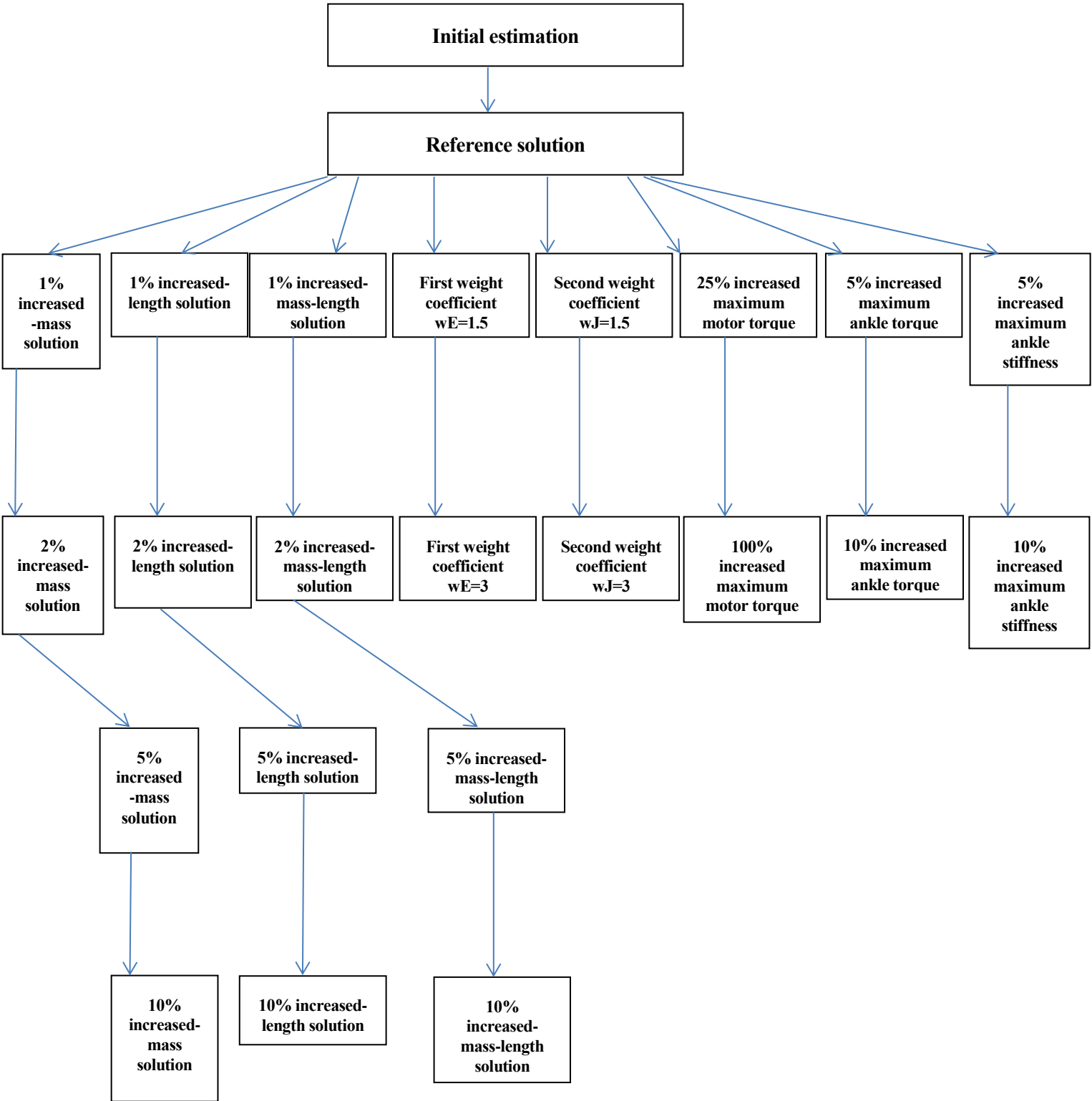
Figure 7-1: Flow diagram representing every phases in the optimization

8 RESULTS

After having presented every theoretical fundamentals required for this research, the optimization problem including the cost function, the bounds and the constraints, and the parameters subject to changes so as to study their influence in the cost function, it is the moment to reveal the results obtained.

As explained before, parameters were subject to small increasements from their reference values, so as to obtain reliable results showing the evolution of the metabolical cost and the design variables. For parameters affecting inertia, these increasements started with a 1% over the reference value, and followed with a 2, 5 and a 10%. In the results, the complete evolution, including these four increasements, will only be shown when the influence of the first parameter studied, the mass, is being analyzed. For the rest of parameters, the comparison will only include the reference and the 10% value. The parameters which do not affect inertia were changed the way explained in the previous Section. The initial reference values were taken from the experiments made in the laboratory with healthy individuals.

On the other hand, the optimization problem has been performed adopting 25 nodes in the interpolation. This number has been selected so as to get reliable results in a reasonable computing time. A solution obtained with 29 nodes during the analysis of the influence of mass will be presented to, and compared with the one obtained with 25 nodes. The 29 nodes solution is more accurate, but increases too much the computing time.

8.1 Reference values

Before starting to study the influence of any parameter, it was useful to build a reference solution, so as not to need to use the initial estimation from the laboratory to perform the optimization algorithm. If the initial estimation is used, the algorithm converges to a feasible solution, but the computing time increases too much, slowing strongly the process down.

Actuating this way, it was only necessary to use the initial estimation to obtain the reference solution; any variation of any parameter could be done from the reference, with the only condition to have the same number of nodes. If a variation of any parameter with a different number of nodes wanted to be studied, another reference solution might be used.

Now, the reference properties of the orthesis are shown in the next table (Figure 8-1).

Parameter	Definition	Value
m_T	Mass of the thigh bars	0.20 kg
I_{G_T}	Inertia moment of the thigh bars about G_T	1.53×10^{-3} kg m^2
l_{KG_T}	Distance from K to G_T	0.13 m
m_K	Mass of the motor, locking system and knee joint (point mass)	1.11 kg
m_S	Mass of the shank bars	0.32 kg
I_{G_S}	Inertia moment of the shank bars about G_S	4.76×10^{-3} kg m^2
l_{AG_S}	Distance from A to G_S	0.17 m
m_A	Mass of the encoder at the ankle (point mass)	0.06 kg
m_F	Mass of the foot support	0.10 kg
I_{G_F}	Inertia moment of the foot support about G_F	1.12×10^{-4} kg m^2
l_{AG_F}	Distance from A to G_F (vertical)	0.07 m
r_{AG_F}	Distance from A to G_F (horizontal)	0.04 m

Figure 8-1: Mass, geometry and inertial orthosis characteristics. Font-Llagunes, García Vallejo and Schliehen [1].

Next, the parameters to list are the characteristical of the human body wearing the orthesis (Table 8-1). These ones remain unchangeable during the whole research.

Table 8-1: Mass, geometry and inertial human subject characteristics

Parameter	Value
Mass of the HAT	44 kg
Inertia of the HAT	1.9178 kgm^2
Length of the hip	0.058 m
Distance joint-Gt of the HAT	0.294 m
Mass of the thigh	10.34 kg
Inertia of the thigh	0.2678 kgm^2
Length of the thigh	0.475 m
Distance joint-Gt of the thigh	0.195 kg
Mass of the shank	3.16 kg
Inertia of the shank	0.0382 kgm^2
Length of the shank	0.429 m
Distance joint-Gt of the shank	0.188 kg
Mass of the foot	1.319 kg
Inertia of the foot	0.0064 kgm^2
Length of the foot	0.117 m
Distance joint-Gt of the foot	0.043 kg

It shall be noted that the values for the thighs, the shanks and the feet are the same in both sides of the body, right and left, so they are listed only once in the table.

To denote the geometrical features of feet according to the model presented in 3.2.1, the height of the individual was needed. It was considered to be 1.792 m. Therefore, those parameters, which are the same for the right and the left foot, have the values appearing in the Table 8-2:

Table 8-2: Feet parameters

Parameter	Value
L_1	0.1792 m
L_2	0.07168 m
L_3	0.10752 m

$$L_{r1} = L_{l1} = 0.10\,H$$
$$L_{r2} = L_{l2} = 0.04\,H$$
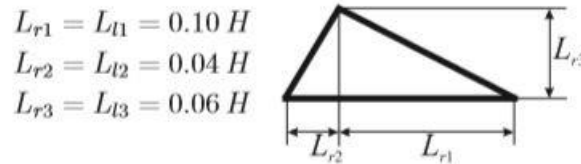$$L_{r3} = L_{l3} = 0.06\,H$$

Figure 8-2: Feet parameters. García Vallejo [3].

8.2   Influence of the number of nodes in the convergence of solutions

As said at the beginning of this section, the number of nodes choosen to run the interpolation process will influence decisively in the speed and the accuracy of the obtained solutions. This way, a bigger number of nodes will lead to a more precise convergency. This could be interesting to design a concrete orthosis, but it will demand a high computational cost that surpasses the limits of available means, as the non-linear constraints already make the optimization problem very burdensome. By contrast, to choose a smaller number of nodes to perform the interpolation will speed the process up, although the found solution could not be as accurate as desired. It will be necessary to reach an agreement between those two factors.

In this report, the results refer to interpolations made with 25 nodes. Firstly, 19 nodes were selected as a starting point, but solutions never converged to a feasible point. Adopting 25 as the number of nodes, the results were found in a reasonable time and always reached a feasible point, fulfilling every constraints. Nonetheless, to compare the speed and precision of using each number of nodes, reference solutions obtained by utilizing both 25 and 29 number of nodes will be compared, so that an analysis in terms of speed and exactitude can be done. Also, this subsection will be drawn to explain the differences in the design parameters among the healthy and the injured individual The green line correspond to the values

obtained in the laboratory [9], the blue refers to the 29-nodes-solution, while the red line references the 25-nodes-solution. In first place, the generalized coordinates will be compared in the Figure 8-3:
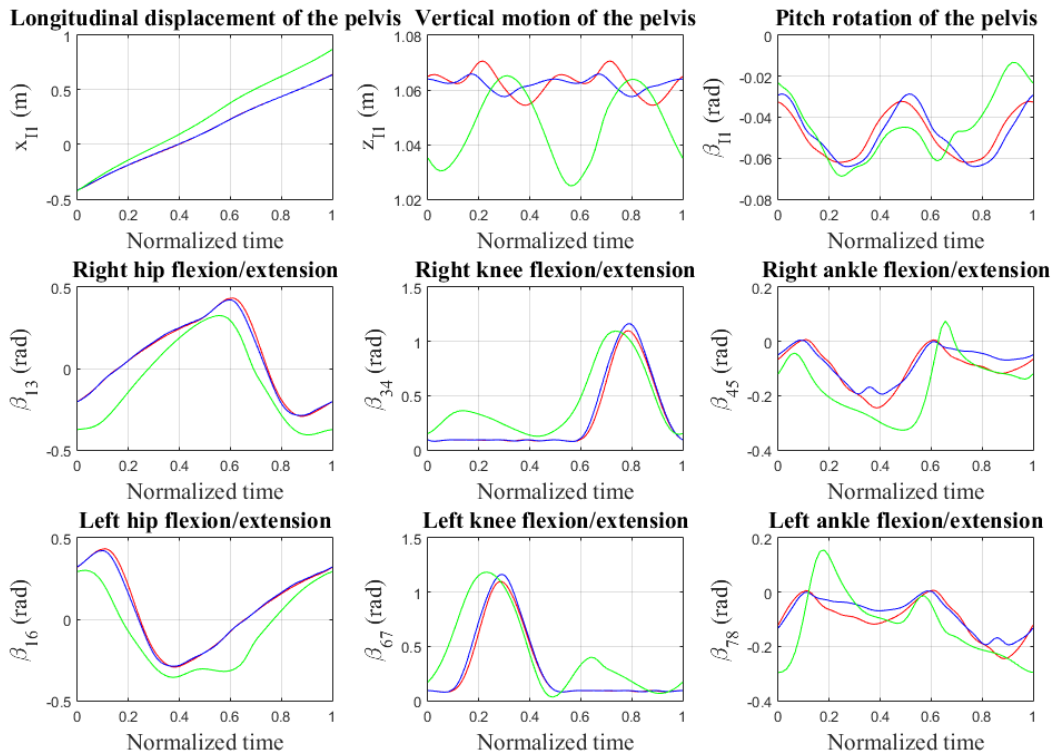

Figure 8-3: generalized coordinates for 25 and 29 nodes.

The two first coordinates (longitudinal and vertical motion of the pelvis) shows the difference between the original motion reference, corresponding to a healthy individual, and the two reference solutions obtained by using MATLAB. The distance walked by the injured individual is a bit smaller than the one walked by the healthy one, and there are no appreciable differences between the two calculated solutions. Besides, the the oscilation experimented in the motion reference is way bigger than the other two, and that can be explained the next way: one of the objectives of the exoskeleton is to add more stability to the body during the act of walking. The 29-nodes solution, as it is more accurate than the 25-nodes one, presents even lower oscillations.

There are no remarkable differences in the rest of generalized coordinates among the solutions, although two facts must be outlined: on the one hand, the knee-locking constraint gets activated, at the beginning of the cycle in the right knee, and at the end in the left one; on the other hand, the ankle angles are always negative zero, as the constraints have been defined to make them always below zero. It can also be remarked than the knee flexion occurs later in the exoskeletal model, although it reaches practically the same value in both cases. Moreover, the amplitude of the ankle flexion and extension is way bigger in the healthy individual.

Concerning to the reaction forces derived from the ground-foot contact, both tangent and normall reactions are plotted as follows:
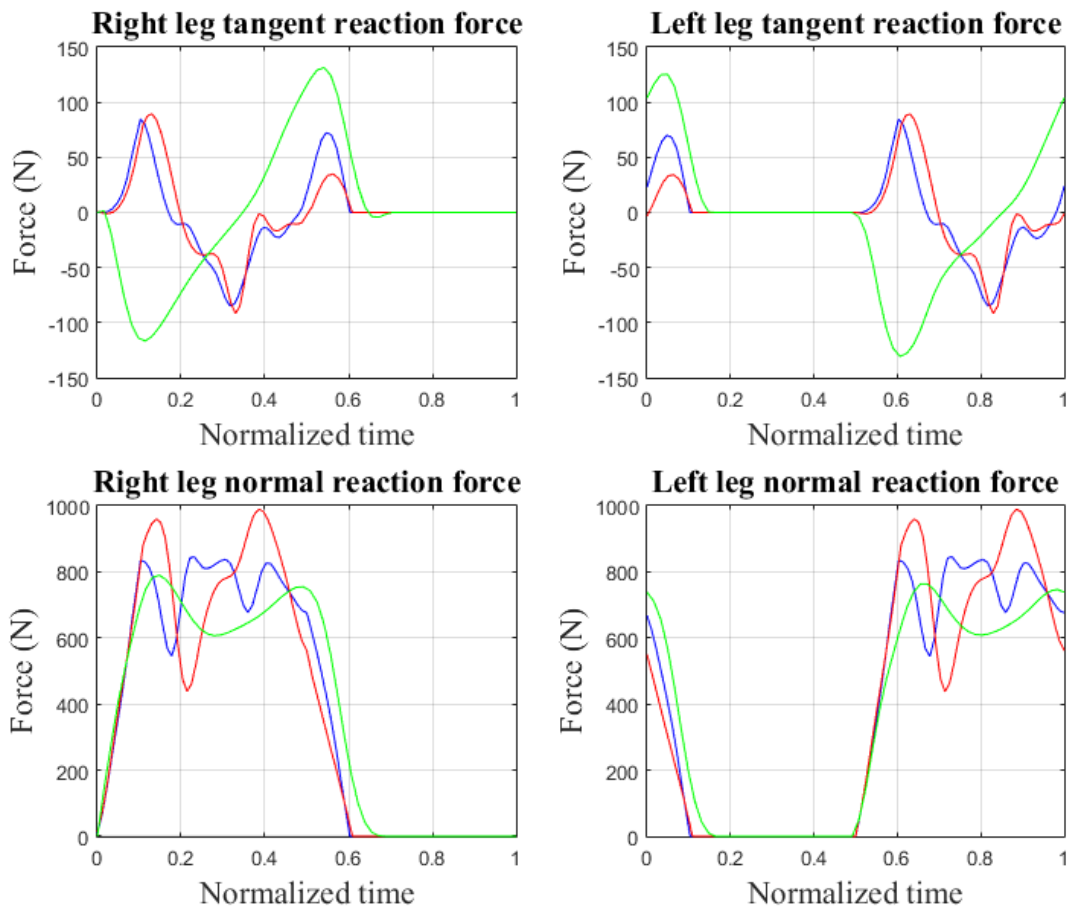
Figure 8-4: Reaction forces for 25 and 29 nodes.

There are no great differences concerning the force exerted among the two different injury-body models, only remarking that the amplitude is a bit smaller using 29 nodes for the interpolation. The explanation for that could reside in the best optimality found in that model, as its solutions are more reliable than using only 25 nodes. However, there are slightly differences between the injuried and the healthy human body models. These differences can be detected in the graphics representing tangent forces, when the foot connected to the studied leg is in contact with the floor. When that happens, a negative tangent force is observed in the healthy walker, while it is positive in the injured individual. The reason for that is the positive sliding on the floor made by the non-skeleton-wearing walker, and the negative made by the injured one. García Vallejo and Schliechen [1] explain that difference with the constraint that makes zero the velocity of the contact point between the foot and the ground.

Now, discordances referring the measured torques in the joints among two injured models will be studied. Firstly, the torques produced by the joints (hip, knees and ankles) by their own, and then, the torques generated by the motor and the flexible Klenzak ankle.
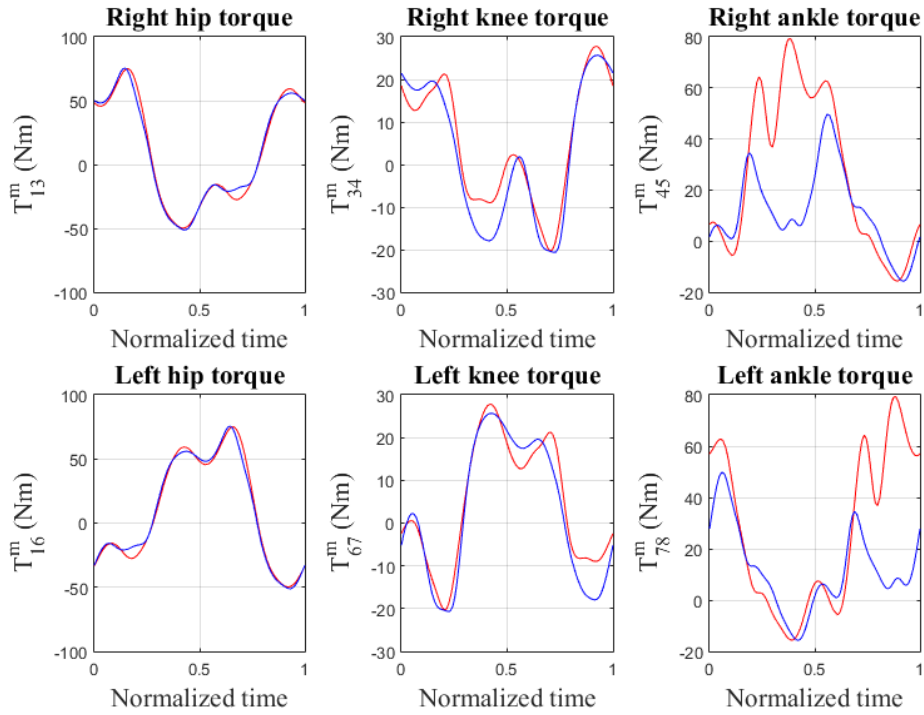
Figure 8-5: Joints torques for 25 and 29 nodes.

As observed before, the absolute value in the model using more nodes uses to be smaller, as it is a more optimal solution. This difference is almost inappreciable in the torque produced by the hip, both for right and left sides, as there is no mechanical device there. More discrepancies appear in the other two joints, especially in the ankle, which containts the Klenzak flexible device. The motive is that the Klenzak produces a big torque when the foot is in contact with the floor, and so the human ankle does not need to exert too much force.
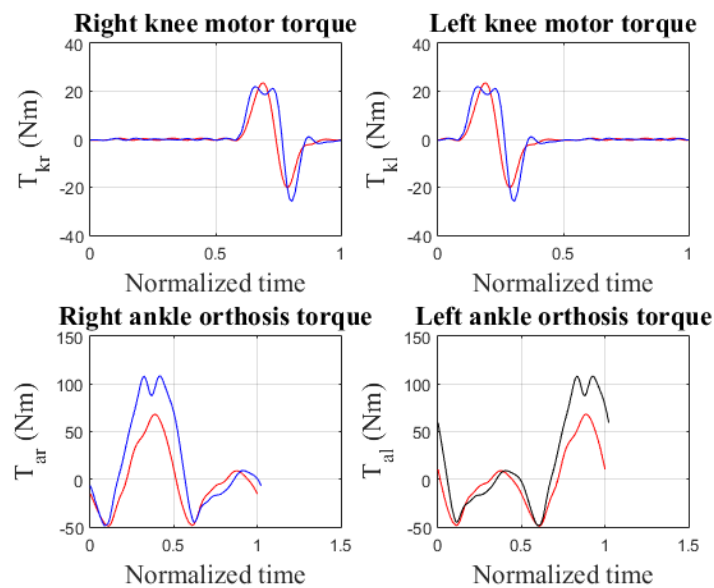

Figure 8-6: Motor and Klenzak torques for 25 and 29 nodes.

Observing the torques yielded by the mechanical units, the phenomenon right explained is confirmed. The solution using 29 nodes finds more optimal to make the Klenzak ankle to generate a bigger torque, and therefore not to strain the ankles a big way when they are in contact with the ground. On the other hand, there are no wide discrepancies in the knee-placed motor torques. It shall be noted that the motor is only active (producing a non-zero torque) when the foot is in the air, performing a step.
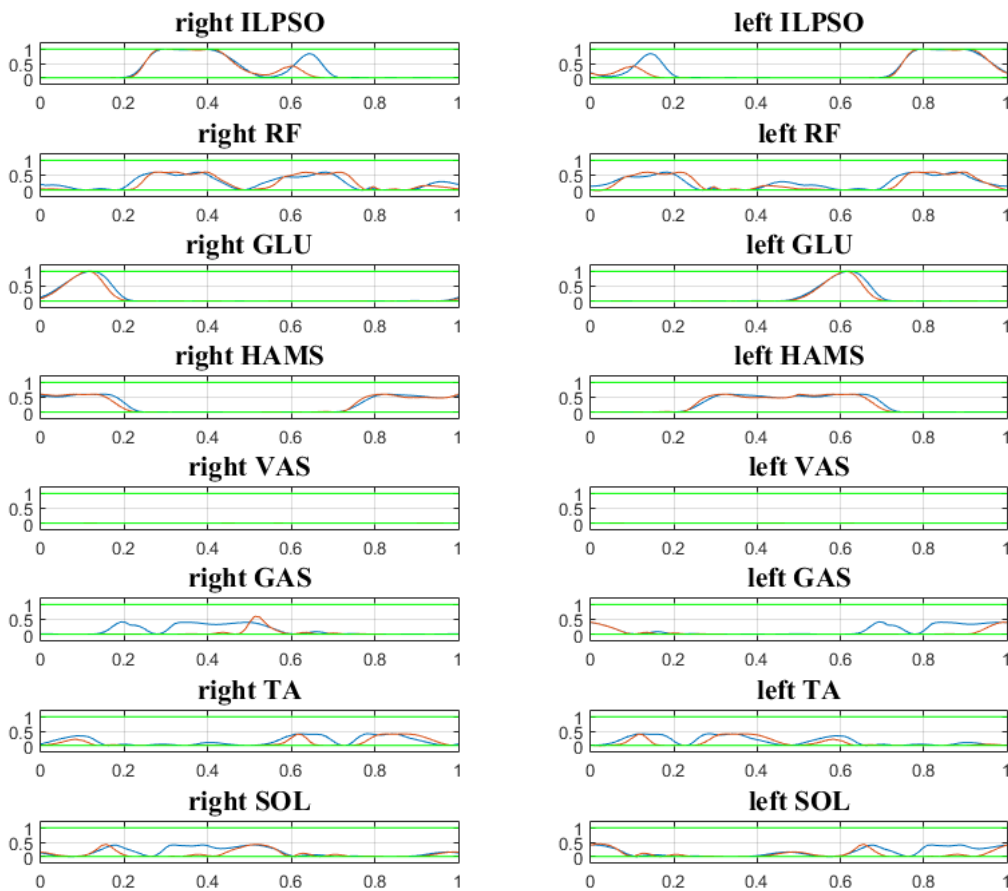
Figure 8-7 Activation and excitation for 25 and 29 nodes.

By last, the activation displayed in the figure above shows that the 29-nodes model uses to present a bigger activation

To summarize, every figures right presented show a more optimal evolution of the design parameters using 29 nodes, but the differences are not big enough to make up the wide bigger computing time. That is the reason for what every optimizations have been made using 25 nodes for the interpolation.

8.3 Influence of intrinsical parameters of the orthesis

The first parameters to be studied their influence in the metabolical cost were those ones intrinsical to the orthosis: its mass and geometry, as well as the inertia, as it is proportional to the mass and the square of the length, as explained before.

To begin with, every mass properties were changed, and so on the ones referred to the inertia. Secondly, geometrical features were affected, and by last, the mass and geometrical characteristics combined. As explained in section 8, the increasements introduced were always symmetrical, to be consistent with the symmetrical 2D musculoskeletal model.

As the first increasements on parameters are very small, especially the 1 and 2%, they hardly introduce changes from the reference motion pattern. The mass will be the only parameter whose analysis includes the whole evolution (1, 2, 5 and 10%), so the graphics showing the evolution after imposing 1% changes will be exploited to explain the form of the curves.

Firstly, graphics exhibiting the design parameters will be exhibited, and then, the evolution of the numerical values of interest will be displayed in a table so as to reach a better understanding of the influence of the introduced changes.

8.3.1 Mass

8.3.1.1 1% increasement

The mass was the first parameter whose influence was analysed. First of all, the mass of every elements of the orthosis were increased a 1%, as well as their contribution to the inertia. Thereby, the new values were:

Table 8-3: Mass and inertia values after 1% increasement

Parameter	Value
Mass of the thigh bars	0.202 kg
Inertia of the thigh bars about Gt	1.5453e-3 kgm^2
Mass of the motor	1.1211 kg
Mass of the shank bars	0.3232 kg
Inertia of the shank bars about Gs	0.0481 kgm^2
Mass of the encoder	0.0606 kg
Mass of the foot support	0.101 kg
Inertia of the foot support about Gf	0.000113 kgm^2

The evolution of the generalized coordinates during the walking cycle after these changes were as follows (the blue line refers to the reference value, the red line to the solutions obtained):
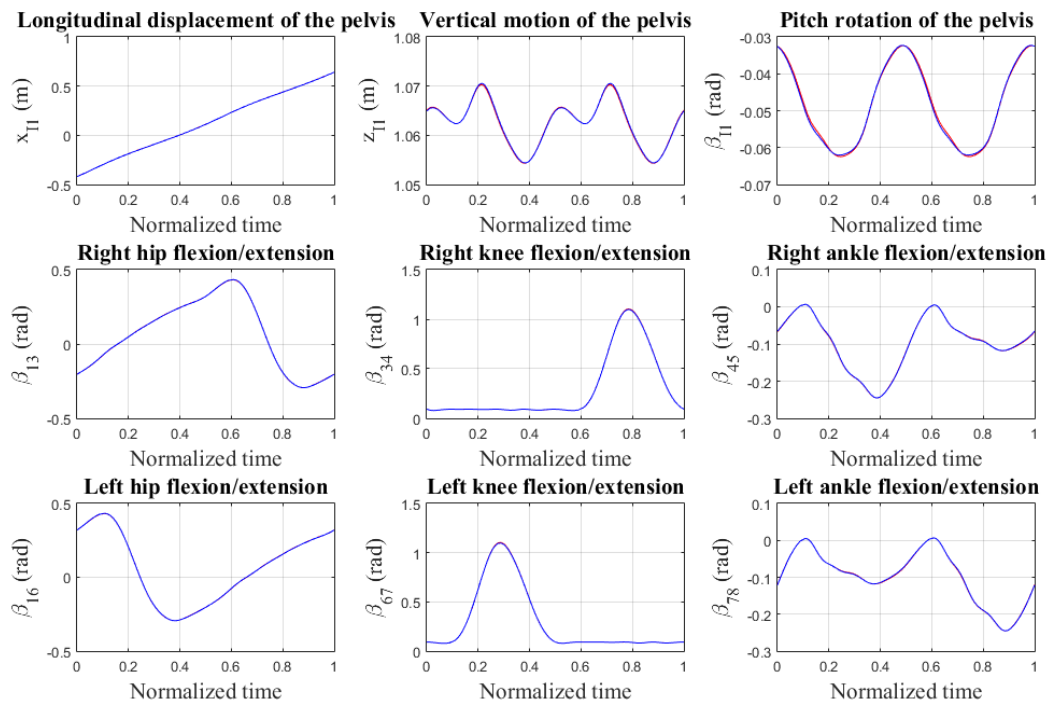
Figure 8-8: Generalized coordinates after 1% mass increment.

As expected, the coordinate x_{11} follows a lineal evolution, as the body model walks at constant speed. The oscilations appearing in the coordinate z_{11} can be divided in two halves, each one with two peaks (one higher than the other one). Each half is related to each of the two steps the body model performs during the cycle, although the variation of the vertical coordinate during the cycle is very low (at around 1.5 cm at most). The variation of the pitch angle in the pelvis follows a very regular, sine wave pattern, and it is also extremely small, in the order of 0.03 rad.

What concerns the leg coordinates, as the left hip angle was defined to the contrary sense than the right one, the angles obtained were very similar in both cases (a bit larger in the right hip case) with different signs. Thereby, the biggest right hip angle was around 0.4 rad, while the largest in the left hip case was close to -0.3 rad.

It does not occur the same with the rest of the coordinates, the ones referred to the knees and the ankles. They were all defined clockwise, so the values obtained for these angles were the same in both cases. The only difference resided in the time instant those angles reached their respective peaks.

Starting with the knees coordinates, as the walking cycle starts with a left step, the left knee angle reaches the first its peak (at about 1.1 rad). Meanwhile, the right knee is subject to the knee-locking constraint, with its angle forced to be 0.0873 rad. The inverse effect happens when the second step is performed: the left knee is locked and the right knee angle reaches its peak.

Concerning the ankle coordinates, they act similarly to the knee ones, with the difference that the Klenzak ankle is flexible and does not have a locking constraint. Taking absolute values for the angles in ankles (as they are negative in the whole cycle due to kinematic constraints), each angle reaches its peak when

opposite leg is performing the step. In other words, if the walking cycle starts with a left step, the right ankle gets its cycle-high (at around 0.25 rad with negative sign) the first. This is because the walker needs to bend his ankle to gain momentum and stand it up easily.

To sum up, the motion is really similar to the reference pattern, with no significant differences between them. Larger increasements were needed to note appreciable variations.
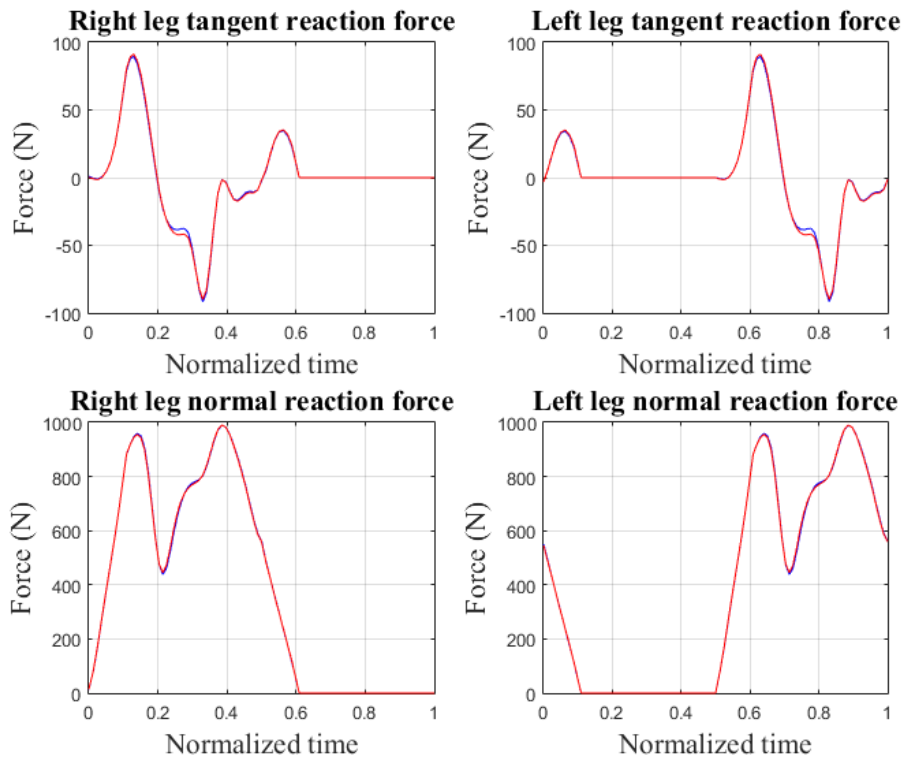

Figure 8-9: Reaction forces after 1% mass increment.

The figure above displays the forces appearing in the contact foot-ground. Not surprisingly, there is no contact force when the foot is in the air. As already known, the walking cycle starts with a left step, what means the left foot will be in the air the first half of the cycle, and therefore the forc. The small peak found right at the start of the cycle in the left tangent force figure can be explained as the momentum performed with the foot to the ground, required to take the foot off to the air. The negative slope in the small linear stretch found in the left normal reaction picture appears because the force exerted with the foot to the ground decreases in a constant way until reaching the zero value, as expected. The same phenomena are observed in the right foot, when it starts its step.

When the foot comes back to the floor, it starts to experiment the reaction forces. In the tangent forces, it shall be noted the change in the sign. It occurs because, during the contact ground-foot, the foot tends to slide with negative sign at the start of the step (what origins a tangent reaction with positive sign), and then slides again with positive sign (creating a negative tangent reaction). Newly, the solution obtained is very reliable to the reference motion. The maximum value for these forces rounds 1000 N (normal forces) and 100 N (tangent forces).
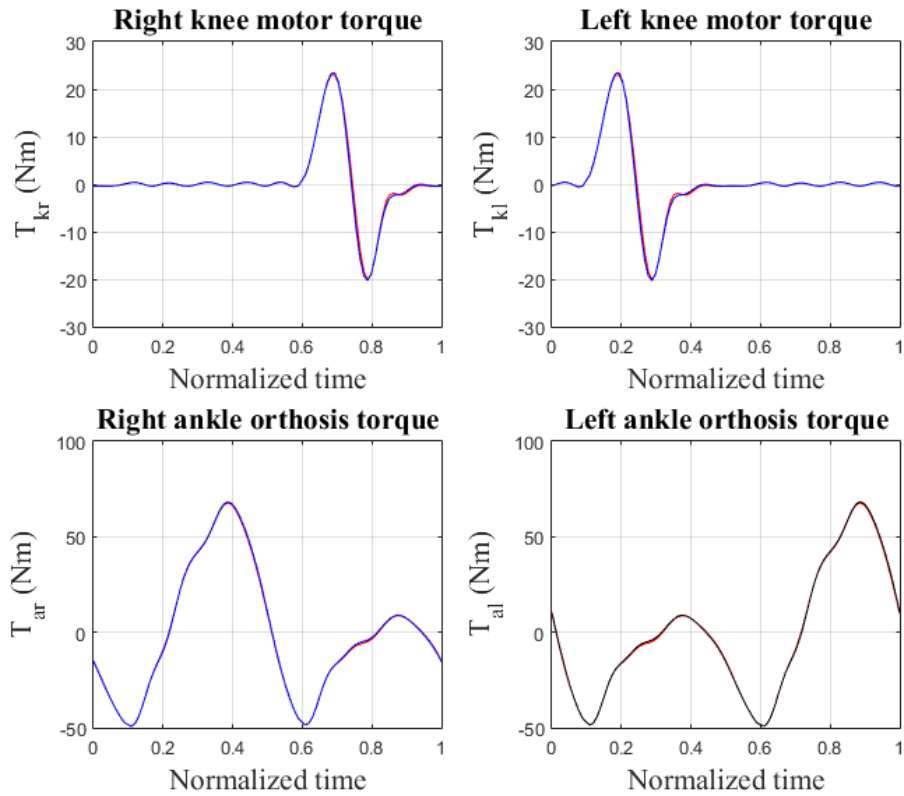
Figure 8-10: Motor and Klenzak torques after 1% mass increment.

Referring to the respective torques exerted by the motor and the Klenzak ankle, they work as expected. The motor, placed in the knee, develops its power when its leg is performing a flexion and extension, and do not exert any torque during the rest of the cycle (only certain vibrations). The change in the sign is due to the change in the movement (from flexion to extension). The obtained values are about 20 Nm (referred in absolute value).

Before it was explained the ankle flexion and extension were bigger when the foot was in the ground. Newly as waited, the torque performed by the Klenzak ankle is larger when the foot is in contact with the floor, to fulfill this requirement, changing the sign because of the same reason as the motor (the flexion-extension movement). As seen in the figures, the obtained torques are between -50 Nm and 70 Nm, in both ankles.
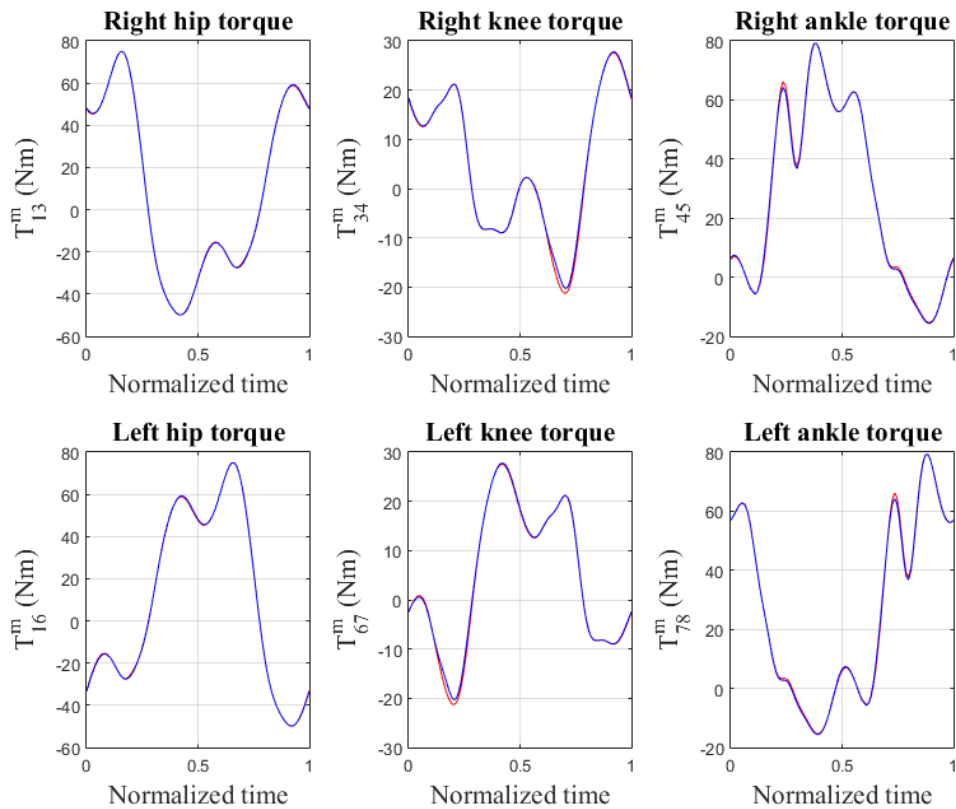
Figure 8-11: Joint torques after 1% mass increment.

Now, the torques appearing in the legs (excepting the ones produced by the motor and the ankle) will be commented. As being a symmetrical motion, the form of the torques charts are symmetrical in the left and right legs, but not so on with the values, as it is logical because the right and the left side of the body are not making the same movements during a step in the walking cycle.

Starting with the ankles, the big torque (about 60 Nm) appearing at the start of the motion of the left ankle is explained due to the impulse on the floor required to lift the foot, while the torque is almost zero in the right ankle. When the foot is in the air, the ankle torque falls to zero, and increases a big way in the right side, reaching 80 almost Nm. The inverse situation occurs when the walker performs the second step in the cycle.

The same is not observed while observing the knee charts, but it is the expected phenomena if common sense is used. Taking absolute values, and considering the sign criterion stablished, the torque experimented by the knee while performing a step changes from negative to positive, as it firstly bends clockwise, and then counterclockwise. During the contact foot-ground, the torque at knees decreases but does not falls to zero, as the knees also suffer part of the reaction forces coming from the ground.

By last, analyzing the torques appearing in the joints leg-hip, the largest torques (about 80 Nm) occur mainly while the contact foot-ground is being produced. A sign change happens from positive to negative, and the opposite fact is appreciable when the foot is in the air.
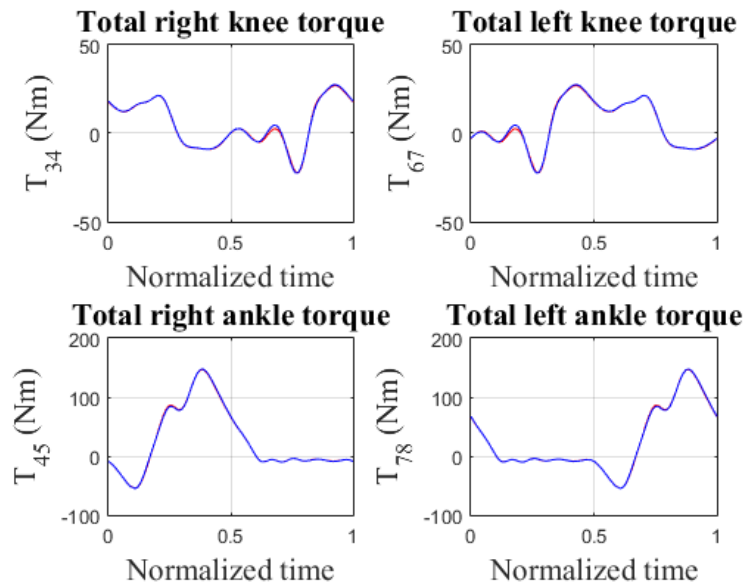
Figure 8-12: Total torques after 1% mass increment.

The figure above shows the total torque in ankles and knees, combining the torque developed by the walker, and the one powered by the motor and the flexible ankle. This one is very near to zero when the foot it is placed in it performing a step, as it was expected.
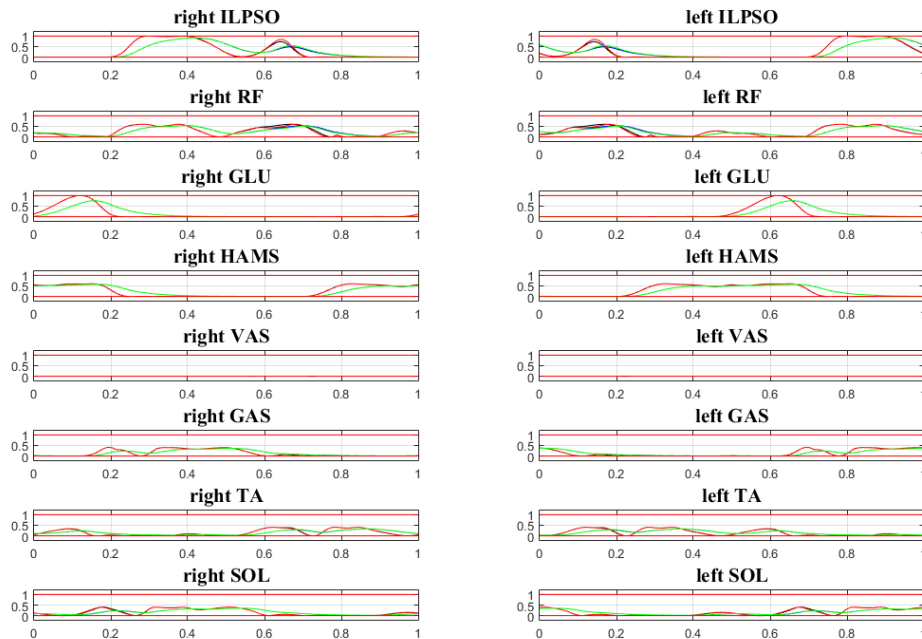

Figure 8-13: Activation and excitation after 1% mass increment.

By last, the muscular activation and the neural excitations are analyzed. The black and the blue line correspond to the activation and excitation, respectively, obtained for the studied model, while the red and the green refer to the reference motion. As it is logical, the activation always appears with a little retard respect to the neural excitation. No slightly discordances are appreciated among the reference and the solution, remarking only that activation decreases a little bit in the second one. Causes will be analyzed later.

8.3.1.2 2% increasement

Secondly, a 2% increasement was imposed, which was equivalent to multiply reference values for orthosis mass by 1.02. These were the new values:

Table 8-4: Mass and inertia values after 2% increment

Parameter	Value
Mass of the thigh bars	0.204 kg
Inertia of the thigh bars about Gt	1.5606e-3 kgm^2
Mass of the motor	1.1322 kg
Mass of the shank bars	0.3264 kg
Inertia of the shank bars about Gs	0.0486 kgm^2
Mass of the encoder	0.0612 kg
Mass of the foot support	0.102 kg
Inertia of the foot support about Gf	0.000114 kgm^2

The new generalized coordinates obtained were (as usual, blue lines refer to the reference motion pattern while red represents the obtained coordinates):
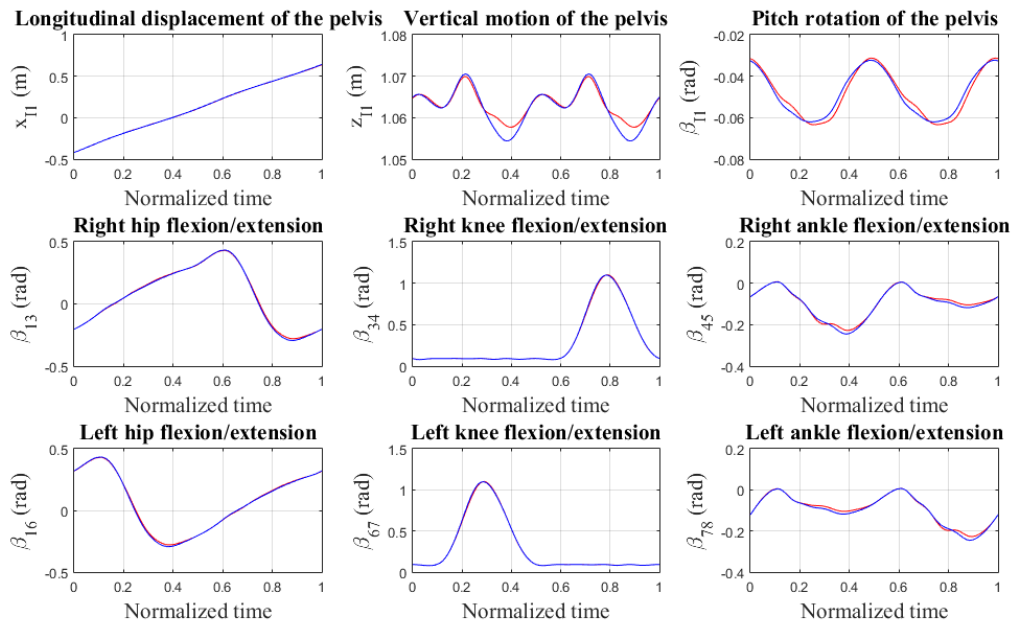

Figure 8-14: Generalized coordinates after 2% mass increment.

Wider deviations start to be detected in the pelvis, specifically in its vertical coordinate. The oscillation in the obtained model is a little smaller than the reference, possibly because the mass increasements tend to stabilize the walker. The rest of coordinates hardly change during the cycle.

Concerning the reaction forces originated in the contact foot-ground, their progress along the cycle follows the next evolution:
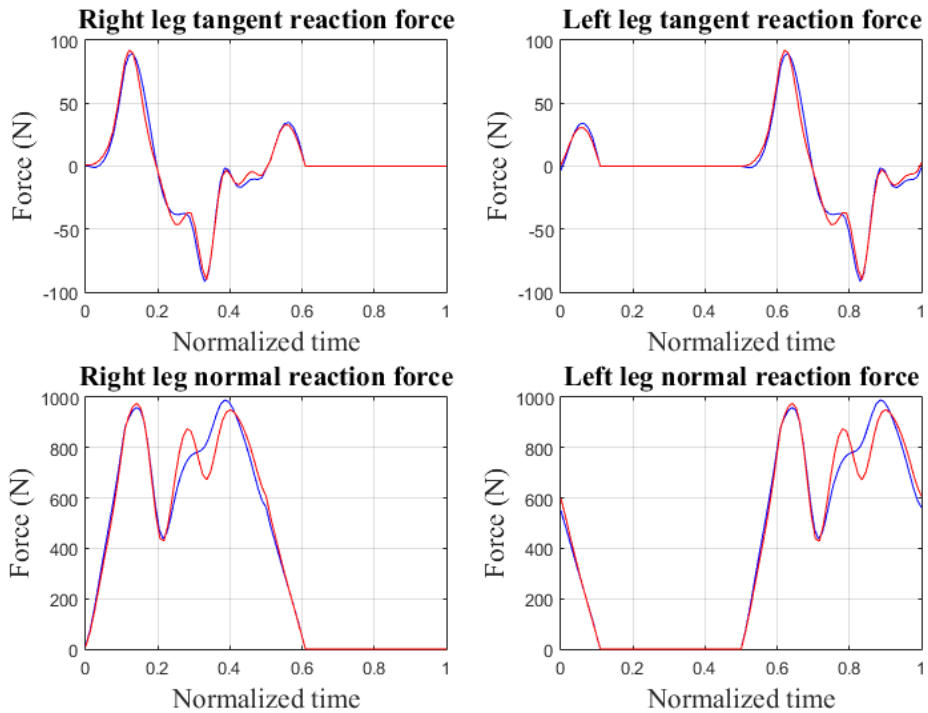

Figure 8-15: Reaction forces after 2% mass increment.

There are no great deviations from the reference pattern, only standing out that the forces oscillate more in the found solution, probably because of a little shaking in the feet while touching the floor after increasing the mass and inertia.
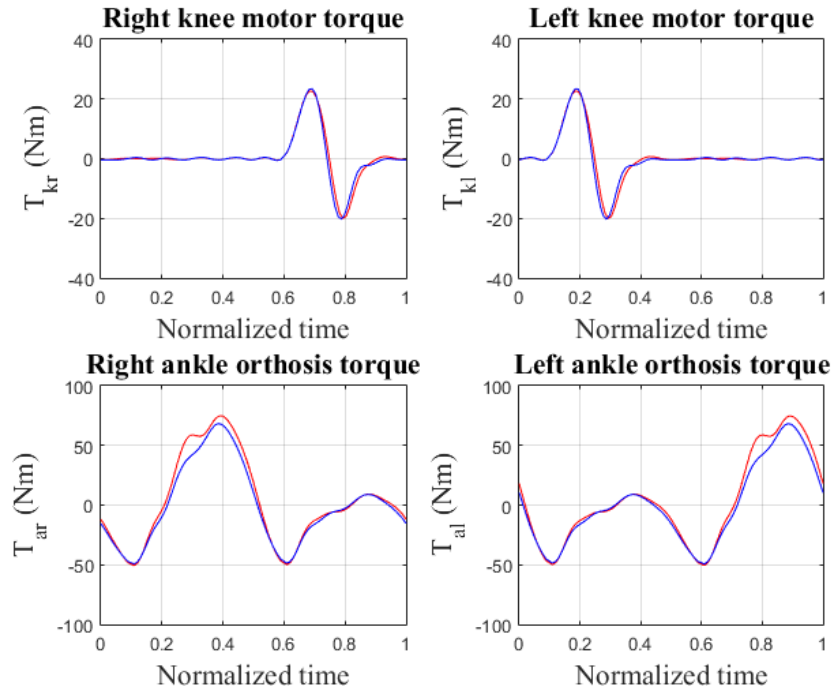
Figure 8-16: Motor and Klenzak torques after 2% mass increment.

Speaking about the torque originated in the mechanical elements, the motor torque slightly experiments important deviations. Meanwhile, although Klenzak torque is almost very similar to the reference, it can be highlighted that the solution is a bit bigger than the torque pattern during the contact to the floor. That can be justified arguing that as the mass increasement makes the walker heavier, and so the contact to the ground is more marked, the torque needs to exert a bigger torque.
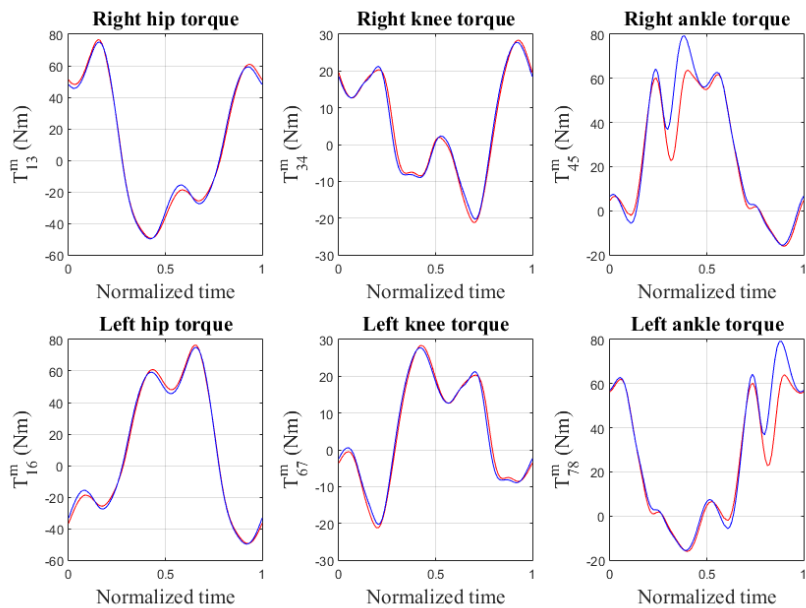
Figure 8-17: Joint torques after 2% mass increment.

The same conclusion is reached when analyzing the natural torques in the joints. While there are variations neither the hip nor the knee, the ankle does present a heavy decreasement while the contact phases, rounding 20 Nm, so as to compensate the larger torque produced by the ankle in that moment. It can be noted that the total torque barely varies during the cycle after implementing a 2% increasement to mass.

Figure 8-18: Total torques after 2% mass increment.

Finally, the muscle activation and the neural excitation are studied:
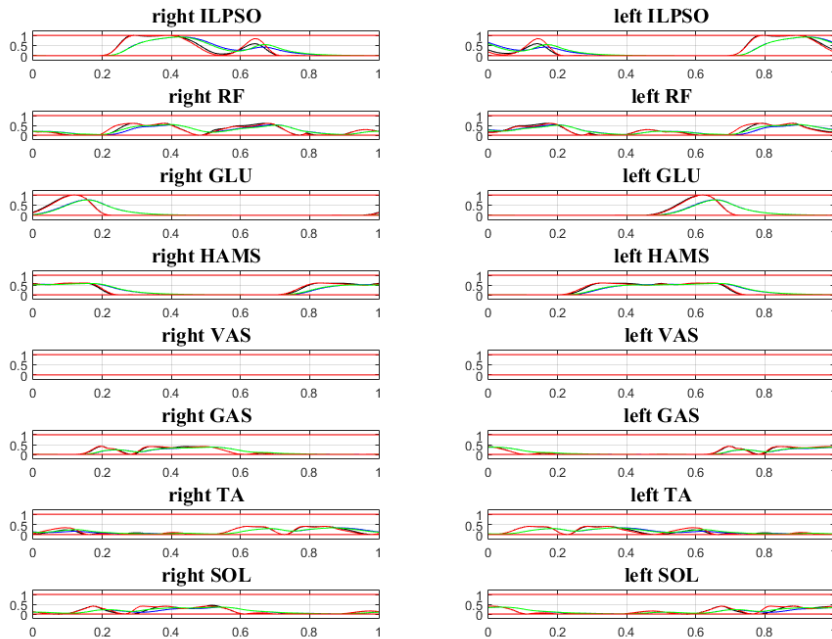
Figure 8-19: Activation and excitation after 2% mass increment.

The colour code is the same as the presented in 9.3.1.1. Significative variances are not discovered.

8.3.1.3 5% increasement

In third place, reference mass and inertia values were increased a 5%, obtaining the new following parameters:
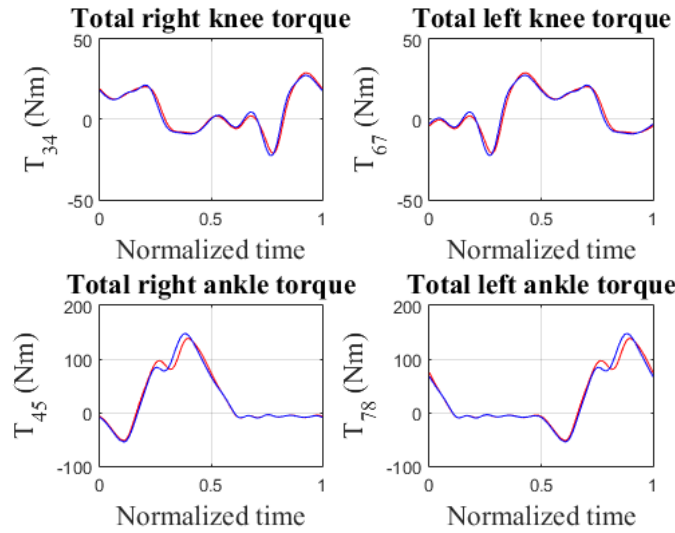
Table 8-5: Mass and inertia values after 5% increment

Parameter	Value
Mass of the thigh bars	0.21 kg
Inertia of the thigh bars about Gt	1.6065e-3 kgm^2
Mass of the motor	1.1655 kg
Mass of the shank bars	0.336 kg
Inertia of the shank bars about Gs	0.05 kgm^2
Mass of the encoder	0.063 kg
Mass of the foot support	0.105 kg
Inertia of the foot support about Gf	0.000117 kgm^2

The resultant generalized coordinates can be displayed as:
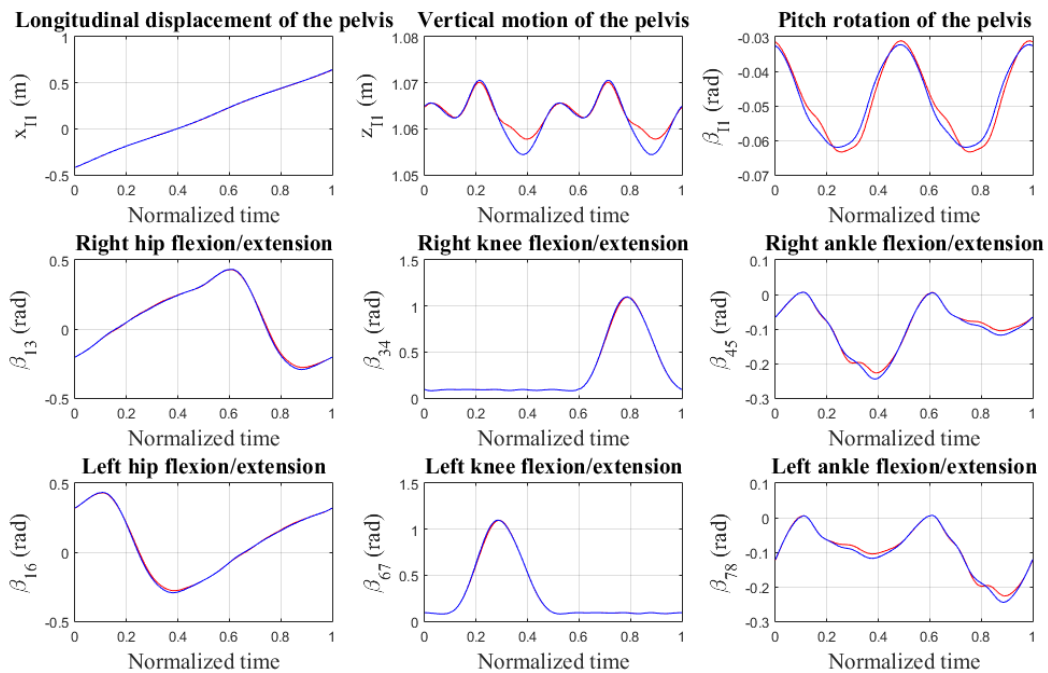
Figure 8-20: Generalized coordinates after 5% mass increment.

Conclusions drawn from the figure above are the same as in the previous case where a 2% increasement was ordered. Bigger deviations from the pattern are observed in the pelvis, especially in its vertical oscillations.
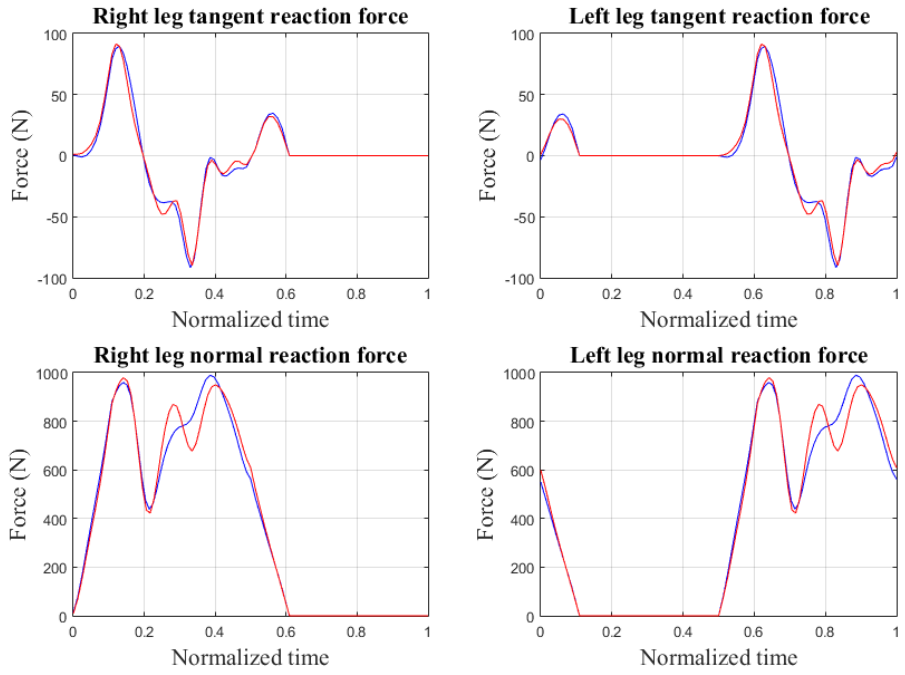
Figure 8-21a: Reaction forces after 5% mass increment.

Regarding the reaction forces, no novelties appear, and the trend detected before gets confirmed: the oscillations grow in the obtained solution.
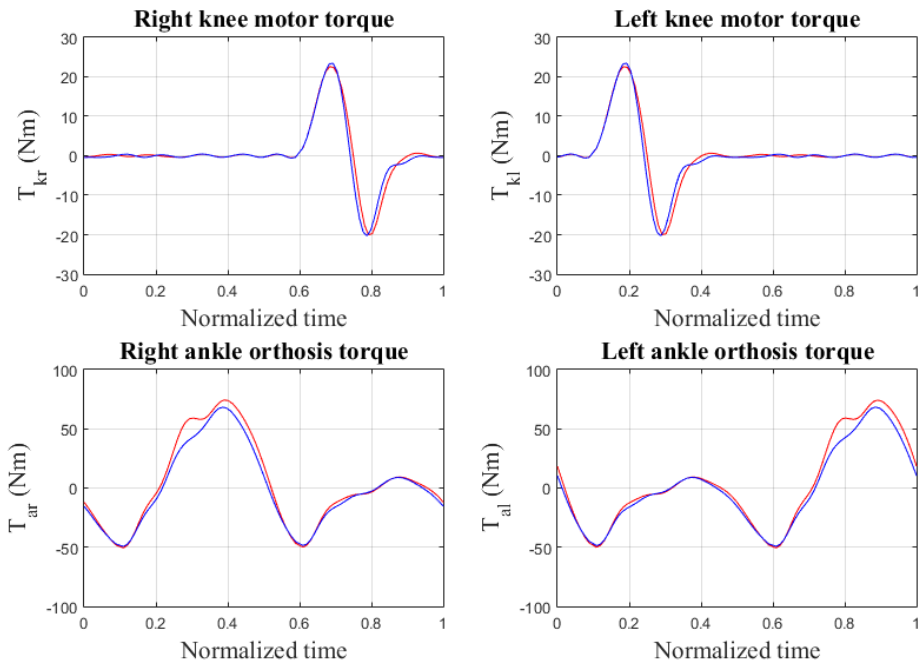
Figure 8-21b: Motor and Klenzak torques after 5% mass increment.

The motor parameters evolution show that, in the solution using a 5% growth, the motor, placed in the knee, produces the torque with a small delay, possibly due to the mass increment in the motor. In the Klenzak orthosis, the torque is a bit larger in the solution, due to same reason explained in the previous subsection.
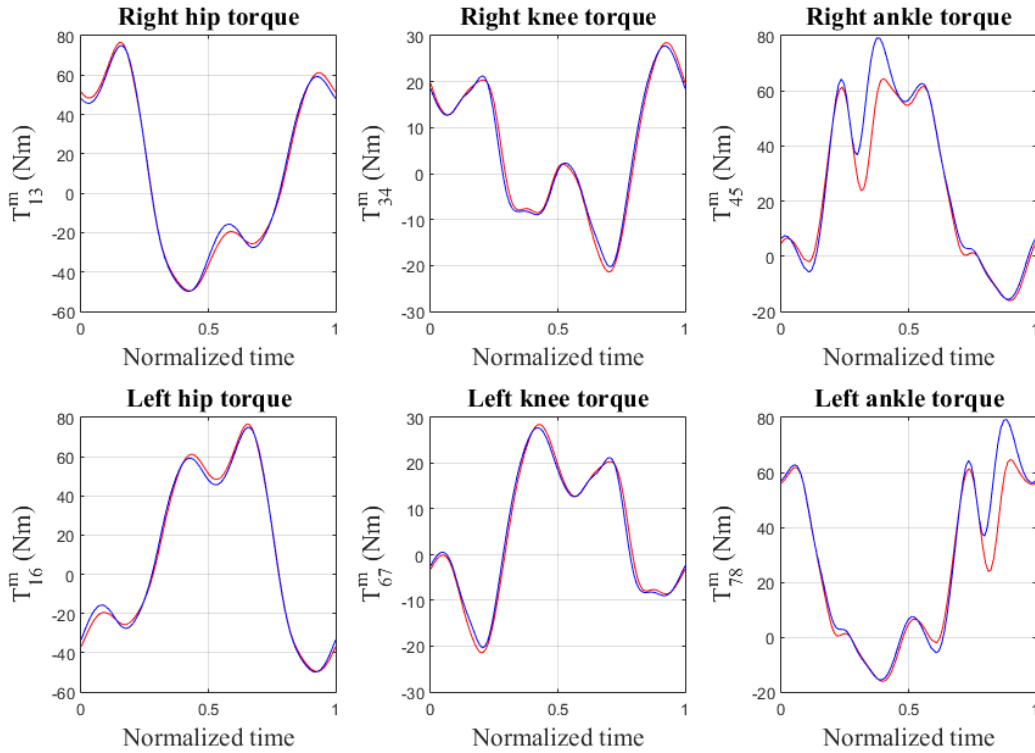
Figure 8-22: Joint torques after 5% mass increment.

Observing the torque generated by the human joints, newly the 20 Nm torque difference is observed in the ankle between the solution and the reference. On the other hand, the torque in the hip and the knee follows accurately the pattern, compensating the small differences appearing in the motor torque plots, as seen in the total torque figures below:
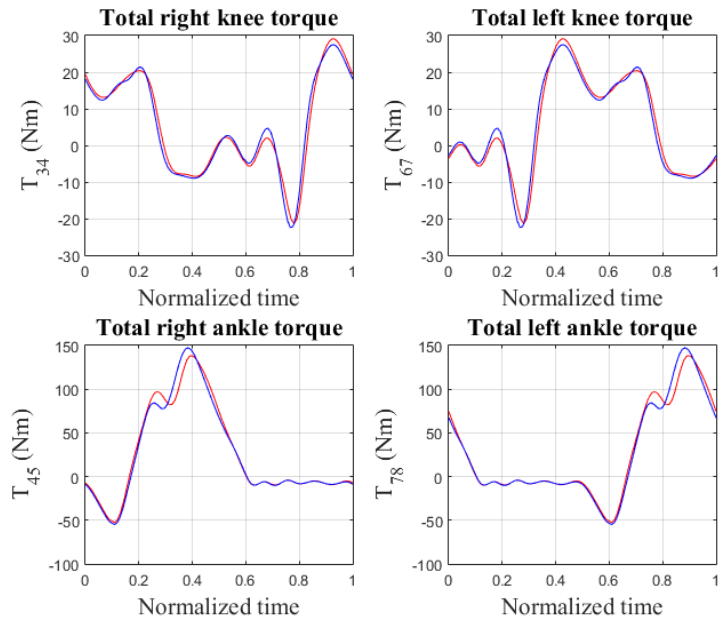
Figure 8-23: Total torques after 5% mass increment.

With respect to the activation and neural excitation:
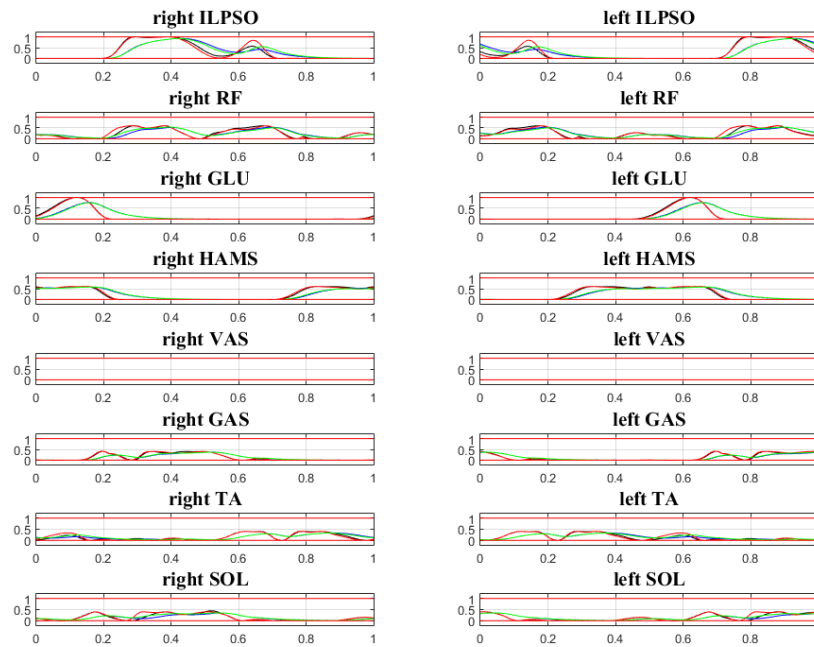
Figure 8-24: Activation and excitation after 5% mass increment.

No appreciable deviations from the results commented in the subsection before are appreciated.

8.3.1.4   10% increasement

By last, the biggest implemented growth was a 10% over the reference, considered to be an important increment. The new values were:

Table 8-6: Mass and inertia values after 10% mass increment.

Parameter	Value
Mass of the thigh bars	0.22 kg
Inertia of the thigh bars about Gt	1.683e-3 kgm^2
Mass of the motor	1.221 kg
Mass of the shank bars	0.352 kg
Inertia of the shank bars about Gs	0.0524 kgm^2
Mass of the encoder	0.066 kg
Mass of the foot support	0.11 kg
Inertia of the foot support about Gf	0.000123 kgm^2

Largest deviations are expected now therefore. Starting with the generalized coordinates:
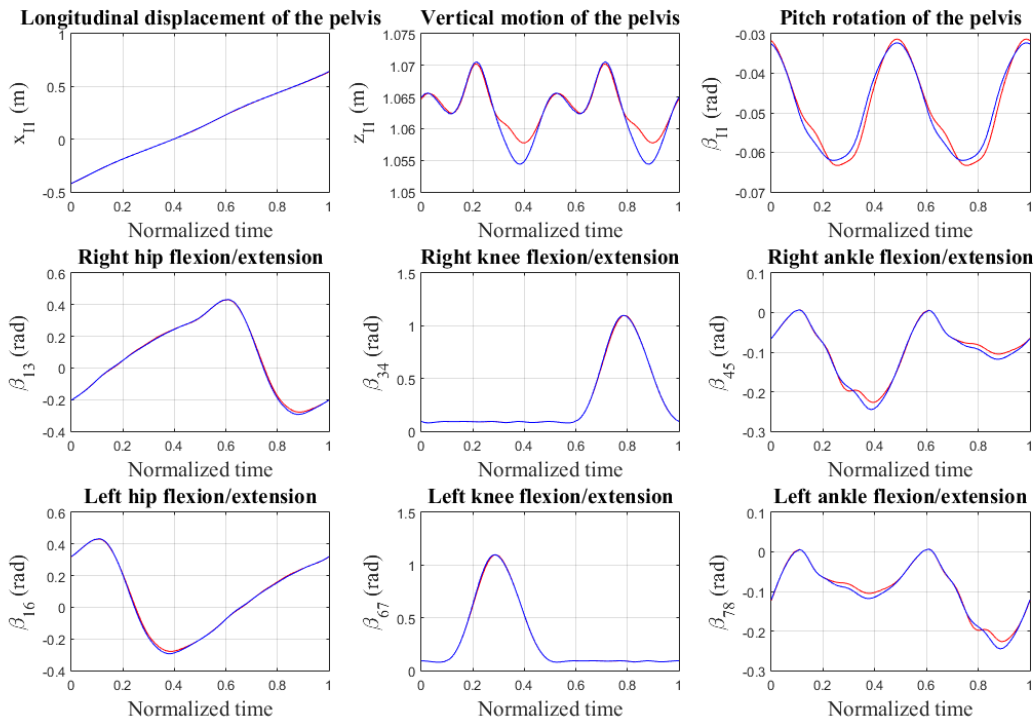
Figure 8-26: Generalized coordinates after 10% mass increment.

The main new observed fact is the small discrepancy in the ankle angle evolution. Remembering that the constraint imposes this coordinate to be below zero, and taking absolute values, the angle obtained in the solution is slightly smaller than the reference one. The reason can be the major inertia of the model, and so on, the bigger opposition to be moved, what makes more difficult to rotate the ankle.
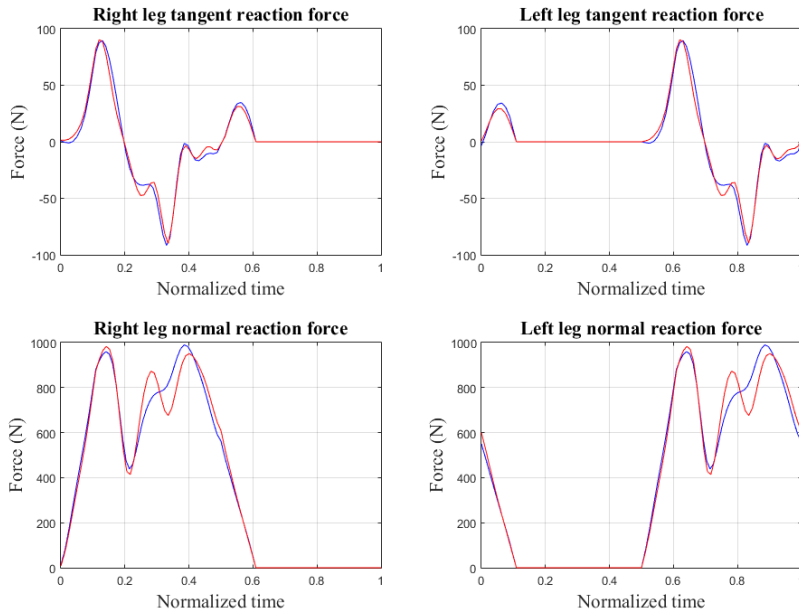
Figure 8-27: Reaction forces after 10% mass increment.

The reaction forces figure confirms the tendency detected with the small increasements implemented in the previous subsections.
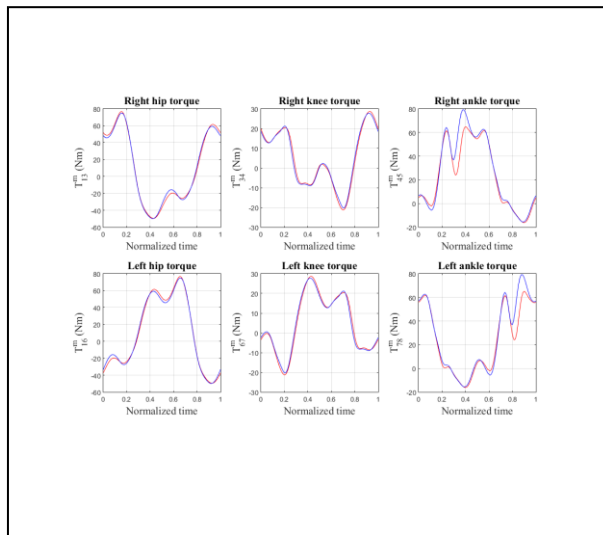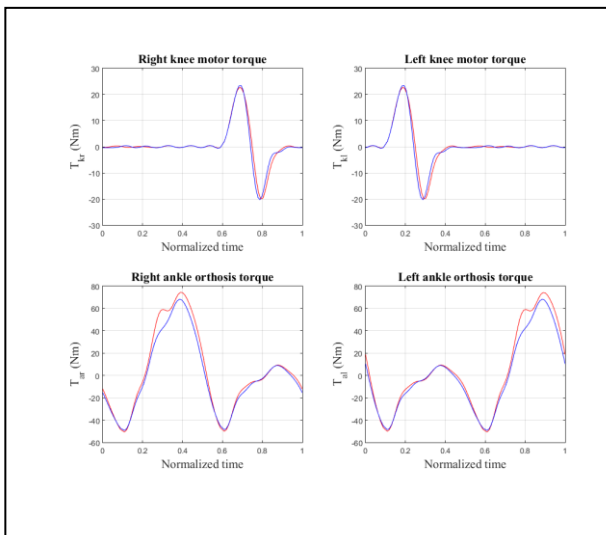
Figures 8-28 and 8-29: Joint, motor and Klenzak torques after 10% mass increment.
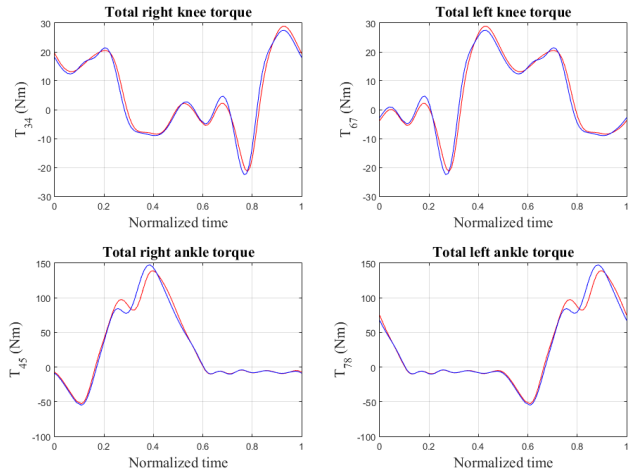
Figure 8-30: Total torques after 10% mass increment.

Now the three figures representing the motor, body and combined torques have been displayed together. The bigger deviation from the pattern is found in the ankle when the foot it is connected to is in contact with the floor.
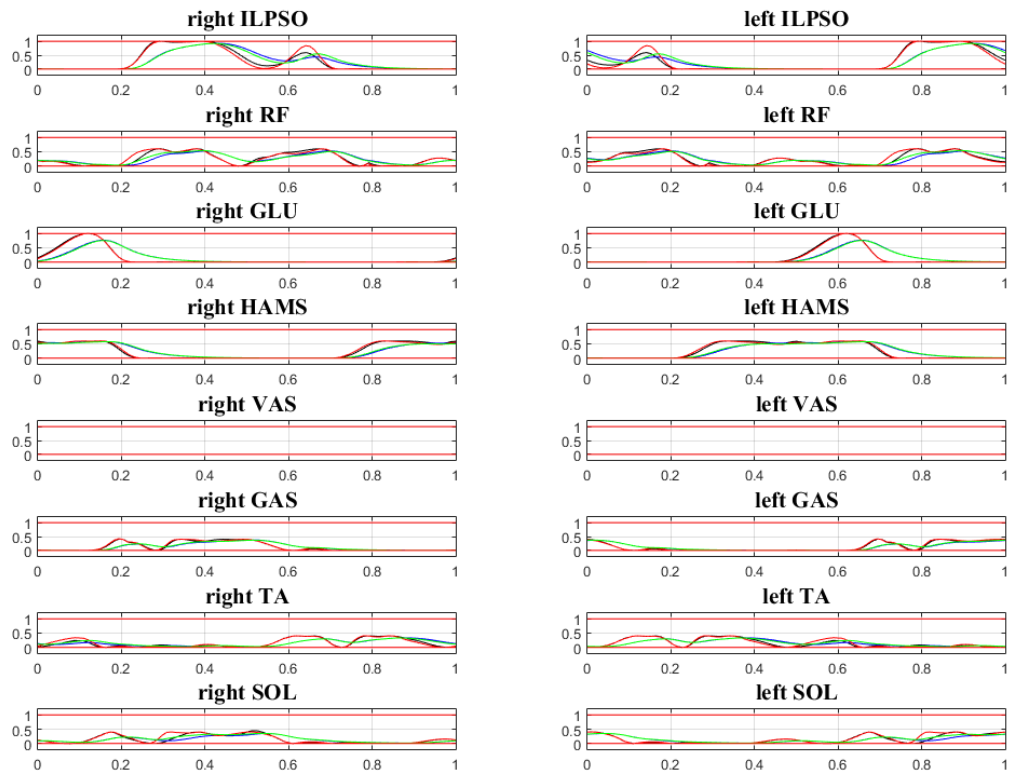
Figure 8-31: Activation and excitation after 10% mass increment.

Differences in the activation and excitation plots are not detected.

Now, it is the moment to analyze the evolution of the metabolical cost and the deviation of the pattern, what will determine if the optimization is successful or not.

Table 8-7: Evolution of expenditure and deviation when mass get increased

Mass increasement	Metabolical expenditure	Deviation from pattern
0 % (Reference)	341.74 J	15.198
1 %	339.33 J	15.102
2 %	333.22 J	14.783
5 %	333.70 J	14.827
10 %	334.39 J	14.901

The metabolical cost decreases from the reference value until imposing a 10% increasement to the mass, when it grows again. This means that, increasing the mass will ease the exoskeleton wearer the act walking, provided that the mass rise do not be over 5%. If so, the walker will have to spend part of his forces to move the exoskeleton itself, and that is non sense, as the objective is to make easier the act of walking.

The results just displayed can be summarized in the Table 8-8. The first column indicates the analyzed variable; the second column contains the maximum amplitude (difference between the maximum amd the minimum value for each variable) for the first increment over the reference, while the third column includes the same as the second, but referring to the last increment. The fourth column reflects the relative increasement between the two measured amplitudes. That will reflect the influence of the studied parameter. The Table 8-7 reflects the legend useful to know what the terms in the first column mean:

Table 8-8. Variables legend.

Variable	Meaning	Variable	Meaning
RT Force	Right tangent force	RK Torque	Right knee torque
RN Force	Right normal force	RA Torque	Right ankle torque
LT Force	Left tangent force	LH Torque	Left hip torque
LN Force	Left normal force	LK Torque	Left normal torque
RM Torque	Right moment torque	LA Torque	Left ankle torque
LM Torque	Left moment torque	TRK Torque	Total right knee torque
RO Torque	Right orthosis torque	TLK Torque	Total left knee torque
LO Torque	Left orthosis torque	TRA Torque	Total right ankle torque
RH Torque	Right hip torque	TLA Torque	Total left ankle torque

Table 8-9. Quantitative summary of mass influence

Variable	Highest amplitude, 1st increment	Highest amplitude, last increment	Relative increasement (%)
x_{11}	1.061 m	1.058 m	0.27
z_{11}	0.016 m	0.012 m	21.73
β_{11}	0.030 rad	0.032 rad	6.27
β_{13}	0.726 rad	0.710 rad	2.16
β_{34}	1.025 rad	1.019 rad	0.58
β_{45}	0.253 rad	0.235 rad	7.14
β_{16}	0.726 rad	0.710 rad	2.16
β_{67}	1.025 rad	1.019 rad	0.58
β_{78}	0.253 rad	0.234 rad	7.25
RT Force	181.228 N	180.211 N	0.56
RN Force	990.122 N	982.866 N	0.73
LT Force	181.196 N	180.088 N	0.61
LN Force	990.124 N	982.875 N	0.73
RM Torque	45.256 Nm	44.793 Nm	1.02
LM Torque	45.256 Nm	44.793 Nm	1.02
RO Torque	117.125 Nm	125.184 Nm	6.88
LO Torque	117.119 Nm	125.026 Nm	6.75
RH Torque	124.908 Nm	126.370 Nm	1.17
RK Torque	48.927 Nm	49.902 Nm	1.99
RA Torque	94.509 Nm	81.034 Nm	14.26
LH Torque	124.900 Nm	126.339 Nm	1.15
LK Torque	48.926 Nm	49.902 Nm	1.99
LA Torque	94.518 Nm	81.278 Nm	14.00
TRK Torque	50.200 Nm	51.196 Nm	1.98
TLK Torque	50.200 Nm	51.196 Nm	1.98
TRA Torque	201.918 Nm	183.364 Nm	9.19
TLA Torque	201.921 Nm	183.545 Nm	9.10

8.3.2 Geometrical parameters

To analyze this second group of parameters, the geometrical characteristics of the orthosis were subjected to increments, as well as their moments of inertia according to the procediment explained in Section 8. The evolution of design parameters will only be displayed for 1 and 10% increasements in the orthosis parameters, as those two increments are enough to calculate the evolution of the studied parameters. The progression of the metabolical cost will be shown for every implemented growths (1, 2, 5 and 10%).

The reference values (appearing in Table…) of the parameters right commented were multiplied by 1.01, ans the referred to the inertia by the square of 1.01, obtaining the next values:

Table 8-10: Geometry and inertia values after increasing geometry 1%

Parameter	Value
Distance from K to Gt	0.1313 m
Inertia of the thigh bars about Gt	1.56e-3 kgm^2
Distance from A to Gs	0.1717 m
Inertia of the shank bars about Gs	0.004858 kgm^2
Distance from A to Gf (vertical)	0.0707 m
Distance from A to Gf (horizontal)	0.0404 m
Inertia of the foot support about Gf	0.000113 kgm^2

Then, a 10% increment was implemented, resulting the next values:

Table 8-11: Geometry and inertia values after increasing geometry 10%

Parameter	Value
Distance from K to Gt	0.143 m
Inertia of the thigh bars about Gt	1.85e-3 kgm^2
Distance from A to Gs	0.187 m
Inertia of the shank bars about Gs	0.005762 kgm^2
Distance from A to Gf (vertical)	0.077 m
Distance from A to Gf (horizontal)	0.044 m
Inertia of the foot support about Gf	0.000134 kgm^2

May the evolution of the generalized coordinates be displayed as follows (the reference motion corresponds to the blue line, the 1% increasement solution to the red line, and the 10% solution to the green line):
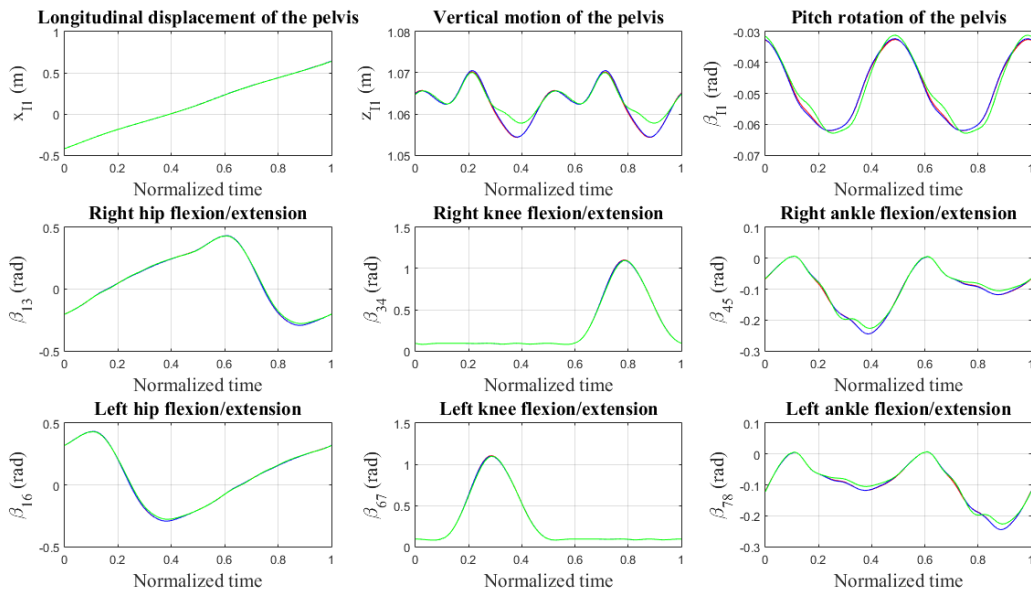
Figure 8-32: Generalized coordinates after increasing geometry 1 and 10%

There are no large discrepancies between the motion pattern and the resulting solutions, even in the one obtained after implementing a 10% increment. The only issues to remark are the lower fluctuations in the vertical motion of the pelvis, due to the reached stability at increasing the moment of inertia. These fluctuations are slightly lower now than the ones appearing after only increasing the mass, as the inertia is proportional to the square of the length, and grows much more than increasing the mass.
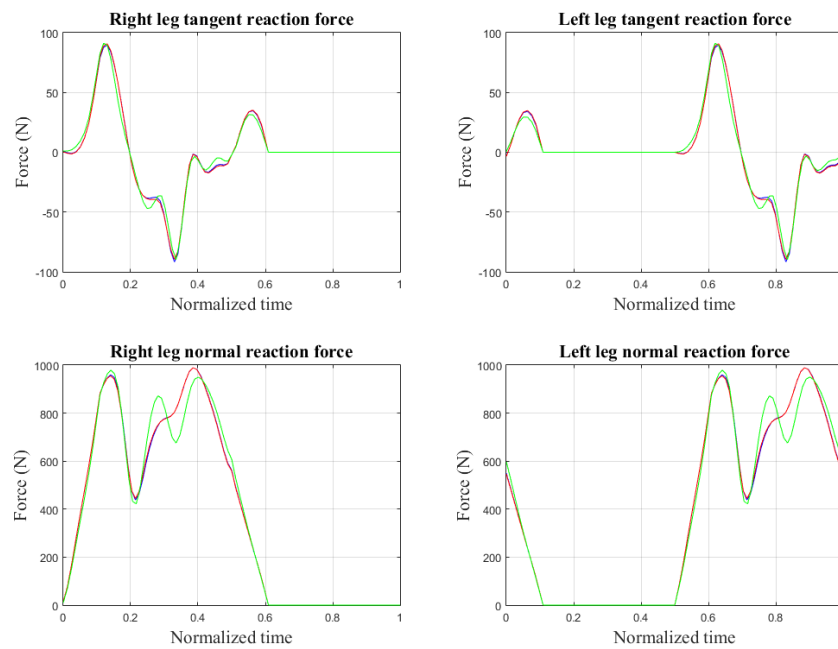
Figure 8-33: Reaction forces after increasing geometry 1 and 10%

The more remarkable fact concerning the reaction forces deals with bigger oscillations observed in the normal reactions. Newly, the larger moment of inertia serves as explanation to this phenomenon. This makes the feet to shake while supporting the feet on the ground, and this shake produces a more inconsistent reaction from the ground. Otherwise, no more important changes with respect to the reference are appreciated.

Now it is the moment to analyze the evolution of the torque. As made before, first the torque generated by the mechanical devices is studied, then the one originated in the joints (hip, ankles and knees), and by last, the combined contribution of every torques (only in the knees and the ankles, as there are no devices in the hips).
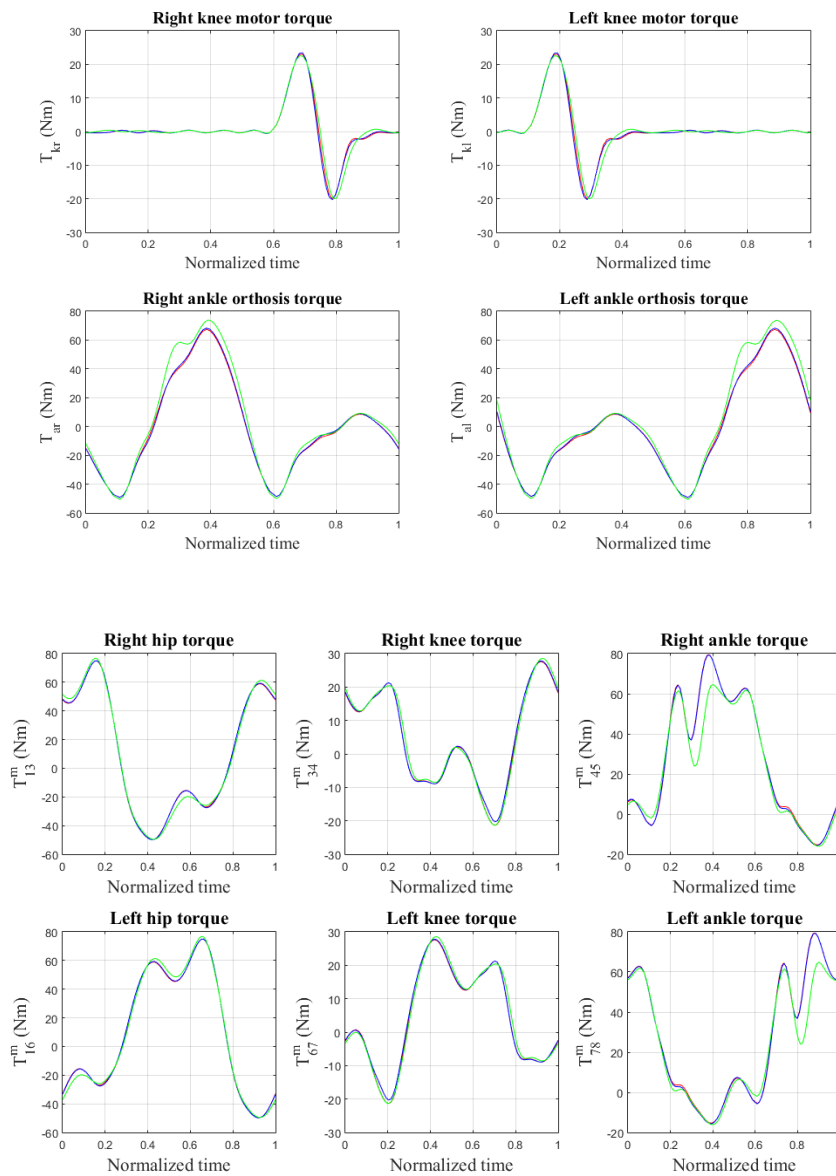
Figure 8-34: Joint, motor and Klenzak torques after increasing geometry 1 and 10%
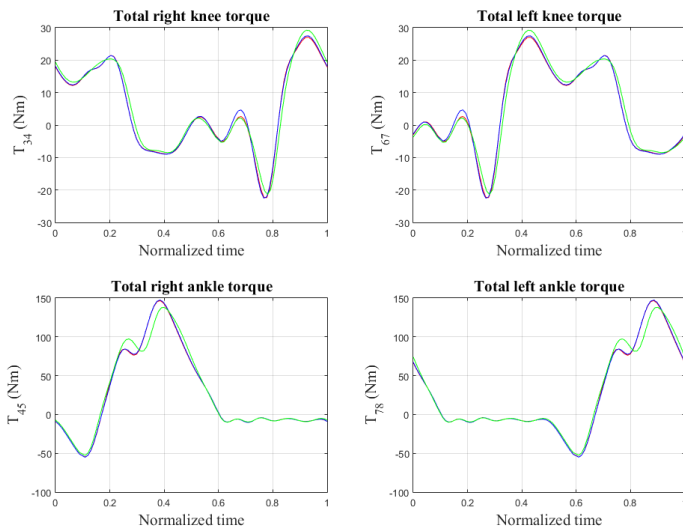
Figure 8-35: Total torques after increasing geometry 1 and 10%

As it happened when the mass was increased, increments in the geometrical characteristics only affect significantly to the torques produced in ankles. First of all, the hip and the knee torques stay with next to no change during the cycle. Secondly, the Klenzak ankle torque is little bigger in the optimization, allowing the human ankle not to make a big effort to move itself. This fact is confirmed in the plots representing the torque in the ankle, which is significantly smaller when the foot is in the air, after increasing a 10% the geometrical features.
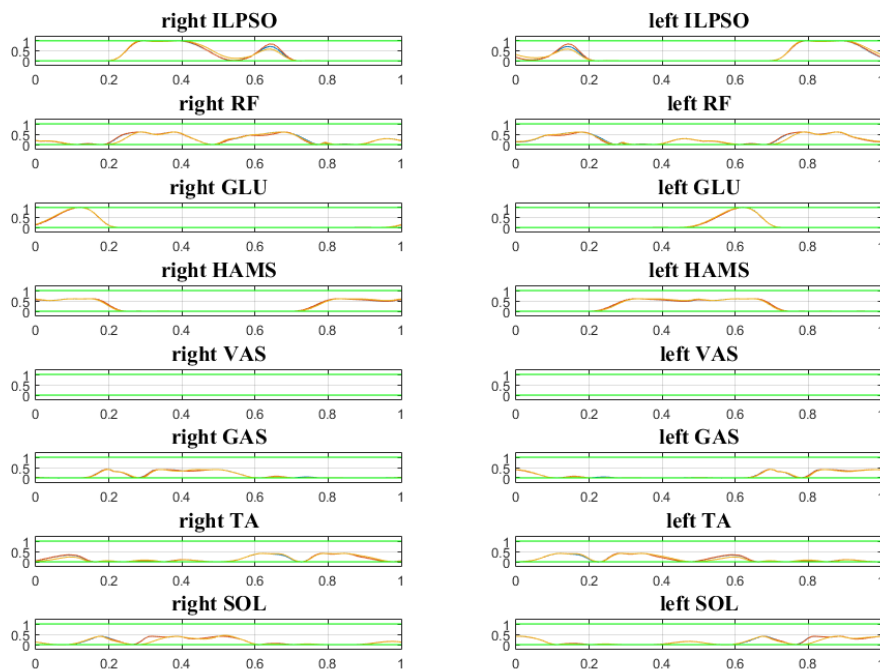
Figure 8-36: Activation and excitation after increasing geometry 1 and 10%

Concerning the activation and excitation graphics (shown in the figure above), the activation is represented with a black line (reference motion), red line (1% solution) and yellow line (10% solution), while the neural excitation is referred with blue, green and cyan lines, respectively. The more standing out fact is the delay in the activation observed in some muscles, like the soleus or the RF. This may well be the result of a more optimal found solution, where the muscle takes a longer time to get activated.

With respect to the evolution of metabolical cost and deviation, the Table collects the following results:

Table 8-12: Evolution of expenditure and deviation when increasing geometry

Geometry increasement	Metabolical expenditure	Deviation from pattern
0 % (Reference)	341.74 J	15.198
1 %	339.56 J	15.096
2 %	333.75 J	14.770
5 %	333.82 J	14.795
10 %	334.26 J	14.836

This time, the lower metabolical cost is reached after implementing a 2% growth to the studied parameter, the geometry of the orthosis. This growth intervenes directly in the inertia, being the moment of inertia proportional to the square of the length. That makes the orthosis more sensitive to this changes than when increasing the mass (only proportional to the moment of inertia), and that provokes that an too large growth could make the walker to spend too much energy to move the orthosis.

The results just displayed can be summarized in the Table 8-12.

Table 8-13. Quantitative summary of geometry influence

Variable	Highest amplitude, 1st increment	Highest amplitude, 2nd increment	Relative increasement (%)
x_{11}	1.061 m	1.059 m	0.26
z_{11}	0.016 m	0.012 m	22.87
β_{11}	0.030 rad	0.032 rad	7.35
β_{13}	0.726 rad	0.709 rad	2.26
β_{34}	1.026 rad	1.018 rad	0.72
β_{45}	0.252 rad	0.234 rad	7.07
β_{16}	0.726 rad	0.709 rad	2.26
β_{67}	1.026 rad	1.018 rad	0.72
β_{78}	0.252 rad	0.234 rad	7.18
RT Force	180.361 N	180.902 N	0.56
RN Force	989.352 N	979.053 N	0.73
LT Force	180.333 N	180.777 N	0.61
LN Force	989.354 N	979.062 N	0.73
RM Torque	45.215 Nm	44.752 Nm	1.02
LM Torque	45.215 Nm	44.752 Nm	1.02
RO Torque	116.692 Nm	124.529 Nm	6.88
LO Torque	116.685 Nm	124.369 Nm	6.75
RH Torque	124.829 Nm	126.397 Nm	1.17
RK Torque	48.999 Nm	49.898 Nm	1.99
RA Torque	94.668 Nm	80.743 Nm	14.26
LH Torque	124.820 Nm	126.362 Nm	1.15
LK Torque	48.999 Nm	49.899 Nm	1.99
LA Torque	94.679 Nm	80.990 Nm	14.00
TRK Torque	50.351 Nm	51.524 Nm	1.98
TLK Torque	50.351 Nm	51.525 Nm	1.98
TRA Torque	201.584 Nm	182.525 Nm	9.19
TLA Torque	201.587 Nm	182.706 Nm	9.10

8.3.3   Mass and geometrical characteristics combined

The third phase in the parameters analysis is indeed a combination of the two first phases right studied. Now, the effects on inertia will be especially important, as both the mass and the geometrical features intervene in the moments of inertia. Therefore, following the procediment explained in section 8, the increment imposed will be cubed.

Moreover, these changes represent a more accurate global view of reality, in that when an orthesis is modified in the real life, mass and geometry should not be changed independently if the density, and so on, the material, must remain with no changes. So, the plots about to be shown reflect a more reliable result.

Taking the same values for the mass and geometry as the shown when 1 and 10% increasements were imposed, the only new magnitudes are the moments of inertia, which gets multiplied by the cube of the growth.

Tables 8-14 and 8-15: Inertial values after increasing mass and geometry 1 and 10%

Parameter	Value
Inertia of the thigh bars about Gt	$1.575\text{e-}3$ kgm^2
Inertia of the shank bars about Gs	0.00491 kgm^2
Inertia of the foot support about Gf	0.000114 kgm^2

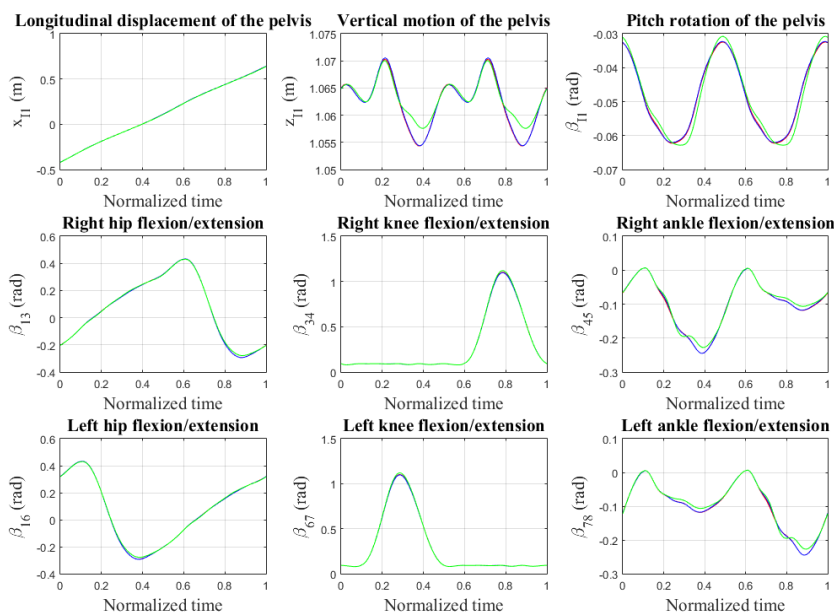| Parameter	Value
Inertia of the thigh bars about Gt	$2.035\text{e-}3$ kgm^2
Inertia of the shank bars about Gs	0.006343 kgm^2
Inertia of the foot support about Gf	0.000147 kgm^2

Figure 8-37: Generalized coordinates after increasing mass and geometry 1 and 10%

Similar results to both the first and second phases in parameterization are found for generalized coordinates, as expected. The 10% solution makes to get newly a major stability during the walking, decreasing the swings in the vertical coordinate of the pelvis (a 30% reduction is obtained). Moreover, following in the pelvis, the pitch angle is a little delayed, what means that the motion gets performed with a very little lag, but does not affect to the movement in a big way. The last noteworthy aspect is the smaller angle obtained in the ankles, possibly because it is more optimal in terms of metabolical cost.
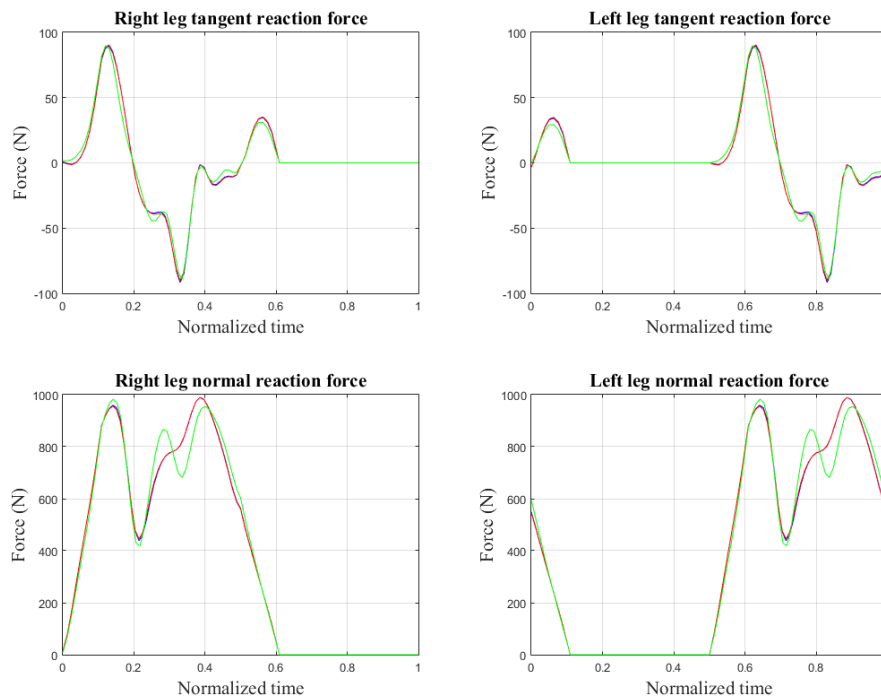
Figure 8-38: Reaction forces after increasing mass and geometry 1 and 10%

The figure above shows the evolution of the reaction forces emerging from the floor. As waited and already observed when studying the mass and geometry influence separately, the biggest fluctuations appear in the normal reactions (around 30-40% over the reference value), due to the same reason as before: the little shake the foot experiments when it gets in contact with the floor. Otherwise there are no other important variations from the reference pattern, neither when implementing a 10% variation.
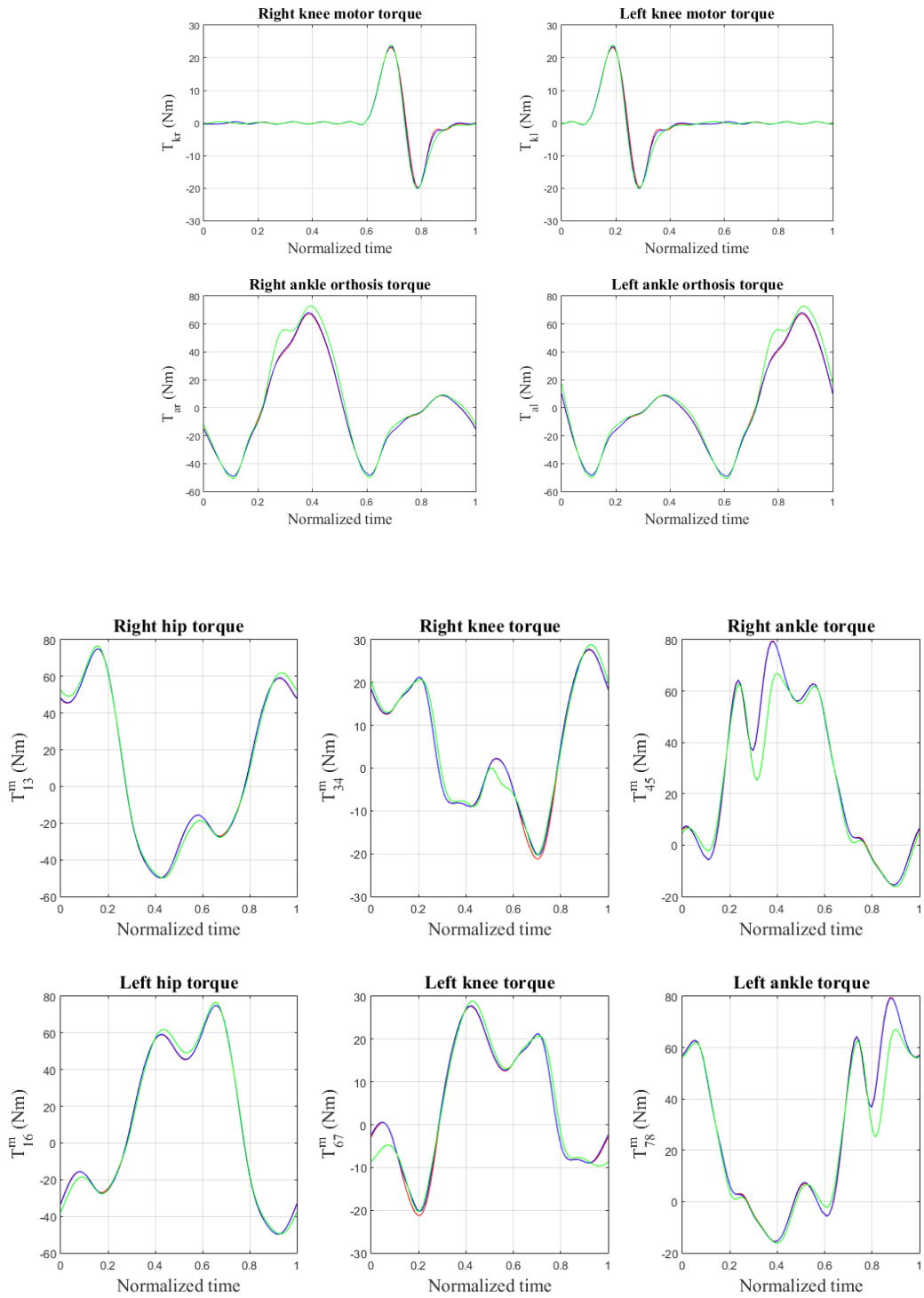
Figure 8-39 and 8-40: Joint, motor and Klenzak torques after increasing mass and geometry 1 and 10%
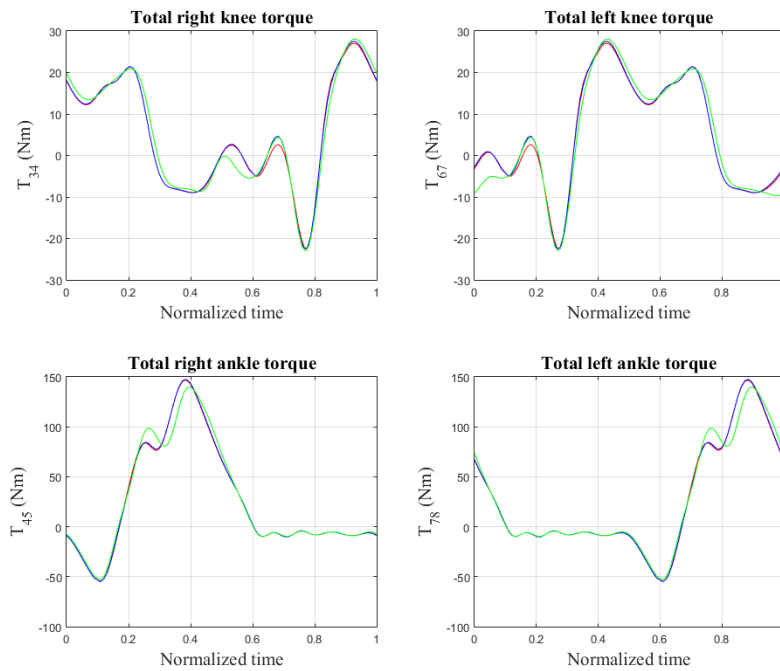
Figure 8-41: Total torques after increasing mass and geometry 1 and 10%

Analyzing the produced torque following the same way as in the previous subsection, a larger torque generated by the flexible ankle is still observed when supporting the feet in the floor, and counterbalanced with a simultaneous smaller torque in the same zone generated by the human ankle. There is also a newness now: a tiny discrepance, around 10 Nm, in the left knee at the beginning of the cycle. The knee can perform the movement by producing less par, thanks to the power supplied by the motor.
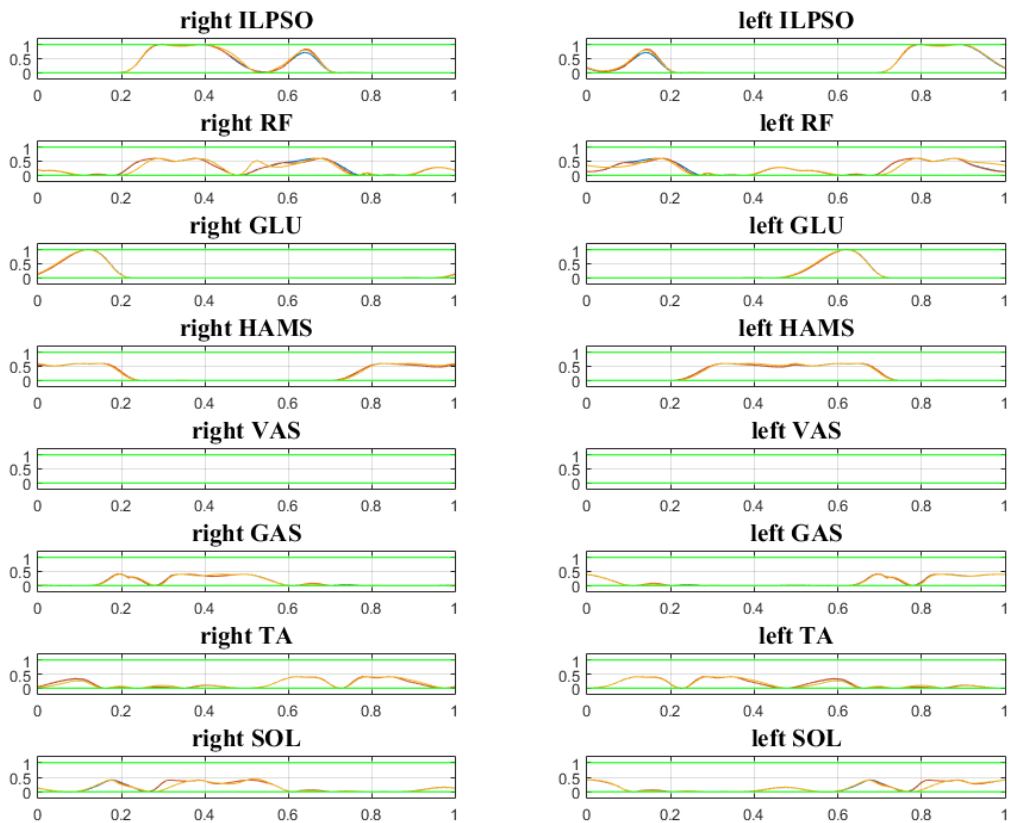
Figure 8-42: Activation and excitation after increasing mass and geometry 1 and 10%

The activation and excitation figure shows no important deviations from the pattern. The only outstanding fact is the absence of any excitation (and thus, activation) in the VAS, as it does not intervene in the walking cycle.

Concerning the metabolical cost evolution during the cycle, the Table shows the following values:

Table 8-16: Evolution of expenditure and deviation when increasing mass and geometry 1 and 10%

Mass and geometry increasement	Metabolical expenditure	Deviation from pattern
0 % (Reference)	341.74 J	15.198
1 %	335.74 J	14.953
2 %	333.75 J	14.770
5 %	334.99 J	14.864
10 %	338.49 J	14.964

As expected, the smallest value for both the metabolical cost and the deviation from reference is reached after imposing the 2% increasement. It was expected because, as it was seen in the previous subsection,

only by increasing the geometry, a 5% growth made the metabolical cost higher. Now, the effect of the mass and the geometry gets combined, making the moment of inertia to be rising with the cube.

The Table 8-17 summarizes in a quantitative way the results just seen.

Table 8-17. Quantitative summary of combined mass and geometry influence

Variable	Highest amplitude, 1st increment	Highest amplitude, 2nd increment	Relative increasement (%)
x_{11}	1.061 m	1.058 m	0.29
z_{11}	0.016 m	0.012 m	22.21
β_{11}	0.030 rad	0.032 rad	7.54
β_{13}	0.726 rad	0.710 rad	2.20
β_{34}	1.024 rad	1.041 rad	1.67
β_{45}	0.252 rad	0.235 rad	6.81
β_{16}	0.726 rad	0.710 rad	2.20
β_{67}	1.024 rad	1.041 rad	1.67
β_{78}	0.252 rad	0.235 rad	6.93
RT Force	180.752 N	179.202 N	0.86
RN Force	989.339 N	982.934 N	0.65
LT Force	180.654 N	179.084 N	0.87
LN Force	989.335 N	982.950 N	0.65
RM Torque	45.308 Nm	46.158 Nm	1.87
LM Torque	45.308 Nm	46.158 Nm	1.87
RO Torque	116.662 Nm	123.986 Nm	6.28
LO Torque	116.660 Nm	123.828 Nm	6.14
RH Torque	124.861 Nm	126.609 Nm	1.40
RK Torque	48.950 Nm	49.100 Nm	0.31
RA Torque	94.872 Nm	83.122 Nm	12.39
LH Torque	124.806 Nm	126.270 Nm	1.17
LK Torque	48.949 Nm	49.107 Nm	0.32
LA Torque	94.881 Nm	83.354 Nm	12.15
TRK Torque	50.415 Nm	51.946 Nm	3.04
TLK Torque	50.415 Nm	51.948 Nm	3.04
TRA Torque	201.720 Nm	185.514 Nm	8.04
TLA Torque	201.726 Nm	185.694 Nm	7.95

8.3.4　Weight coefficients of the cost function

The fourth phase in the analysis of the responsiveness of the orthosis to changes in their parameters will not consist on manipulating a intrinsical parameter of the orthosis itself, but it will only deals with the optimization problem, concretely the cost function, defined in Section 6. The weight coefficients will be modified so as to give more importance to one of the following features: the metabolical expenditure (represented with the coefficient w_E) and the deviation from the reference pattern (weighted by the coefficient w_J), just as explained in Section 6.

So far, these coefficients have always been 1, so the same importance has been given to both the metabolical cost and the discrepance with the reference motion. In this analysis, each coefficient will be given the values of 1.5 and 3, while remaining the other one with no change.

8.3.4.1　Coefficient w_E

In the next figures the result of give more emphasis to metabolical cost in the optimization problem will be displayed. As usual, the reference motion is represented by the blue line. The motion obtained after imposing w_E=1.5 appears as a red line, while the green line refers to the motion after increasing w_E to 3.
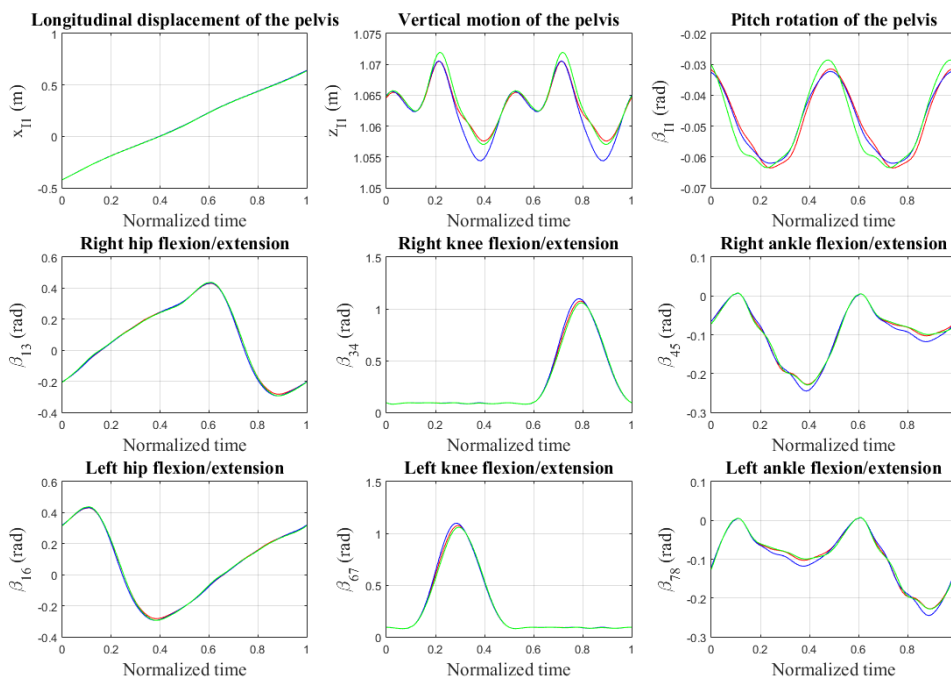
Figure 8-43: Generalized coordinates after imposing w_E=1.5 and 3

The introduced changes are really important, especially the second one, as it gives three times more weight to the expenditure over the deviation. Watching the generalized coordinates evolution in the figure above, the resemblance between solutions is the prevailing trend, the biggest discrepancies appearing in the pelvis, as it happened before. The gain imposed to this weight factor makes more stable the walking cycle, as the

oscilations are smaller. Moreover, the vertical coordinate is somewhat higher, being this one a more interesting solution in energetical terms. The flexion and extension of the ankle experiments a vaguely smaller variation in this approximation.

Now the reaction forces in the contact will be reviewed:

Figure 8-44: Reaction forces after imposing w_E=1.5 and 3
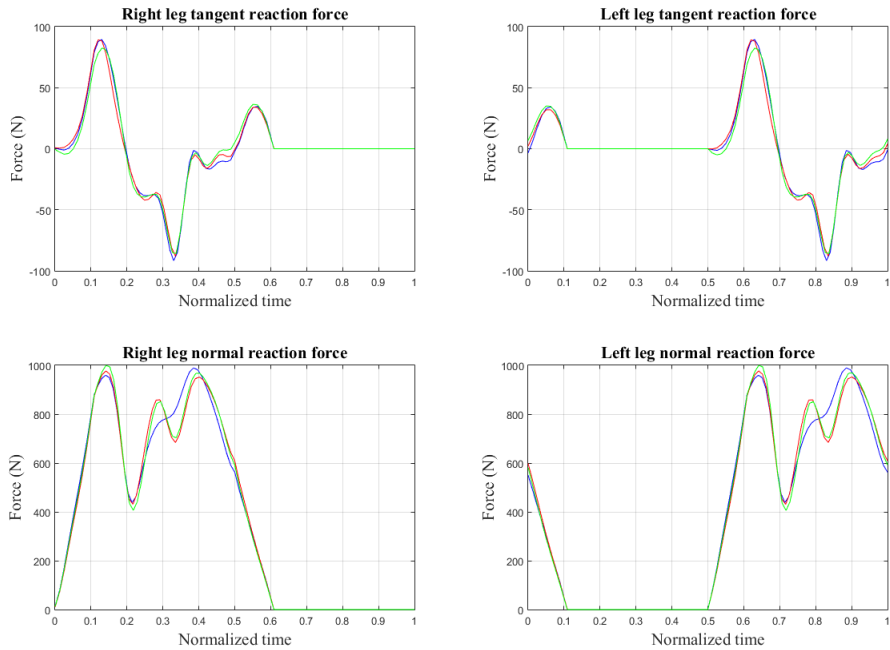
The most important detail to comment held in the largest fluctuation appearing in the normal reactions when holding the foot on the floor, the same way as in previous phases in the analysis. No more deviations are outstanding.
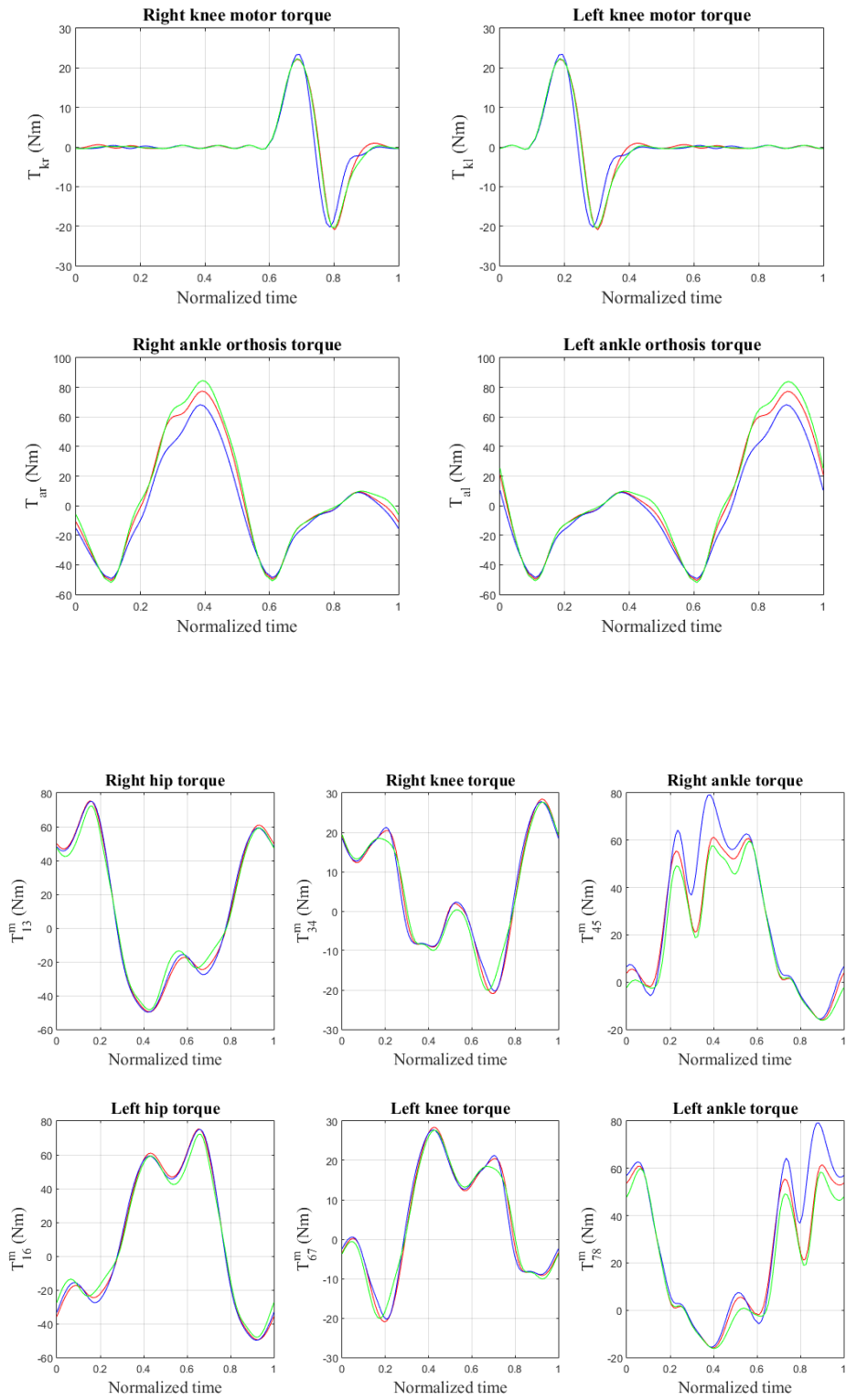
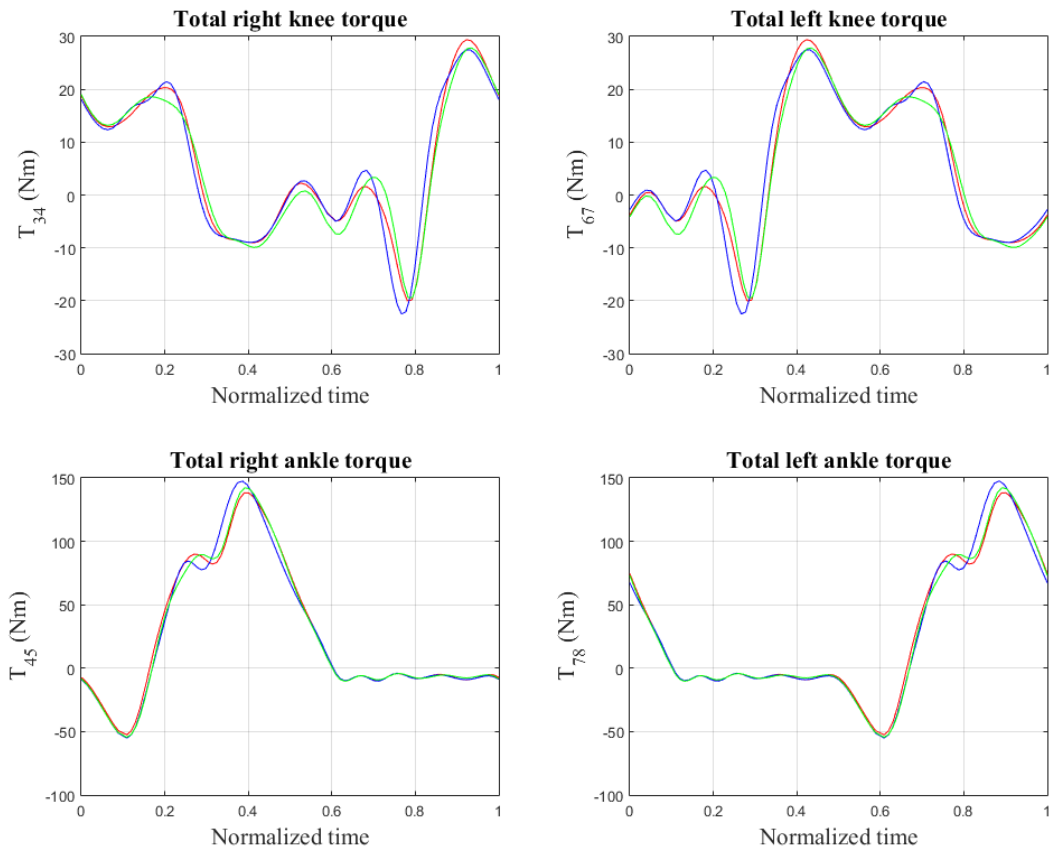Figure 8-45: Joint, motor and Klenzak after imposing w_E=1.5 and 3

Figure 8-46: Total torques after imposing w_E=1.5 and 3

Concerning the torque moments, biggest differences with respect to the reference appear in the ankle, as happened in other sections. Although it will be commented later, it seems the ankle is the most affected part of the musculoskeletal body during the walking cycle. Watching the graphics, the mechanical torque produced by the Klenzak ankle gets increased a 30% when the coefficient wE is imposed to be 3. Simultaneously, the moment originated in the human ankle is way smaller (a 25% between the reference and the solution), what is logical as the metabolical cost is getting much more importance now, and the optimization algorithm has found a very optimal solution which allows to reduce the torque in the joints, and so on the stress in that zone. Deviations are slightly larger than in previous cases because their reduction is being given less importance than the metabolical cost in the cost function.

The total torque plots display that the resulting moment is slightly smaller in the solutions, although the reduction is difficult to appreciate. It can be considered that the Klenzak ankle compensates the little torque in the human ankle.
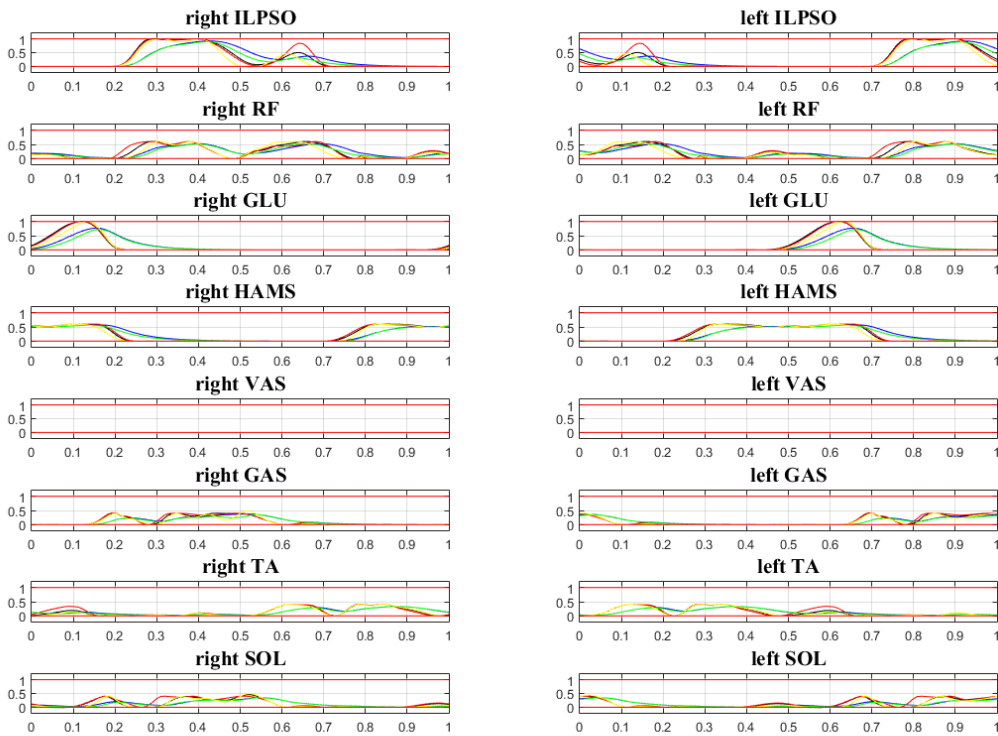
Figure 8-47: Activation and excitation after imposing w_E=1.5 and 3

The figures above show the evolution of the activation and the neural excitation for each muscle. The table below indicates the meaning of each line:

Table 8-18. Key table for activation-excitation plots

Solution	Activation	Neural excitation
Reference	Blue	Black
When wE = 1.5	Green	Red
When wE = 3	Cyan	Yellow

Observing the plots right presented it is worth mentioning a fact already commentated when analyzing the torque generated. It was determined that the moment exerted by the muscles was smaller by making the first weight coefficient to be 3 (especially in the ankles, where the reduction reached a 25% from the reference). So it is logical to wait the activation and excitation to get reduced as well. And that is what is observed in the figure. The cyan and yellow lines displayed prove the activation and excitation are way smaller when amplifying wE.

Now, the Table 8-18 displays the evolution of the energetic cost:

Table 8-19: Evolution of expenditure and deviation when imposing w_E=1.5 and 3

w_E	Metabolical expenditure	Deviation from pattern
1 (Reference)	341.74 J	15.198
1.5	326.42 J	14.866
3	297.88 J	15.532

The metabolical cost decreases considerably when increasing w_E, almost a 15% when trebling the coefficient w_E. This is not surprising, as the cost function is focused on reducing the energetical expenditure in the optimization problem. On the other hand, the deviation pattern increases for $w_E = 1.5$ and decreases for $w_E = 3$, just like happened in the activation of the gluteus.

The Table 8-19 includes the quantitative information appearing in the graphics just shown:

Table 8-20. Quantitative summary of coefficient w_E influence

Variable	Highest amplitude, 1st increment	Highest amplitude, 2nd increment	Relative increasement (%)
x_{11}	1.059 m	1.058 m	0.07
z_{11}	0.013 m	0.015 m	15.22
β_{11}	0.032 rad	0.035 rad	8.73
β_{13}	0.714 rad	0.732 rad	2.48
β_{34}	0.997 rad	0.981 rad	1.57
β_{45}	0.236 rad	0.238 rad	0.79
β_{16}	0.714 rad	0.732 rad	2.48
β_{67}	0.997 rad	0.981 rad	1.58
β_{78}	0.236 rad	0.237 rad	0.45
RT Force	177.395 N	168.331 N	5.11
RN Force	977.307 N	999.653 N	2.29
LT Force	177.258 N	168.259 N	5.08
LN Force	977.321 N	999.678 N	2.29
RM Torque	45.261 Nm	44.761 Nm	1.10
LM Torque	45.261 Nm	44.761 Nm	1.10
RO Torque	128.130 Nm	136.605 Nm	6.61
LO Torque	127.993 Nm	135.999 Nm	6.26
RH Torque	124.950 Nm	120.608 Nm	3.48
RK Torque	49.405 Nm	47.803 Nm	3.24
RA Torque	77.245 Nm	75.841 Nm	1.82
LH Torque	124.914 Nm	120.301 Nm	3.69
LK Torque	49.412 Nm	47.804 Nm	3.25
LA Torque	77.457 Nm	76.127 Nm	1.72
TRK Torque	50.309 Nm	48.242 Nm	4.11
TLK Torque	50.310 Nm	48.241 Nm	4.11
TRA Torque	190.808 Nm	188.304 Nm	1.31
TLA Torque	190.843 Nm	188.782 Nm	1.08

8.3.4.2 Coefficient w_J

After studying the influence of giving more emphasis to the metabolical cost by making the coefficient wE bigger, now it is the moment to study the effect provoked by increasing the other coefficient in the cost function, w_J. As already described, this coefficient measures the weight of the deviation from the reference motion pattern when performing the optimization problem. The procediment is analog to the one right followed: the coefficient is multiplied by 1.5 (red lined solutions) and 3 (green lined solutions), and they will

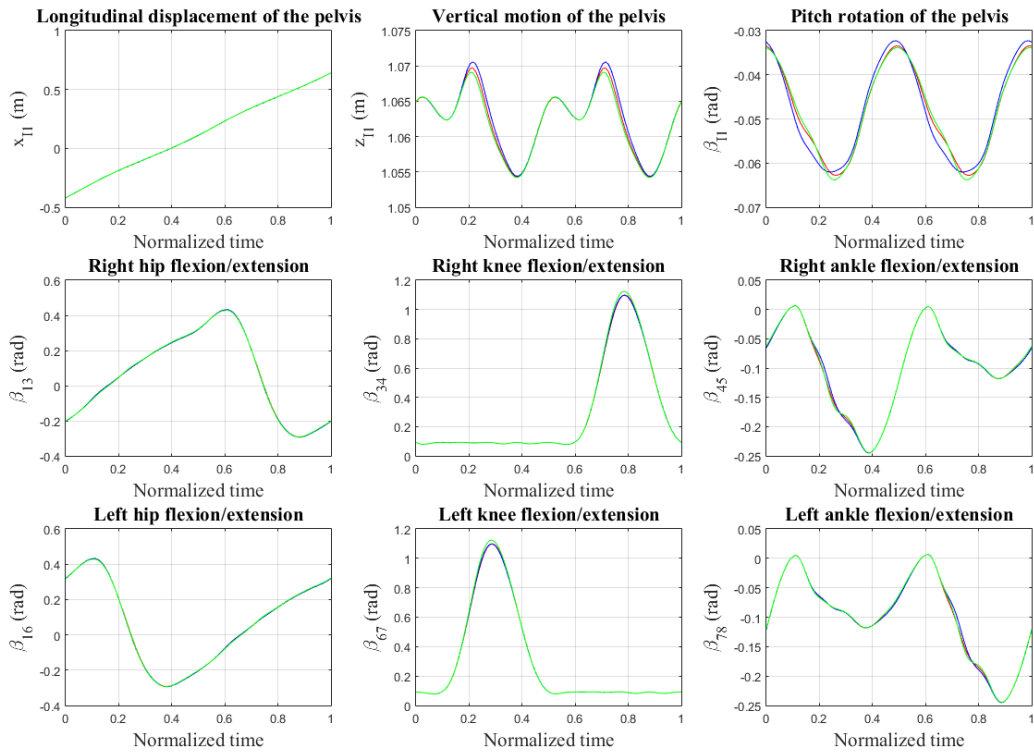be compared to the reference (blue lined solutions).

Figure 8-48: Generalized coordinates after imposing w_J=1.5 and 3

The solutions follow the reference pattern and it can be said there are hardly variations in any coordinates. This can be considered as expected as the effect of giving more emphasis the deviation from the reference motion will make the optimization algorithm to find a solution minimizing the differences from the pattern. As it happened when changing other parameters, the pelvis is the zone where there are more discrepancies, but now they are almost unnoticeable.

Similar conclusions can be reached after analyzing the reaction forces, the torque moments and the activation and excitation.
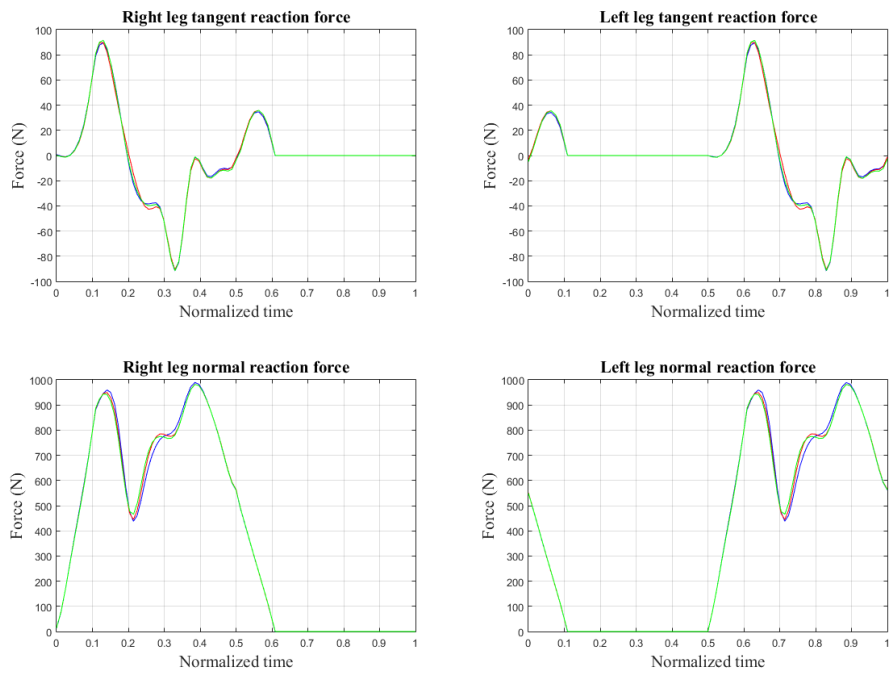
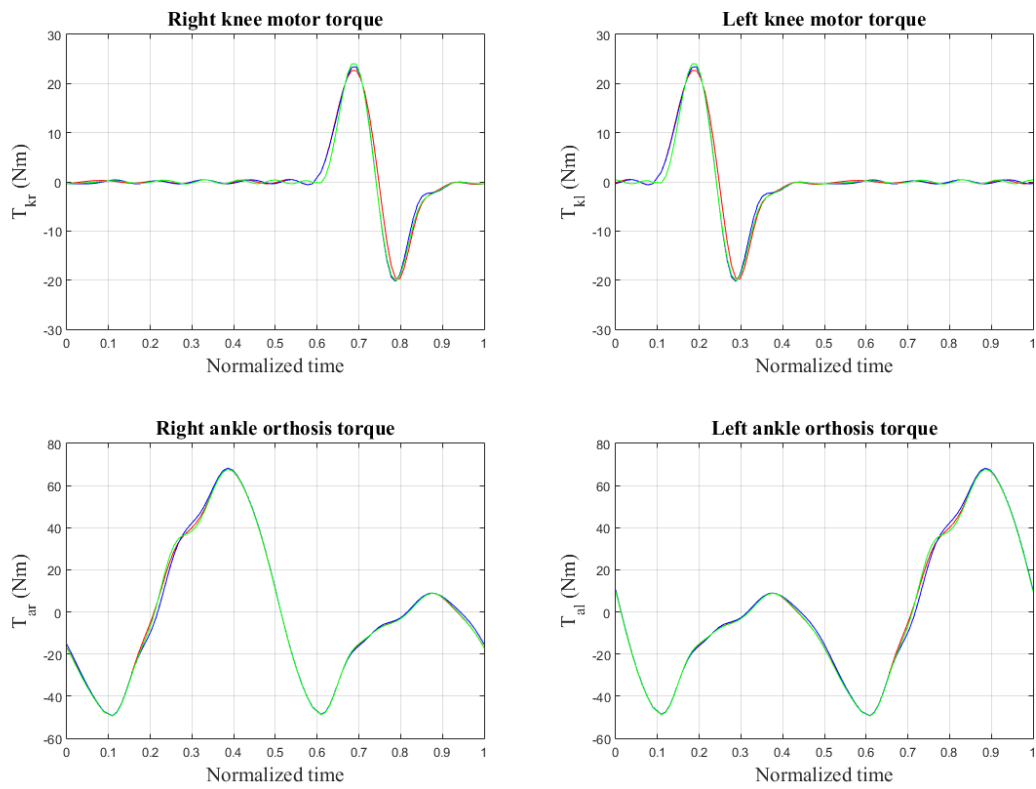Figure 8-49: Reaction forces after imposing w_J=1.5 and 3

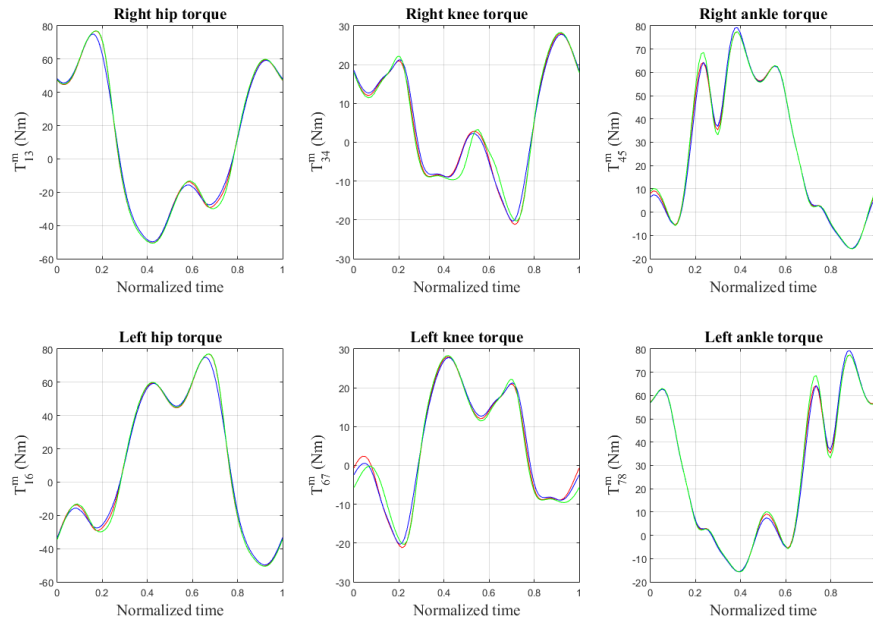Figure 8-50: Motor and Klenzak torques after imposing w_J=1.5 and 3

Figure 8-51: Joint torques after imposing w_J=1.5 and 3
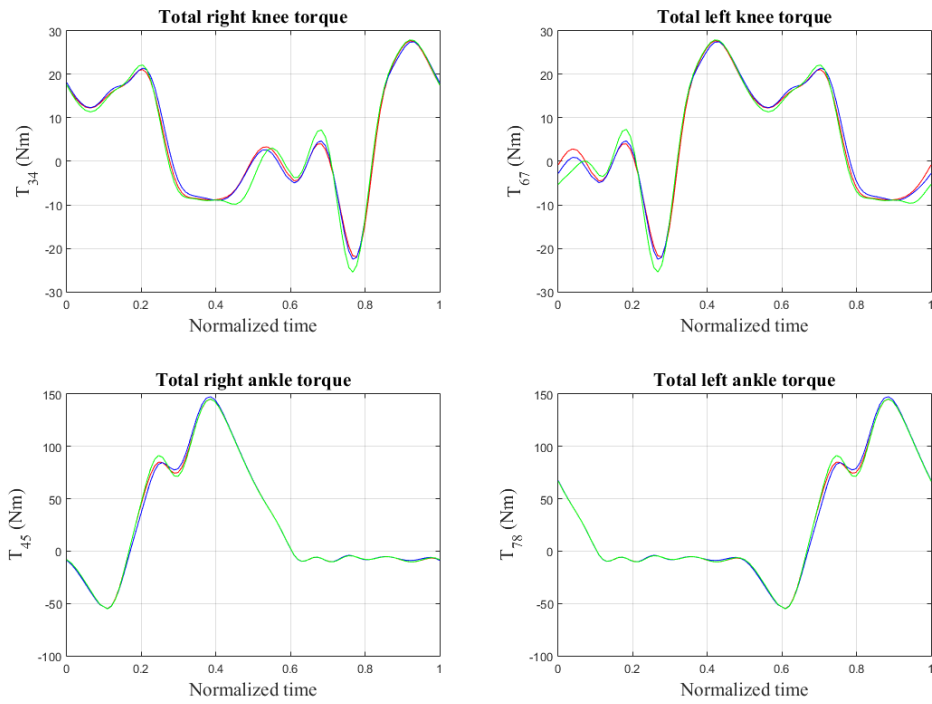
Figure 8-52: Total torques after imposing w_J=1.5 and 3

Small disagreements appear in the knee total torque, in particular when the coefficient wJ is 3. The oscillation of the torque is now slightly larger, although the discrepancy is not important enough to consider a change in the trend.
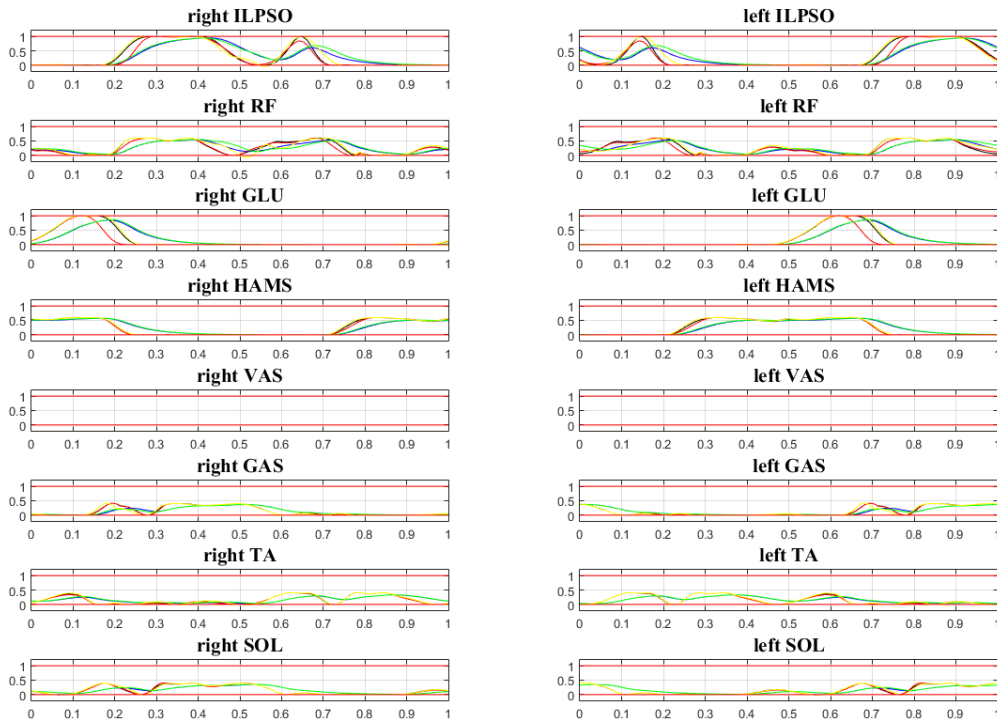
Figure 8-53: Activation and excitation after imposing w_J=1.5 and 3

Following the same colour code as described in the previous subsection, a curious fact can be observed in the gluteus. Taking $w_J = 1.5$, the gluteus activation (red-lined) gets sooner than the reference does, but when increasing the coefficient to 3 (yellow-lined), the activation gets the same time, practically, as the reference (black-lined) does.

This inconsistency apparently may occur because the algorithm has found a more optimal solution by finishing the gluteus activation before. It is worth mentioning this circumstance only appears in the gluteus; in the rest of the muscles intervening on the cycle, the activation gets sooner when w_J gets the 1.5 value rather than it is 3.

Now, the Table 8-20 displays the evolution of the energetic cost:

Table 8-21: Evolution of expenditure and deviation when imposing w_J=1.5 and 3

wJ	Metabolical expenditure	Deviation from pattern
1 (Reference)	341.74 J	15.198
1.5	365.96 J	14.906
3	382.22 J	14.831

Contrary to increasing the first weight coefficient, now the goal of the objective function is to reduce the deviation from the reference, as it was checked in the displays just finished. The metabolical expenditure gets increased while the deviation gets decreased, but in a small way. The decreasement calculated in the deviation from the pattern only gets a 7%, much smaller than the obtained when changing the wE coefficient, when the metabolical cost decreased a 15%.

A quantitative vision of the influence exerted by this second coefficient appear in the Table 8-21:

Table 8-22. Quantitative summary of coefficient w_J influence

Variable	Highest amplitude, 1st increment	Highest amplitude, 2nd increment	Relative increasement (%)
x_{11}	1.061 m	1.061 m	0.01
z_{11}	0.015 m	0.015 m	3.57
β_{11}	0.029 rad	0.030 rad	2.23
β_{13}	0.723 rad	0.723 rad	0.02
β_{34}	1.021 rad	1.045 rad	2.40
β_{45}	0.252 rad	0.252 rad	0.08
β_{16}	0.723 rad	0.723 rad	0.02
β_{67}	1.021 rad	1.045 rad	2.40
β_{78}	0.252 rad	0.252 rad	0.08
RT Force	180.428 N	182.947 N	1.40
RN Force	981.786 N	981.654 N	0.01
LT Force	180.377 N	182.864 N	1.38
LN Force	981.786 N	981.652 N	0.01
RM Torque	44.509 Nm	46.404 Nm	4.26
LM Torque	44.509 Nm	46.404 Nm	4.26
RO Torque	117.137 Nm	117.246 Nm	0.09
LO Torque	117.133 Nm	117.243 Nm	0.09
RH Torque	127.532 Nm	127.758 Nm	0.18
RK Torque	49.220 Nm	48.571 Nm	1.32
RA Torque	93.168 Nm	93.274 Nm	0.11
LH Torque	127.481 Nm	127.730 Nm	0.20
LK Torque	49.218 Nm	48.624 Nm	1.21
LA Torque	93.175 Nm	93.282 Nm	0.11
TRK Torque	50.548 Nm	54.210 Nm	7.24
TLK Torque	50.549 Nm	54.188 Nm	7.20
TRA Torque	200.229 Nm	200.447 Nm	0.11
TLA Torque	200.231 Nm	200.450 Nm	0.11

8.3.5 Maximum orthosis torque

This part of the analysis will consist on increasing the maximum value the orthosis motor can generate, and evaluate how it influences in the walking and energy expenditure. In order to see better the effect of changing the maximum torque, the increments implemented have been way bigger than usual, so that the first increment consisted on a 25% over the reference value (24 Nm, its paraemeters are represented with a red lined), and the second one a 100% over the same one (40 Nm, green lined parameters). The reference remains represented

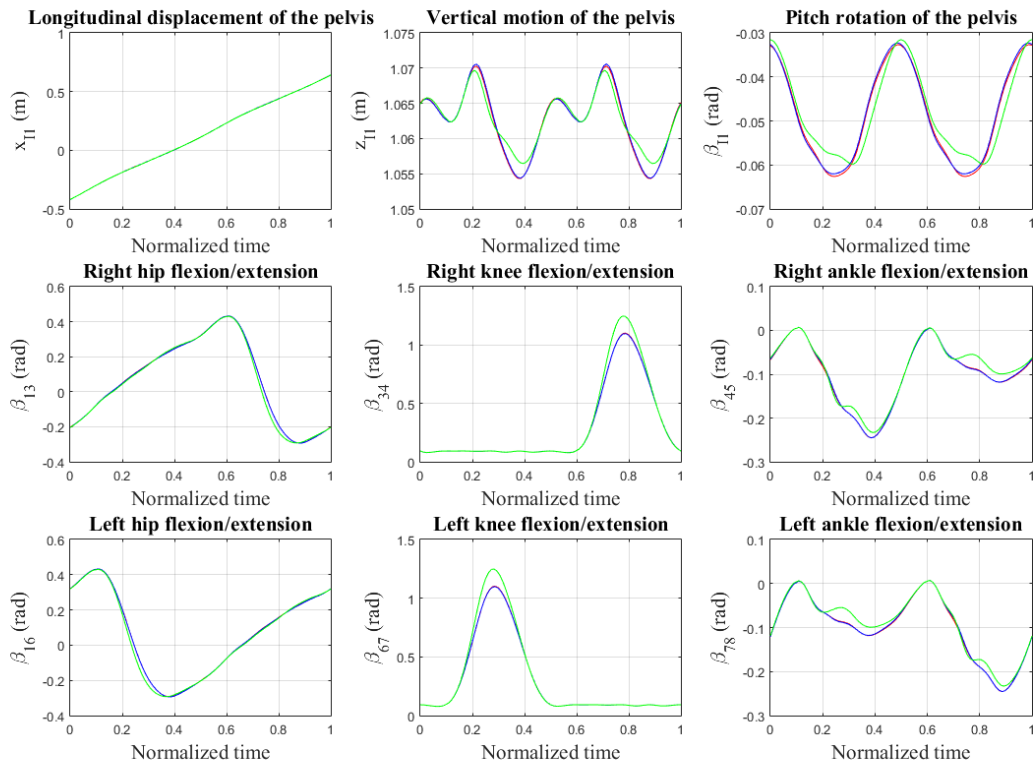with a blue line. Results are displayed as follows:

Figure 8-54: Generalized coordinates after increasing maximum orthosis torque

The Figure shows that increasing only a 25% the maximum possible torque, even being an important increment compared to other made in this research, hardly makes the coordinates to change from the reference. The red line even overlays the blue, due to their similarities between them. So, the most interesting to study is clearly the solution obtained after the 100% increasing imposed to the motor torque, placed in the knee.

Given that the motor has a wider range of torque to exert, it makes also bigger the range of angles possible to be performed by the joints, especially in the knee (the place where the motor is located). The peak in the knee flexion/extension movement is a 25% bigger now.

The other conclusion reached is not new: the pelvis motion is more stable, because the motor provides an additional moment with stabilizes the body, and so on, the walking. This effect can be observed in both the vertical motion and the pitch rotation.
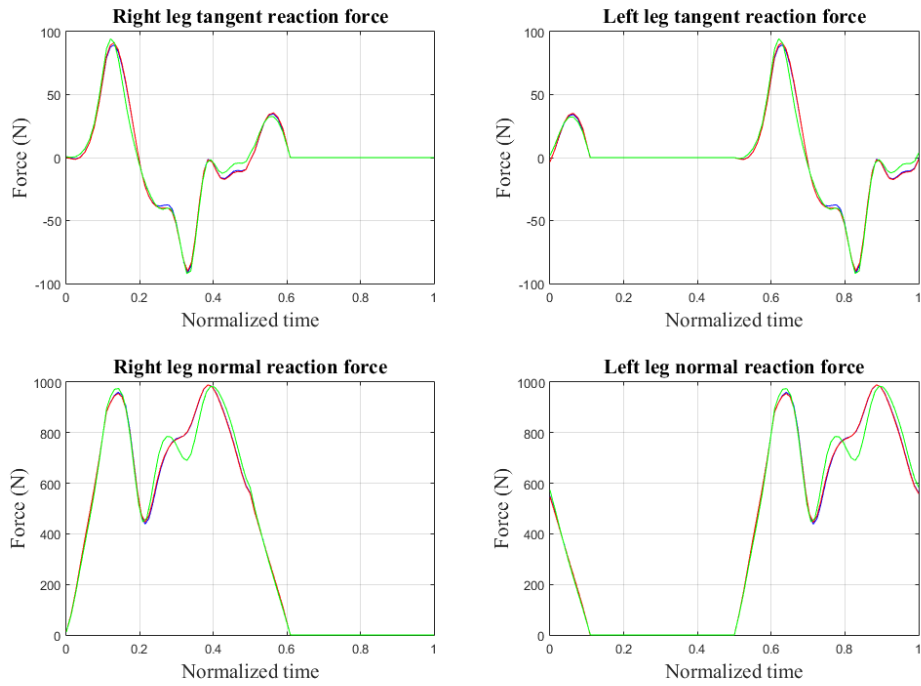
Figure 8-55: Reaction forces after increasing maximum orthosis torque

The only incidence observed in the evolution of reaction forces emerging from the ground is the little swing appearing in the normal reactions, already observed when increasing other parameters in previous phases in the optimization.
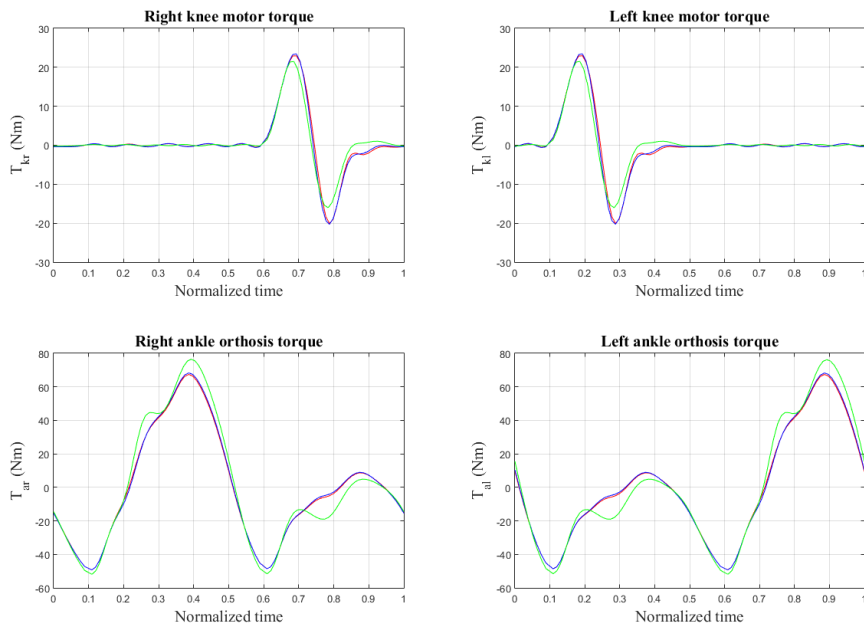

Figure 8-56: Motor and Klenzak torques after increasing maximum orthosis torque
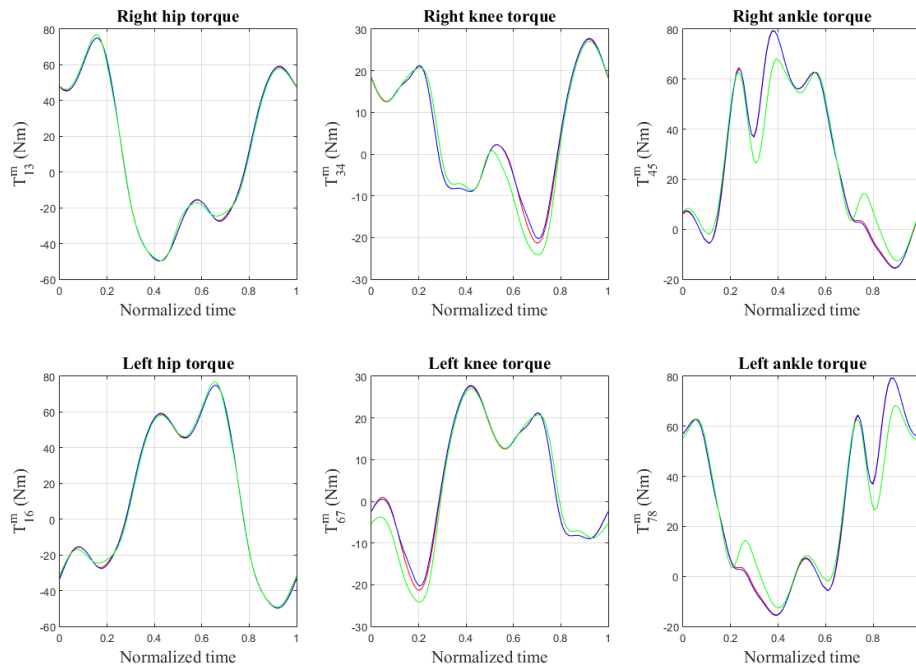
Figure 8-57: Joint torques after increasing maximum orthosis torque

It is worth commenting the evolution of the torque, especially the generated by the motor in the knees. The torque range the orthosis can embrace now is way bigger (it has been doubled, after all). However, contrary to what is expected, the Figure shows how the torque triggered in the knee, where the motor is placed, not only is not bigger than the appeared in the reference, but its peak is smaller. It shall be remembered that the peak gets produced when the foot is not in contact with the ground. Possibly it may be because it is not optimal in terms of efficiency for the motor, to give the maximum level of power during a big amount of time in the cycle.

To compensate this discrepancy, the registered torque produced by the knee is bigger (taking absolute values) with the torque increment. Curiously, the resultant combination of every torques gives a total moment, way bigger than the obtained with the reference, as it can be observed in the Figure below. It seems the walker must overcome the opposition created by the orthosis itself, what may result inconvenient in energetics term.

Observing the ankle torque figure (Figure), there are phases in the cycle when the solution torque is bigger and other phases when it is smaller. On the one hand, analog to previous studied cases, it is smaller when the foot is in contact with the ground. On the other hand, the obtained torque is bigger with the foot in the air. At any rate, these differences are compensated with the Klenzak torque, as it can be observed in the figures below.
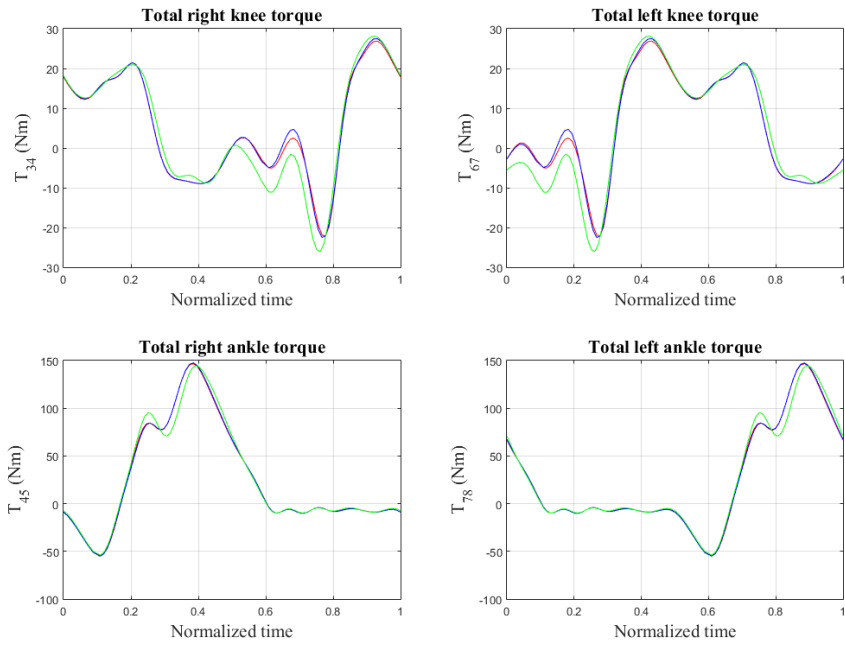
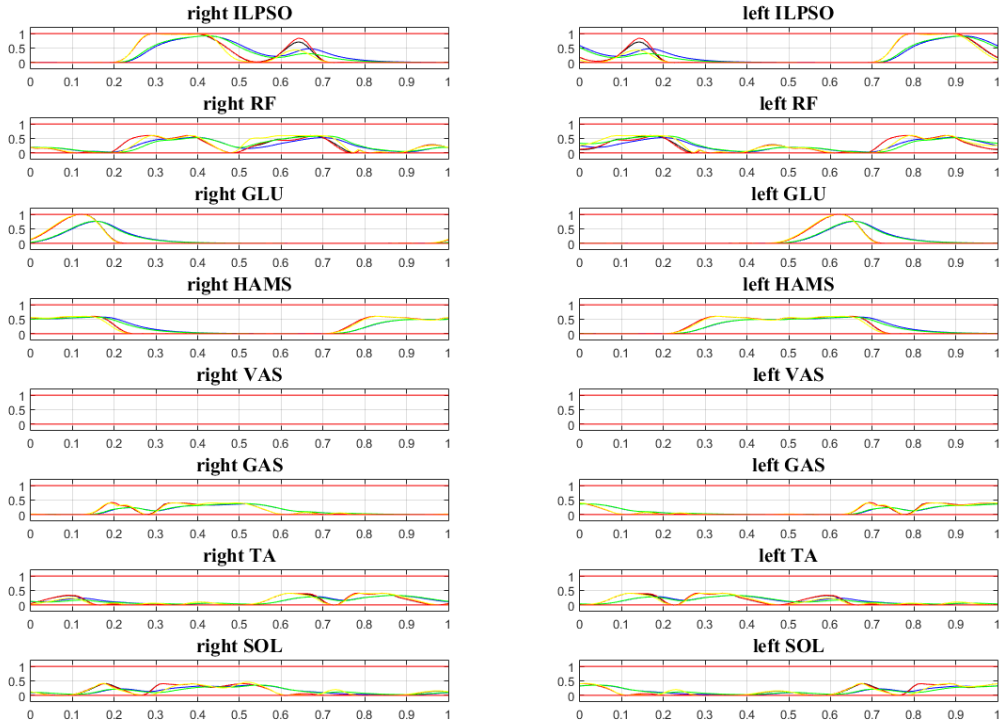Figure 8-58: Total torques after increasing maximum orthosis torque

Figure 8-59: Activation and excitation after increasing maximum orthosis torque

114

The activation and excitation plots (Figure above) show a curious circumstance already appeared and described in previous sections. The muscle activation for the doubled-motor-torque solution (cyan-lined) is lower than the reference and the obtained after the 25% increment. That can be observed in the ilpsoas, placed very near to the hip, where the muscle efforts were detected to be lower during the optimization (as it can be seen in the Figure…). In other muscles, especially those closer to the knee, this phenomenon does not occur.

Table 8-23: Evolution of expenditure and deviation when increasing maximum orthosis torque

Maximum orthosis torque increment	Metabolical expenditure	Deviation from pattern
0 % (Reference)	341.74 J	15.198
25 %	338.91 J	15.089
100 %	326.29 J	14.870

The Table above shows clearly how it seems optimal in energetical terms to double the maximum torque bound imposed to the orthosis, as the metabolical cost gets reduced a 5%. The deviation from the reference gets reduced as well, although to a lesser extent. Now, the Table 8-23 collects the quantitative summary of the results:

Table 8-24. Quantitative summary of maximum motor torque influence

Variable	Highest amplitude, 1st increment	Highest amplitude, 2nd increment	Relative increasement (%)
x_{11}	1.061 m	1.060 m	0.11
z_{11}	0.016 m	0.013 m	17.02
β_{11}	0.030 rad	0.028 rad	5.60
β_{13}	0.726 rad	0.723 rad	0.33
β_{34}	1.023 rad	1.170 rad	14.34
β_{45}	0.252 rad	0.241 rad	4.71
β_{16}	0.726 rad	0.723 rad	0.33
β_{67}	1.023 rad	1.170 rad	14.34
β_{78}	0.252 rad	0.240 rad	4.87
RT Force	181.370 N	186.400 N	2.77
RN Force	989.393 N	983.078 N	0.64
LT Force	181.331 N	186.337 N	2.76
LN Force	989.394 N	983.339 N	0.61
RM Torque	45.172 Nm	39.399 Nm	12.78
LM Torque	45.172 Nm	39.399 Nm	12.78
RO Torque	116.656 Nm	128.389 Nm	10.06
LO Torque	116.651 Nm	128.169 Nm	9.87
RH Torque	124.819 Nm	126.733 Nm	1.53
RK Torque	48.938 Nm	51.227 Nm	4.68
RA Torque	94.668 Nm	80.853 Nm	14.59
LH Torque	124.806 Nm	126.324 Nm	1.22
LK Torque	48.938 Nm	51.227 Nm	4.68
LA Torque	94.676 Nm	81.071 Nm	14.37
TRK Torque	49.931 Nm	54.832 Nm	9.82
TLK Torque	49.931 Nm	54.832 Nm	9.82
TRA Torque	201.581 Nm	186.847 Nm	7.31
TLA Torque	201.584 Nm	187.061 Nm	7.20

8.3.6 Ankle parameters: torque and stiffness

The sixth and last phase of this analysis will comprise the Klenzak ankle. Its two mechanical characteristics, the generated torque and the typical stiffness of the ankle, will be modified so as to see their influence in the optimization.

8.3.6.1 Klenzak torque

The colour code is the same as the followed in the previous phases of the optimization: the blue line correspond to the reference motion (the reference value for the Klenzak torque is 17.156 Nm), the red refers to a 5% increment in the torque, while the green line makes reference to the solution obtained after implementing a 10% growth.
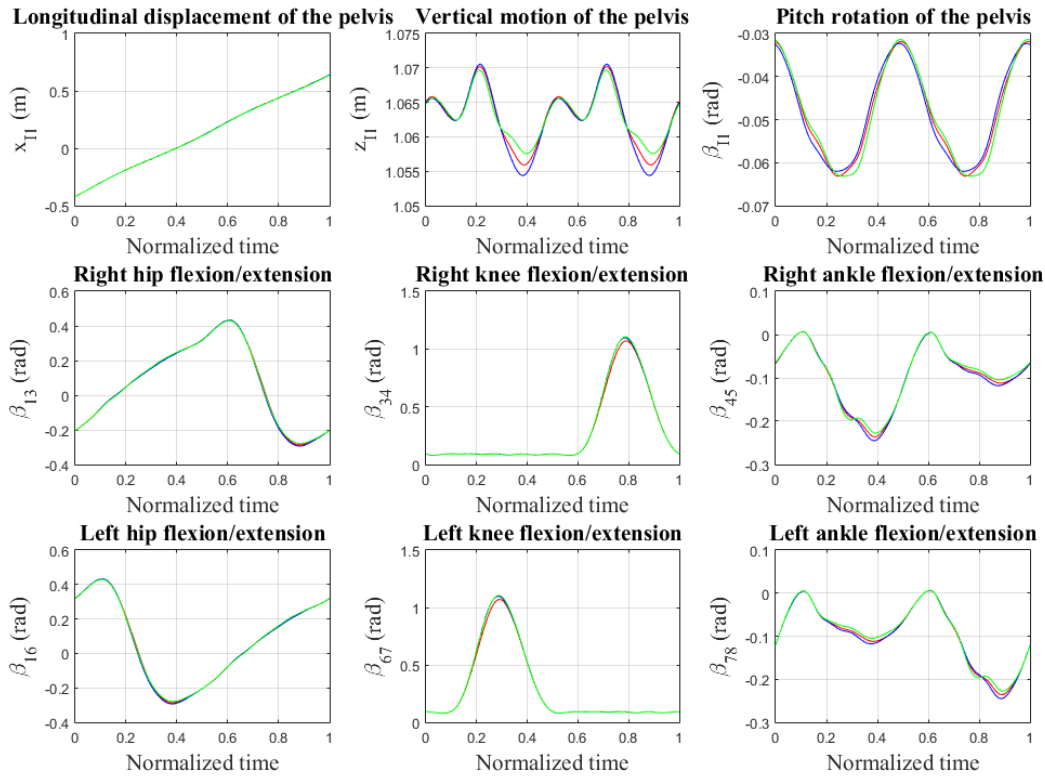

Figure 8-60: Generalized coordinates after increasing maximum Klenzak torque

Discrepancies between the model and the solutions use to appear in the ankle and, especially, the pelvis. To increment the maximum possible torque allows the Klenzak ankle to carry out a bigger moment, and that makes the act of walking more stable, reducing the oscillations in the pelvis. That can explain why the amplitude of the vertical motion of the pelvis is slightly shorter when incrementing the maximum torque.

In the ankle, the flexion movement is less ample in the solution, although it can not be considered as an important reduction. It can be explained with optimal reasons: the ankle does not need to bend itself such a big angle, thanks to the larger torque generated by the Klenzak ankle.
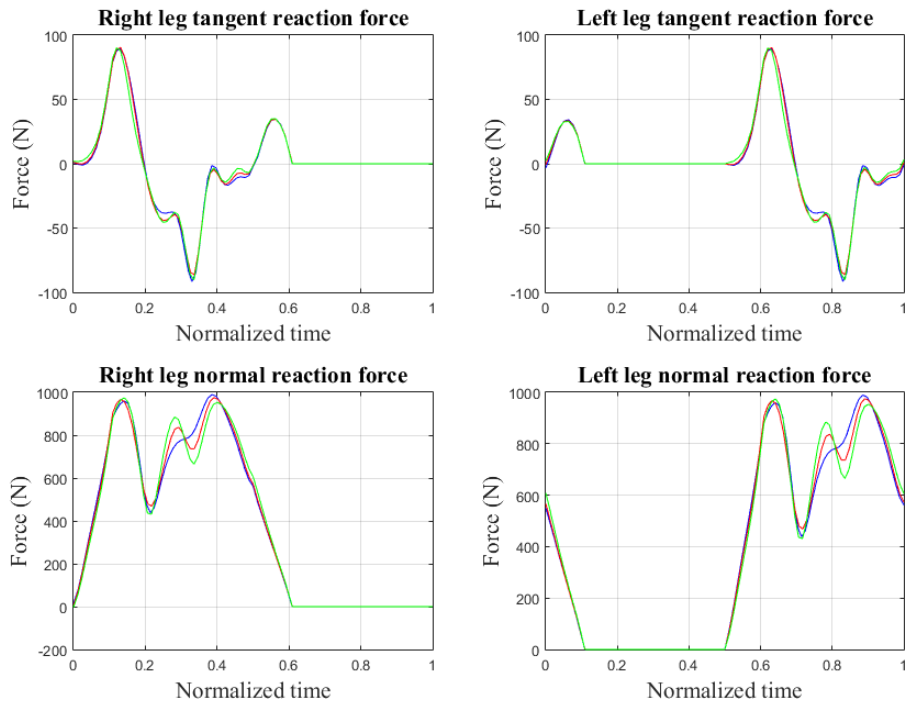
Figure 8-61: Reaction forces after increasing maximum Klenzak torque

Regarding the reaction forces, the observed effect is similar to previous cases: the higher maximum torque generates oscillations in the normal reaction forces in the contact feet-ground. The bigger torque range the ankle disposes of makes larger reactions to appear in the ground, so it is logical to expect this result. Otherwise, the solutions follow almost truly the pattern.

Figure 8-62: Motor and Klenzak torques after increasing maximum Klenzak torque

Figure 8-63: Joint torques after increasing maximum Klenzak torque

Figure 8-64: Total torques after increasing maximum Klenzak torque

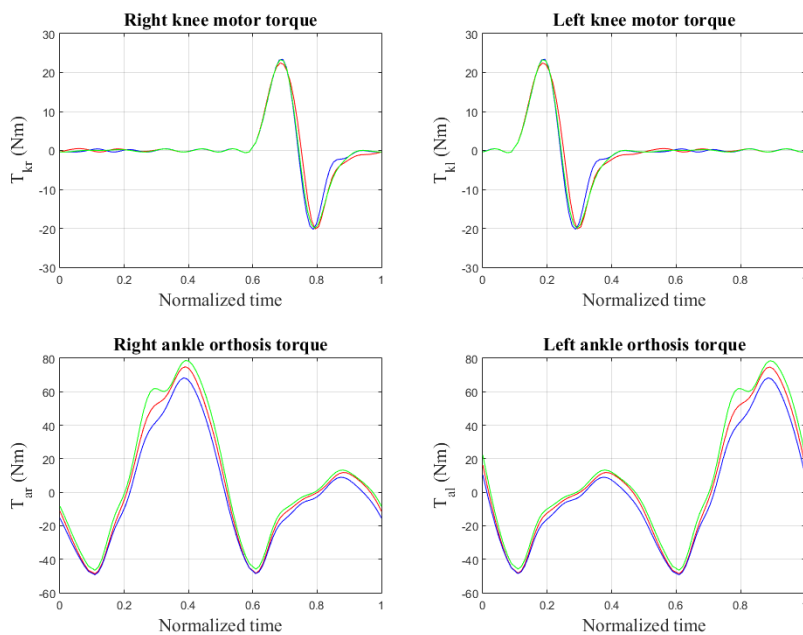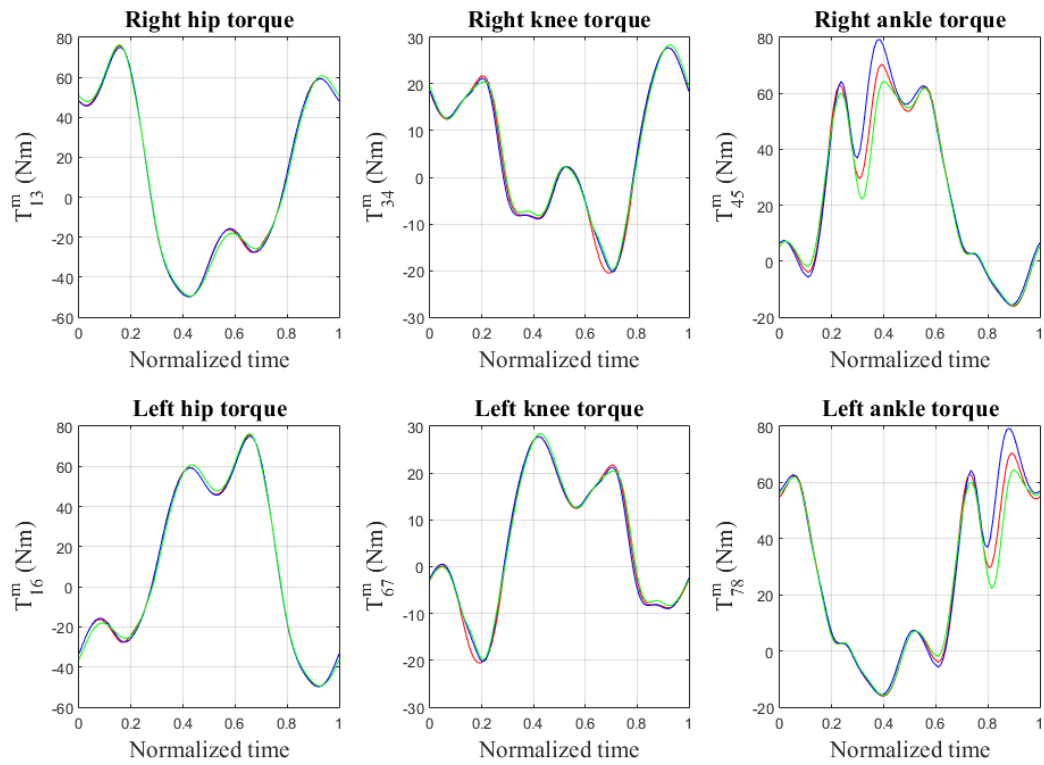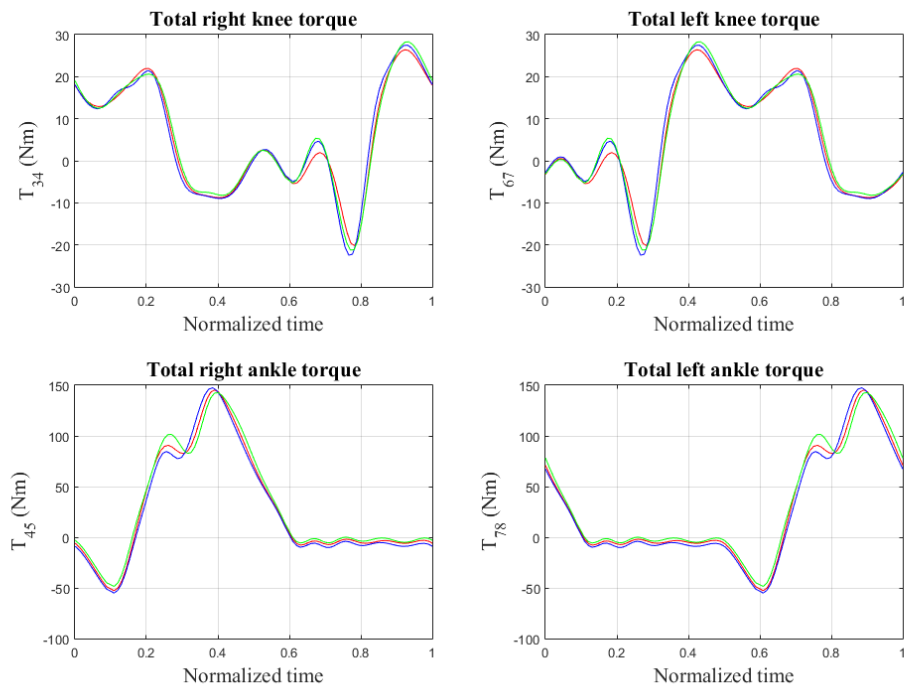It is easy to understand now the evolution of the torque plotted in the figures above. The range amplitude of the torque produced by the mechanical ankle has been incremented, so the reached peak is way bigger. Newly, in order to optimize the energy, the human ankle must reduce its moment, and that is what is observed in the figures.
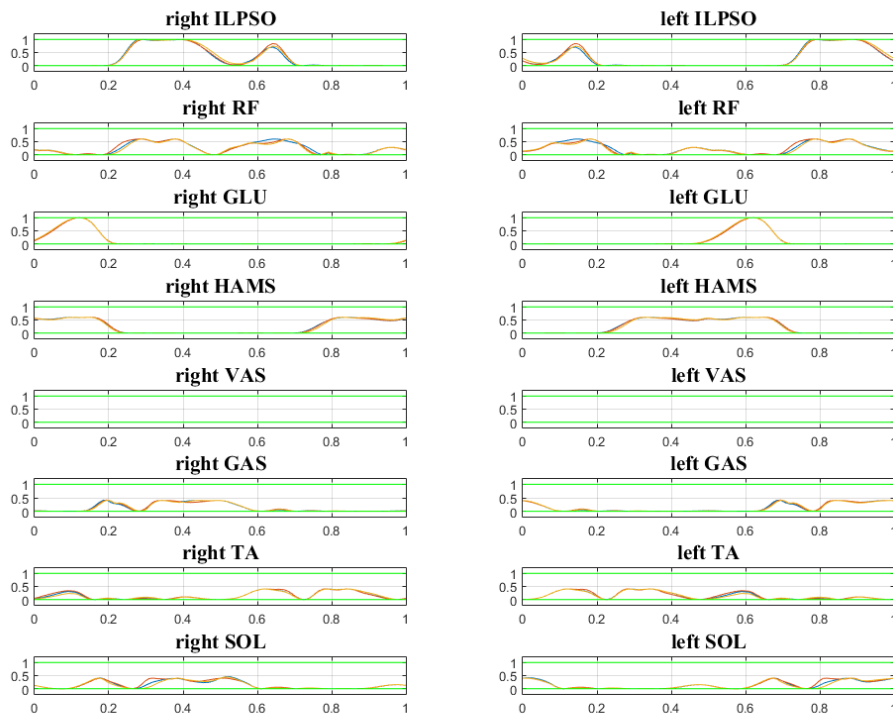
Figure 8-65: Activation and excitation after increasing maximum Klenzak torque

In concordance with the results right presented, where the moment exerted by the muscles was always smaller when increasing the maximum torque in the ankle, and so on the muscle force, the figure above, representing the muscle activation and excitation, shows how the activation has reduced as it is not necessary to force too much the muscle. This general rule serves for each muscle.

Table 8-25: Evolution of expenditure and deviation when increasing maximum Klenzak torque

Ankle torque increasing	Metabolical expenditure	Deviation from pattern
0 (Reference)	341.74 J	15.198
5 %	336.80 J	14.878
10 %	335.11 J	14.688

Now studying the evolution of the energetical cost, it decreases from the reference value, although there is no a remarkable reduction (the order of 1%). More increasings would be needed to reach a notable depletion of the spent energy. The Table 8-25 shows the quantitative analysis of the influence of the Klenzak torque:

Table 8-26. Quantitative summary of Klenzak torque influence

Variable	Highest amplitude, 1st increment	Highest amplitude, 2nd increment	Relative increasement (%)
x_{11}	1.061 m	1.058 m	0.25
z_{11}	0.014 m	0.012 m	15.05
β_{11}	0.031 rad	0.032 rad	1.54
β_{13}	0.719 rad	0.710 rad	1.27
β_{34}	0.992 rad	1.025 rad	3.36
β_{45}	0.243 rad	0.235 rad	3.27
β_{16}	0.719 rad	0.710 rad	1.27
β_{67}	0.992 rad	1.026 rad	3.37
β_{78}	0.243 rad	0.235 rad	3.25
RT Force	176.764 N	180.508 Nm	2.12
RN Force	975.077 N	977.088 Nm	0.21
LT Force	176.684 N	180.362 Nm	2.08
LN Force	975.2578 N	974.271 Nm	0.10
RM Torque	44.747 Nm	45.454 Nm	1.58
LM Torque	44.747 Nm	45.454 Nm	1.58
RO Torque	123.597 Nm	125.293 Nm	1.37
LO Torque	123.420 Nm	125.141 Nm	1.39
RH Torque	125.686 Nm	125.801 Nm	0.09
RK Torque	48.2978 Nm	48.306 Nm	0.02
RA Torque	86.473 Nm	80.152 Nm	7.31
LH Torque	125.573 Nm	125.778 Nm	0.16
LK Torque	48.297 Nm	48.305 Nm	0.02
LA Torque	86.669 Nm	80.390 Nm	7.24
TRK Torque	47.452 Nm	50.378 Nm	6.17
TLK Torque	47.452 Nm	50.378 Nm	6.17
TRA Torque	198.063 Nm	189.103 Nm	4.52
TLA Torque	198.083 Nm	189.113 Nm	4.53

8.3.6.2 Klenzak stiffness

Analog to the torque, the sensivity of the orthosis subject to changes in the stiffness of the Klenzak device is analyzed. The reference value for the Klenzak stiffness is 293.886 N/m. The same colour code is used to represent the design parameters. As it will be seen in the following figures, the stiffness will hardly have an important weight in the optimization process.
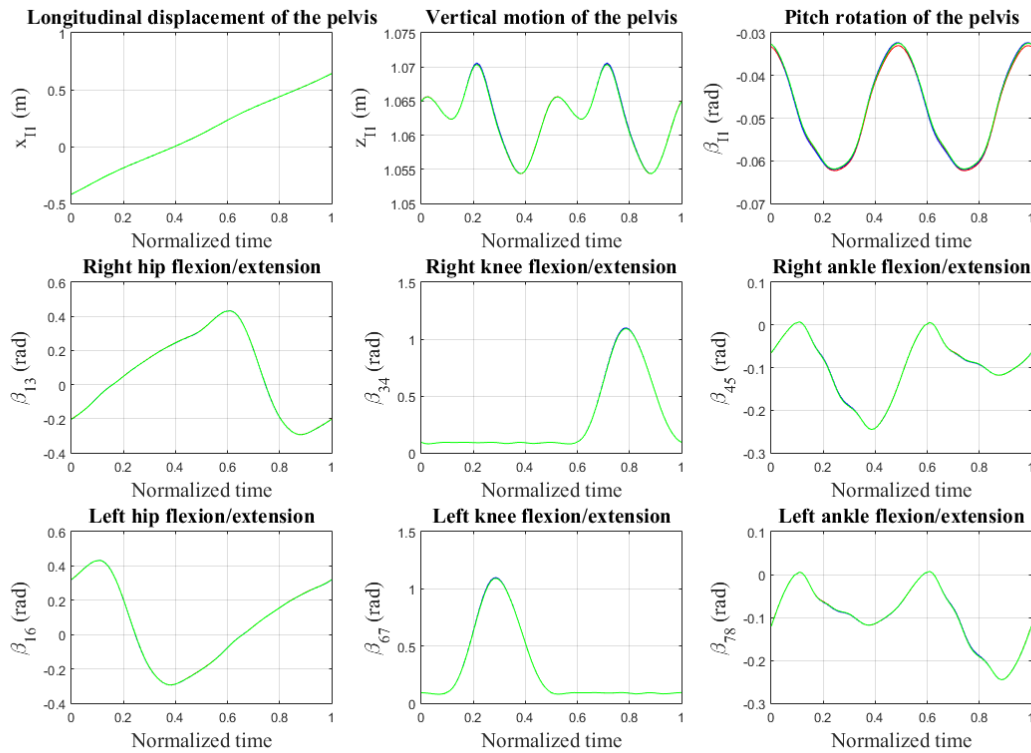
Figure 8-66: Generalized coordinates after increasing maximum Klenzak stiffness.

This time there are no appreciable differences in any coordinate between the reference and the solutions, neither in the pelvis, where they had always appeared until now. The logical deduction would be to think that increasing the stiffness would make more difficult to the walker to bend the Klenzak ankle, as by the definition of stiffness, it consists on the opposition to be bent in a determined direction.

Figure 8-67: Reaction forces after increasing maximum Klenzak stiffness.

No discrepancies were found between the model and the solution with respect to the reaction forces emerging from the ground, originated in its contact with the floor.
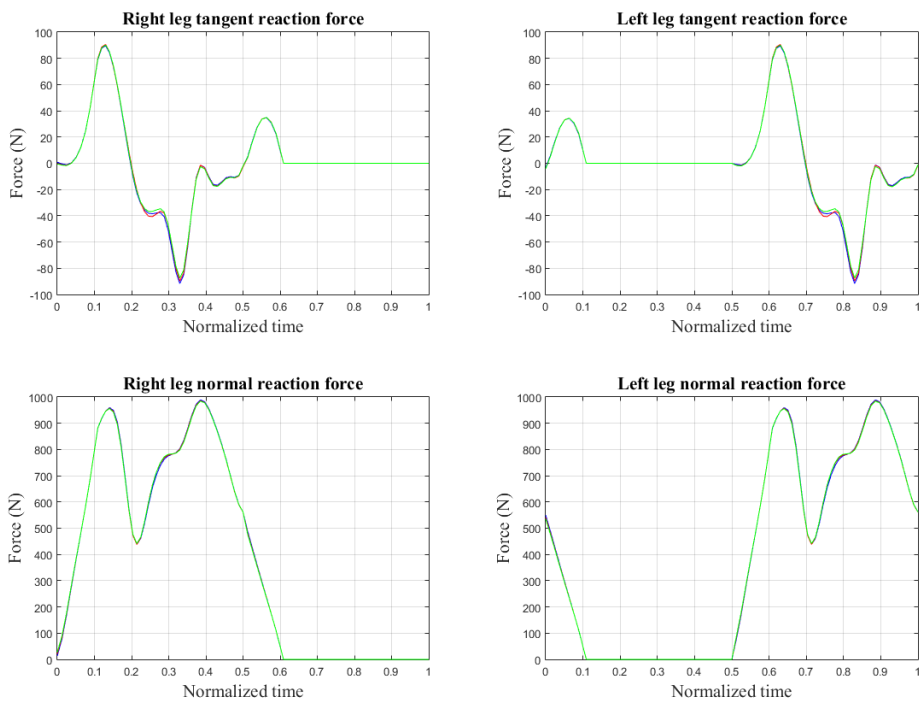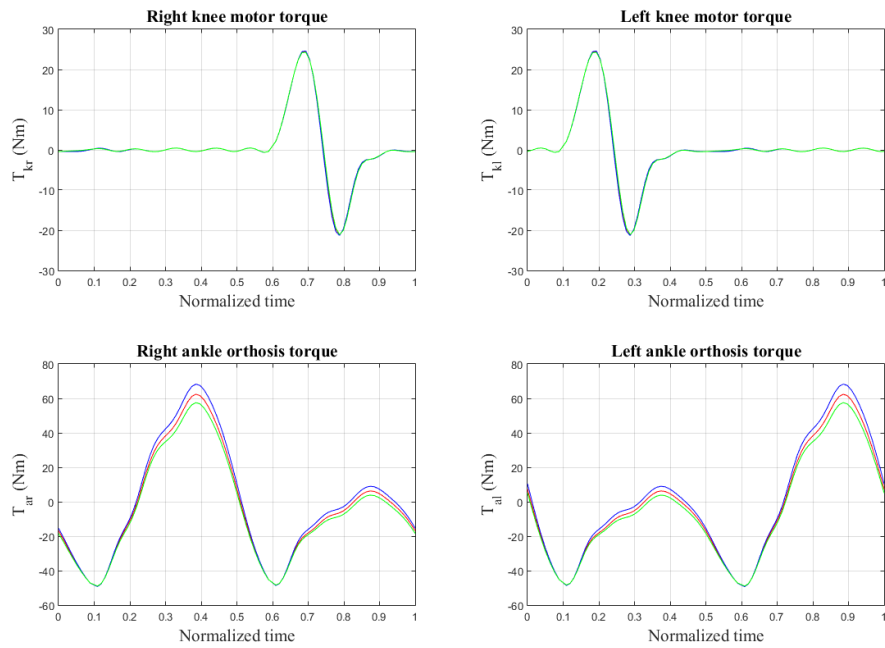

Figure 8-68: Motor and Klenzak torques after increasing maximum Klenzak stiffness.

The Figure shows the first important deviation in this phase of the parameterization, concretely in the ankle. Contrary to the results studied before, when imposing the parameter to grow meant a larger moment produced by the ankle, now the Klenzak device originates a smaller torque (decreasing it at around a 20% from the reference). The reason is easy to explain: the ankle must overcome a bigger resistance as the stiffness is larger now, so if the angle bent is maintained almost the same (as seen in Figure), the registered torque will be smaller.
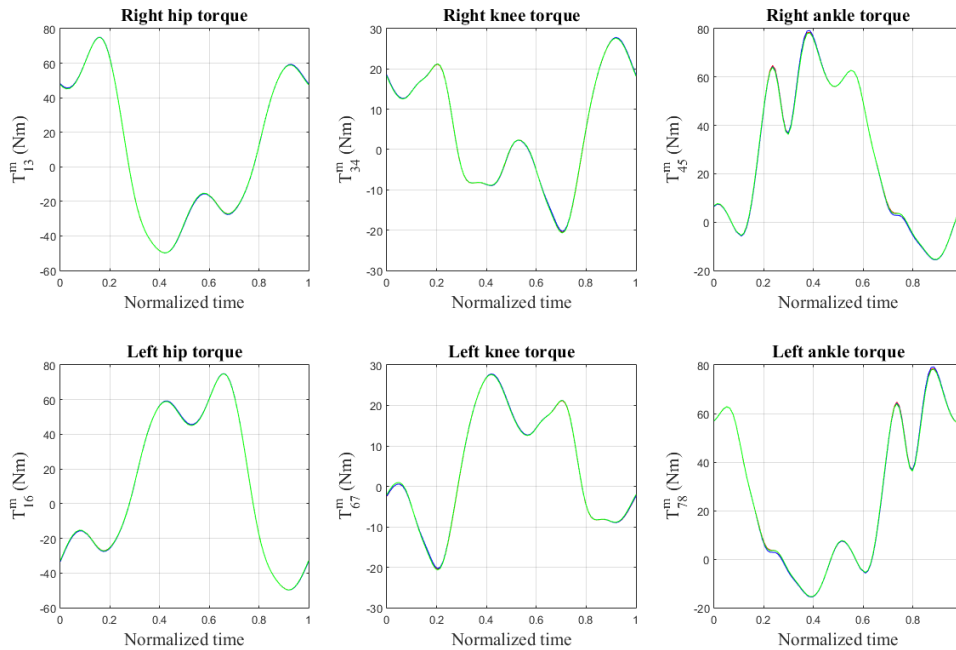
Figure 8-69: Joint torques after increasing maximum Klenzak stiffness.
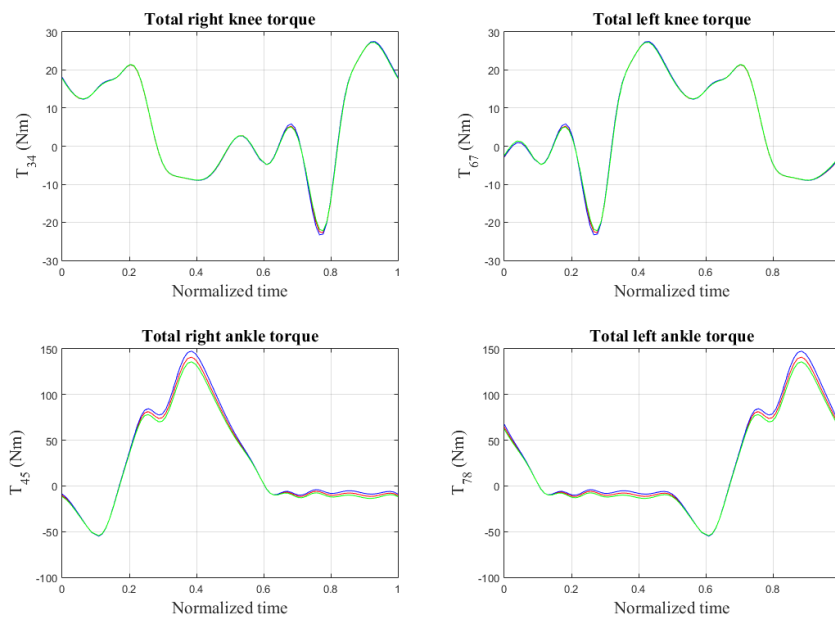
Figure 8-70: Total torques after increasing maximum Klenzak stiffness.

The figures above, displaying the total combined torque, shows how the moments produced by both the human walker and the mechanical devices get compensated. The only discrepance observed between the model and the solutions, the smaller torque in the ankle, already commented, is easily seen in the plots.
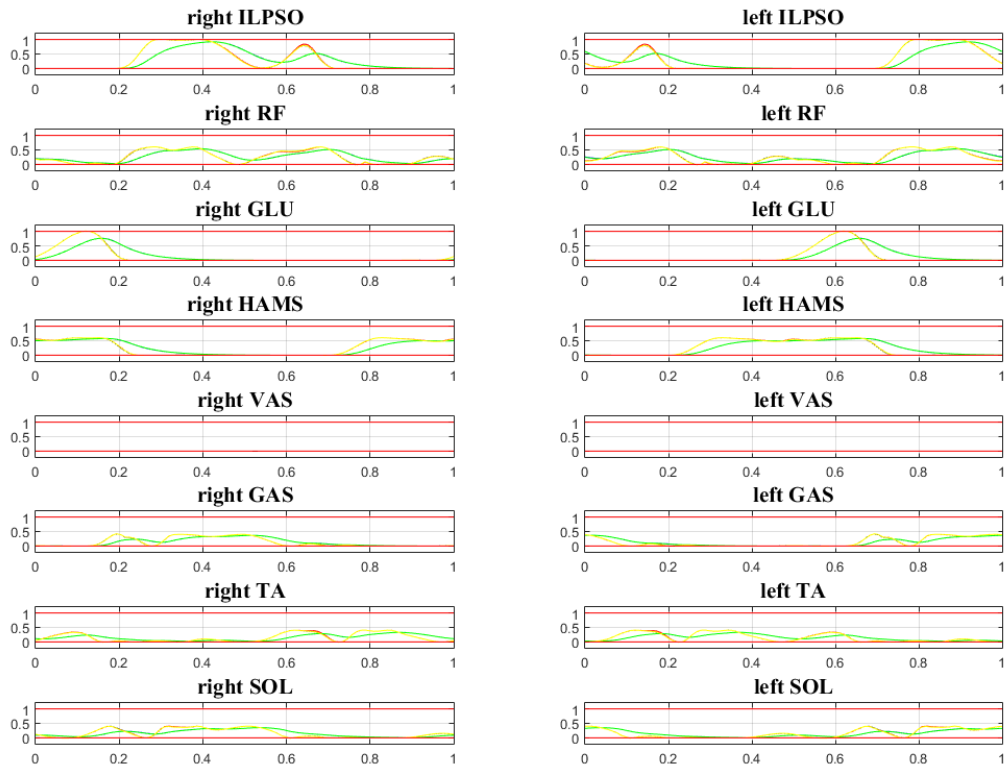
Figure 8-71: Activation and excitation after increasing maximum Klenzak stiffness.

By last, the activation graphics does not present important deviations from the reference. It is easy to reach the conclusion that the stiffness is not an important parameter in this optimization. Anyway, the material of the orthosis will not be likely to change in other orthosis, so this part of the analysis is not as important as other studied in this research.

Concerning the energy expenditure and deviation:

Table 8-27: Evolution of expenditure and deviation when increasing maximum Klenzak stiffness.

Ankle stiffness increasing	Metabolical expenditure	Deviation from pattern
0 (Reference)	341.74 J	15.198
5 %	340.55 J	15.116
10 %	340.60 J	15.131

The energy hardly varies when increasing the stiffness, confirming the point right described: it is non influential in this research. By last, the correspondent Table 8-27, showing the quantitative analysis:

Table 8-28. Quantitative summary of Klenzak stiffness influence

Variable	Highest amplitude, 1st increment	Highest amplitude, 2nd increment	Relative increasement (%)
x_{11}	1.061 m	1.061 m	0.01
z_{11}	0.016 m	0.016 m	0.44
β_{11}	0.029 rad	0.029 rad	0.57
β_{13}	0.726 rad	0.726 rad	0.02
β_{34}	1.016 rad	1.014 rad	0.21
β_{45}	0.252 rad	0.252 rad	4.11e-05
β_{16}	0.726 rad	0.726 rad	0.02
β_{67}	1.016 rad	1.014 rad	0.201
β_{78}	0.252 rad	0.252 rad	8.98e-04
RT Force	180.266 N	177.574 N	1.49
RN Force	986.148 N	984.544 N	0.16
LT Force	180.197 N	177.518 N	1.49
LN Force	986.147 N	984.544 N	0.16
RM Torque	45.532 Nm	45.378 Nm	0.34
LM Torque	45.532 Nm	45.378 Nm	0.34
RO Torque	111.509 Nm	106.5373 Nm	4.46
LO Torque	111.505 Nm	106.534 Nm	4.46
RH Torque	124.767 Nm	124.720 Nm	0.04
RK Torque	48.228 Nm	48.343 Nm	0.24
RA Torque	94.023 Nm	93.698 Nm	0.35
LH Torque	124.742 Nm	124.696 Nm	0.04
LK Torque	48.225 Nm	48.342 Nm	0.24
LA Torque	94.034 Nm	93.706 Nm	0.35
TRK Torque	49.982 Nm	49.495 Nm	0.98
TLK Torque	49.980 Nm	49.494 Nm	0.97
TRA Torque	195.661 Nm	195.314 Nm	0.18
TLA Torque	195.667 Nm	195.317 Nm	0.18

9 ANALYSIS OF RESULTS. FUTURE

After performing every optimizations in the orthosis by increasing the magnitudes described in Chapter 8, and obtaining the effects in terms of variation of the energetical cost, generalized coordinates, motor and joints torques, muscle forces, muscle activation and neural excitations, further conclusions about the influence of these changes in the human walking cycle can be obtained. This is what this chapter deals with.

To start, the influence of mass and geometry in the orthosis was studied by separately in the two first phases of the optimization. Then, both effects were analyzed simultaneously in the third phase, what was considered a more reliable approximation to reality, as a change in mass must take account a change in the geometry if the density remains unchangeable. Therefore, it can be considered that the third phase includes the same conclusions as the first and second phases together.

So, the most remarkable changes affects to the pelvis movement and the generated torque in the joints. On the one hand, the increasement of the moment of the inertia in the orthosis makes more stable the movement, as the fluctuation in the vertical coordinate are smaller. These can be explained the next way: the center of gravity has been displaced to a lower position, reducing the appearing of forces which could destabilize the movement.

On the other hand, the inertial gain makes bigger the mechanical torque produced by the artificial devices, especially the one generated by the Klenzak ankle. This allows the walker not to make such an enormous effort to perform a movement, as it is reflected in the natural torque in the ankle joint, and so on, it eases him his walking. Not great changes were detected in the muscle activation or the neural excitation, so the impact provoked by increasing the moment of inertia in the orthosis can be considered as positive, and that makes a potential innovation facing the development of future orthosis.

Regarding the influence of the weight coefficients in the cost function, the expected results were obtained. Giving more importance to the first coefficient, wE, concretely by trebling its value, the metabolical cost was reduced a 15%, with no great effects in the deviation from pattern. The work by García Vallejo [3] explains that aesthetics in the movement is a bit sacrificed in favor of reducing the expenditure cost. The observed fact is that, effectively, the metabolical cost gets smaller, but the deviation from pattern hardly grows. However, when making the coefficient wJ bigger, the decreasement detected in the deviation is not really important, around 7%. Moreover, the energy expenditure increases, what makes worthless to give more importance to reduce deviation from the pattern. The main conclusion obtained from there is that the fundamental task regarding the future of active orthosis will be to reduce the metabolical expenditure rather than focus on the difference from the reference motion.

Concerning the maximum motor torque rising, it has both positive and negative impacts in the walking cycle. Firstly, it must be highlighted that the movement is way more stable because the motor can now generate more power to produce forces which stabilize the walking. However, what refers to the torque, the impact cannot be considered as fully positive. The major range of torque the motor can embrace does not imply a bigger torque during the cycle. In fact, it is observed that the maximum reached torque is smaller than the measured in the reference motion. This means that it is not costeffective in terms of efficiency to increase the maximum torque. At least, the metabolical cost gets a small reduction, rounding the 5%, smaller than other reductions obtained in other phases during the optimization.

To end this summary, it may be commented that the increasements in the mechanical characteristics of the Klenzak ankle infludes positively in the walking cycle, although not in large-scale. Some variations already commented appear again, such like the lesser swings in the vertical motion of the pelvis, or the small

decreasement in the metabolical cost. Moreover, the generated torque in the motor is bigger during the cycle, especially when the maximum Klenzak torque is the increased magnitude. This can be considered as a positive effect which may be taken into account regarding future active orthosis designing. However, the increasement of the stiffness does not impact positively in the cycle.

BIBLIOGRAPHY

[1] Font-Llagunes, J.M., García-Vallejo, D., Schiehlen, W, *Dynamical analysis and design of active orthoses for spinal cord injured subjects by aesthetic and energetic optimization,* Nonlinear Dynamics, 2014.

[2] García-Vallejo, D., Schiehlen, W, *3D-Simulation of human walking by parameter optimization,* Nonlinear Dynamics, 2014.

[3] García-Vallejo, D., *Three-Dimensional Simulation of Human Walking Optimizing Aesthetics and Energy*, University of Stuttgart, 2010.

[4] Mayo Clinic, *Spinal Cord Injury,* Rochester, Minnesota, December 2017. Available online: https://www.mayoclinic.org/diseases-conditions/spinal-cord-injury/symptoms-causes/syc-20377890

[5] Johns Hopkins Medicine, *Spinal Cord Injury,* The Johns Hopkins University, Baltimore, Maryland, Available online:
https://www.hopkinsmedicine.org/healthlibrary/conditions/physical_medicine_and_rehabilitation/spinal_cord_injury_85,P01180

[6] Shepherd Center, *Spinal Cord Injury Information*, Atlanta, Georgia. Available online: https://www.shepherd.org/patient-programs/spinal-cord-injury/about

[7] Daniel Barranquero, *'Boban' Jankovic, el guerrero sin alas,* Asociación de Clubes de Baloncesto, Barcelona, Spain, July 2006. Available online: http://www.acb.com/redaccion.php?id=32435

[8] Tolo Leal, *Boban Jankovic, el momento más trágico en una cancha de baloncesto,* Libertad Digital, September 2014. Available online: https://www.libertaddigital.com/deportes/baloncesto/2014-09-04/boban-jankovic-el-momento-mas-tragico-en-una-cancha-de-baloncesto-1276527297/

[9] Ackerman, M. and Gross, H., *Measurements of Human Gaits,* Institut für Technische und Numerische Mechanik, University of Stuttgart, December 2005

[10] Graham, R.B., Agnew, M.J., Stevenson, J.M., 2009. *Effectiveness of an on-body lifting aid at reducing low back physical demands during an automotive assembly task: assessment of EMG response and user acceptability.* Appl. Ergon. 40, pp. 936–942.

[11] De Rijcke, L., Näf, M., Rodriguez-Guerrero, C., Graimann, B., Houdijk, van Dieën, J., Mombaur, K., Russold, M., Sarabon, N., H., Babič, J., Lefeber, D., 2017. *SPEXOR: Towards a passive spinal exoskeleton.* Biosystems and Biorobotics 16, pp. 325-329.

[12] Wikipedia, the free encyclopedia. *Powered exoskeleton,* June 2018. Available online: https://en.wikipedia.org/wiki/Powered_exoskeleton

[13] Exoskeleton report, *Types and Classifications of exoskeletons,* March 2017. Available online: https://exoskeletonreport.com/2015/08/types-and-classifications-of-exoskeletons/

[14] Yale University, *Active Orthosis and Exoskeletons*, New Haven, Connecticut, 2012. Available online: https://www.eng.yale.edu/grablab/research_orthoses.html

[15] School of Medicine and Public Health, *Classification of Spinal Cord Injuries,* University of Wisconsin-Madison, October 2017. Available online: https://www.uwhealth.org/health/topic/special/classification-of-spinal-cord-injuries/ug2627.html

[16] Martínez Reina, J. *Comportamiento mecánico del músculo esquelético*. Bioengineering, University of Seville, 2018.

[17] Mathworks, *fmincon Active Set algorithm*, The Mathworks, inc. 2018. Available online: https://es.mathworks.com/help/optim/ug/constrained-nonlinear-optimization-algorithms.html#bsgppl4

[18] Mathworks, *fmincon,* The Mathworks, inc. 2018. Available online: https://es.mathworks.com/help/optim/ug/fmincon.html#busog7r-options

[19] Umberger,B.R., Gerritsen,K.G.M., Martin,P.E.: *A model of human muscle energy expenditure*. Comput. Methods Biomech. Biomed. Eng. 6 (2), 99–111 (2003).

[20] Nagano, A., Gerritsen, K.G.M.: *Effects of neuromuscular strength training on vertical jumping performance—a computer simulation study*. J. Appl. Biomech. 17, 113–128 (2001).

[21] Riener, R., Edrich, T.: *Identification of passive elastic joint moments inthe lower extremities*. J. Biomech. 32, 539–544 (1999).

[22] Stein, R.B., Zehr, E.P., Lebiedowska, M.K., Popovic, D.B., Scheiner, A., Chizeck, H. J.: *Estimating mechanical parameters of leg segments in individuals with and without physical disabilities.* IEEE Trans. Rehabil. Eng. 4(3), 201–211 (1996).

[23] García Vallejo, D., MATLAB, *Algorithm to evaluate the energetic cost during a human walking cycle when wearing an active orthosis.* Stuttgart, Germany, 2010.